Characterization of Macro-Length Conducting Polymers and the Development of a Conducting Polymer Rotary Motor

by

Bryan D. Schmid

B.S. Mechanical Engineering (2003)
Massachusetts Institute of Technology

Submitted to the Department of Mechanical Engineering
in Partial Fulfillment of the Requirements for the Degree of

Master of Science in Mechanical Engineering

at the

MASSACHUSETTS INSTITUTE OF TECHNOLOGY

MAY 2005 [June 2005]

Signature of Author _____
Department of Mechanical Engineering
May 17, 2005

Certified by _____
Ian W. Hunter
Hastopolous Professor of Mechanical Engineering
Thesis Supervisor

Accepted by _____
Lallit Anand
Professor of Mechanical Engineering
Chairman, Department Committee on Graduate Students

Characterization of Macro-Length Conducting Polymers and the Development of a Conducting Polymer Rotary Motor

by

Bryan D. Schmid

Submitted to the Department of Mechanical Engineering
on May 17, 2005 in Partial Fulfillment of the
Requirements for the Degree of Master of Science in
Mechanical Engineering

Abstract

Conducting polymers are a subset of materials within the electoractive polymer class that exhibit active mechanical deformations. These deformations induce stresses and strains that allow for conducting polymers to be used as an actuator for mechanical devices. Incorporation of conducting polymer actuators into mechanical devices requires electrochemical and mechanical characterization of varying polymer sample sizes and their active properties. Of particular interest, is the characterization of macro-length polymer samples, which have yet to be investigated. An understanding of conducting polymer films and their feasibility as an actuator in a mechanical device are required for the development of a conducting polymer based rotary motor.

The conducting polymer, polypyrrole, was studied for its feasibility as an actuator for control surfaces on autonomous underwater vehicles. Enhancements to the actuator's performance were addressed following the feasibility study. The development of an electrochemical dynamic mechanical analyzer provides an instrument for characterization of the polymer's properties over a variety of sample sizes and actuation conditions. Finally, the application of polypyrrole as an actuator and possible enhancements combined with the characterization of macro-length polymers provides the necessary tools to develop a rotary motor.

Enhancements to polypyrrole actuators in this study account for an increase in tip force of 350% and a seven fold increase in achievable strain. Completion of a novel electrochemical dynamic mechanical analyzer, construction of a finite rotary motor able to subtend angular displacements, and the developed embodiment of a polymer based rotary eccentric motor are accomplished in this study.

Thesis Supervisor: Ian W. Hunter
Title: Professor of Mechanical Engineering

Acknowledgements

I thank the Lord for the past years that have blessed me with opportunities, friendships, and challenges which have shaped me into who I am today. It is a wonderful privilege to reflect upon and recognize those around me who have colored my education with thought, friendship, guidance, laughter, and support.

I owe great thanks to Ian Hunter and the members of the BioInstrumentation Laboratory. I have been fortunate to benefit from his unending efforts to provide the resources for my research, and for that I am thankful. Ian's supervision has opened my mind to the expansive scope of truly understanding a problem.

Working with "the polymer group" has been a pleasure. My interest and understanding of conducting polymers is greatly due to my introduction into the field by John and Peter Madden. Patrick and Naomi have been wonderful colleagues who have helped foster my interest in entrepreneurship and helped me maintain my sanity through conversation in our area. I would like to thank Rachel for her hard-working example and for flattering me by being the first to use my ECDMA.

I am very grateful for the friendships that have carried me through the past years in and out of lab. Thank you, Nate, for the laughs, supportive guidance, camaraderie, and good times. Thank you, Sasha, for your friendship, smile, and support throughout our time at MIT. The many memories from trips to the Muddy, Thirsty, coffee shop, Miracle, etc. with you will always be appreciated.

Other colleagues in the BioInstrumentation Lab have always offered the support and guidance which I appreciate. During the pressure and stress of the last few months, I appreciate the time, guidance, and listening ear that Andrew always offered. I would also like to thank Cathy for her kindness and fresh orange juice after long nights in lab.

Very special thanks to my parents who have always supported me and given me opportunities at their own sacrifice. My family has been a constant source of encouragement and love whom without, I wouldn't be here today as the person I am.

I am also indebted to Elaine for her patience, support, and ability to make me forget about MIT. My time and memories of her will always be treasured.

I would like to thank the U.S. Army and The Institute of Soldier Nanotechnologies at MIT for the wealth of resources that have allowed this research to take place.

Contents

List of Figures

List of Tables

Chapter 1

Introduction

Electroactive polymers (EAPs) are a class of materials that respond to an electrical or chemical stimulus with an active response. Active EAP material responses can include mechanical deformations inducing a stress, varying optical coloration effects, and changes to the material's electrical conductivity. Polymers in this class include conducting polymers, ionic polymer metal composites, electrostrictive polymer actuating materials (EPAMs), and others.

The capability of EAPs to produce active strains and stresses with an electrical or chemical stimulus is of special interest to mechanical engineers. An active shape change allows for the polymer to be used as an actuator in mechanical systems [1,2]. Some of the EAP materials exhibit active mechanical stresses and strains that allow for them to be suitable substitutes of more traditional actuator technologies [3]. A comparison between EAPs and other actuators such as mammalian skeletal muscle, DC motors, and ultrasonic motors provide a benchmark for the polymer's potential as an actuator.

In vitro mammalian skeletal muscle exhibits a peak strain rate of ± 10 %/s active strain [4] whereas EAPs have demonstrated active peak strains ranging from 2 to 300 % [5]. EAPs are able to achieve active tensile stresses of 20 to 450 MPa [1, 3] compared to the peak achievable active *in vitro* stresses in mammalian skeletal muscle of 350 kPa [4]. The power density of EAP actuators ranges from 5.8 W/kg up to 150 W/ kg [3,6,7,8,9] with the expected possibility of achieving 4 kW/kg [10] in the future with polymer advances. By comparison, the peak power densities of mammalian skeletal muscle (50 to

200 W/kg) [4], ultrasonic motors (70 to 100 W/kg) [11], and DC motors (5 to 3000 W/kg) [12] reveal comparable to inferior performance against EAP actuators.

Traditional actuators, such as DC motors, are limited in their evolution without advances in raw materials, i.e. copper. Over the past 100 years there has been little advancement in actuator technologies compared to the advancement of the devices they power. Developments in actuator technologies including ultrasonic, piezo electric, and hyrbrid electrical and internal combustion motors have all failed to match the power to mass ratios of the first internal combustion engines. In addition, all of the traditional actuators above do not scale well below 1.0×10^{-6} m^3 without sacrificing power and efficiency [13]. In contrast, EAP actuators size down very well and in many cases become more efficient and exhibit higher strain rates. The promise of EAP actuators and their mechanical properties has improved significantly since the 1990s [5] with the advancement of new polymer materials and techniques. EAPs continue to advance everyday on the material level through the efforts of many research groups throughout the world, such as at the Institute for Soldier Nanotechnologies at the Massachusetts Institute of Technology.

1.1 Motivation

Employing EAPs as the actuating material for a motor provides a novel solution to motor development since the materials can be structured on the molecular level [14]. Research has already demonstrated large active stresses in conducting polymers and some EAPs, such as polypyrrole, increase in efficiency as they are used at smaller length scales. In particular, the advancements of technology today seek to move into the micro and nano scale with motors that are scalable without sacrificing the actuator's power to mass ratio.

Conducting polymers, a subset of EAP polymers, exhibit active mechanical deformations with an electrical or chemical stimulus. Polypyrrole (PPy) is particular conducting polymer which has been studied exclusively in the BioInstrumentation Laboratory at the

Massachusetts Institute of Technology. PPy's active mechanical properties are superior to most conducting polymers and electrochemical deposition of PPy films is simple and inexpensive. The incorporation of PPy films into a rotary motor provides a novel solution to finite or infinite motion that can be scaled down to meet the trends of today's technology

1.2 Background: Principles of Polypyrrole Actuation

The exact mechanical and structural behaviors of polypyrrole actuation are not completely understood. Different models presented from research typically suggest that PPy, as depicted in Figure 1-1, either undergoes a structural phase change due to an electrochemical stimulus or an active bulk swelling of ions in the polymer film due to an electrochemical stimulus. The subsequent Chapters assume an active bulk swelling of PPy as described by the diffusive elastic model.

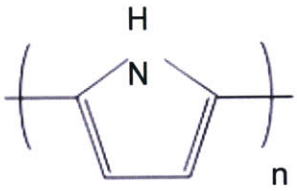

Figure 1-1: Chemical structure of polypyrrole.

The principles of active mechanical expansion and contraction for PPy can be described by the diffusive elastic model developed by J. Madden [10]. The model accurately describes the behavior of a PPy film in an electrolyte solution stimulated within an electrochemical cell at frequencies from 10^{-3} to 10^{5} Hz as depicted in Figure 1-2 [15]. The PPy is actuated in an electrolyte solution that consists of a dissolved salt, such as tetraethylammonium hexaflourophosphate (TEAP), in a solvent, such as propylene carbonate. Active mechanical deformation of the PPy occurs when a potential is applied between the conducting polymer and counter electrode.

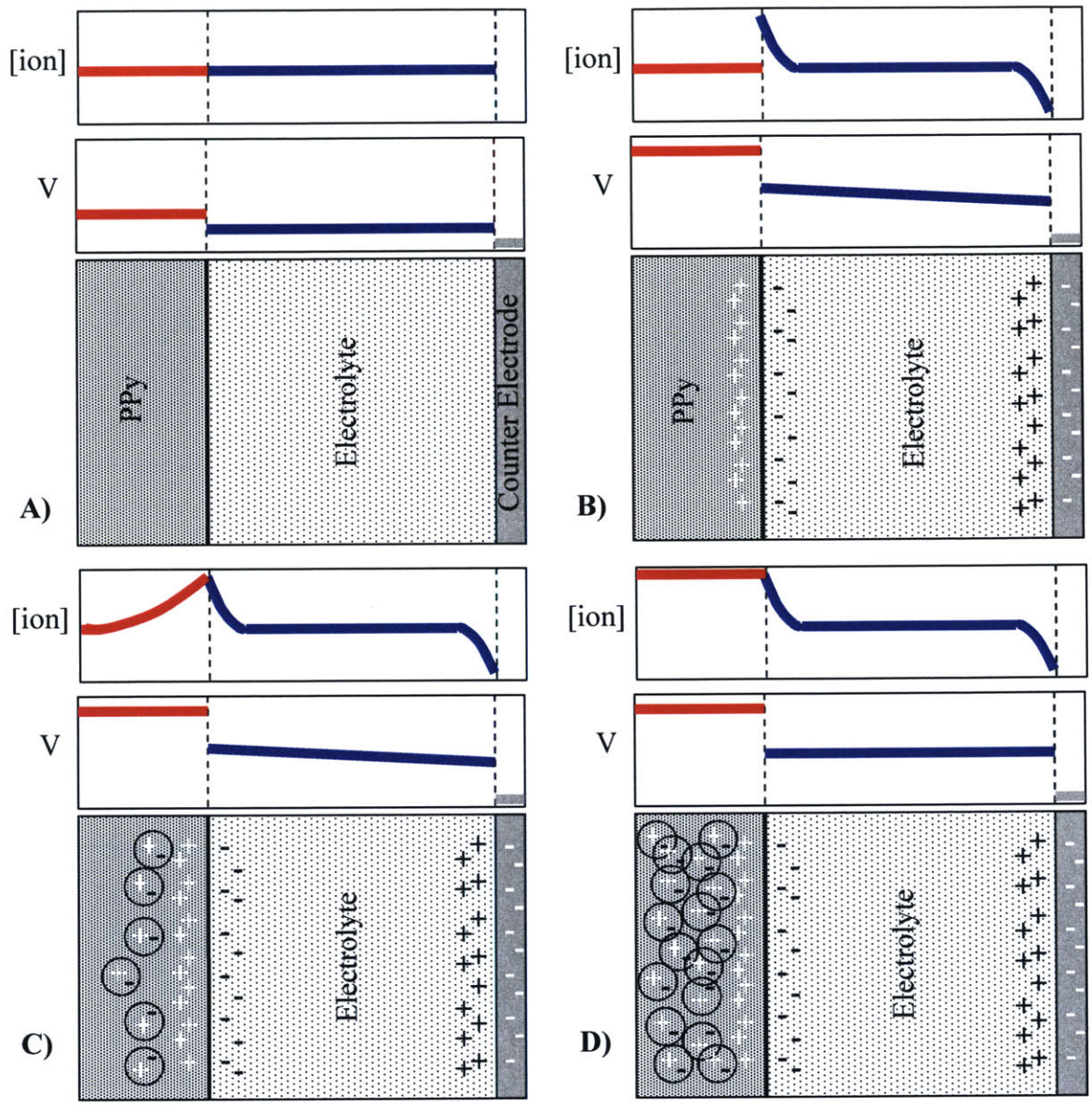

Figure 1-2: Polymer, Electrolyte, and Electrochemical cell schematic during actuation [15]. A) The PPy system at rest and the open circuit potential represented by the voltage difference. B) Applied potential and charge buildup at double layers. C) The diffusion of ions into the polymer brings the system to equilibrium and depicts bulk material swelling. D) Fully charged polymer at peak mechanical deformation for the applied potential.

The potential charges ions at the double layer capacitance of the film's surface as pictured in Figure 1-2B. The concentration of ions at the double layer drives the diffusion of ions in or out of the PPy (Figure 1-2C) as the system moves toward

equilibrium of the applied potential. The steady state result (Figure 1-2D) is achieved when the charge between the double layer and the polymer is at equilibrium. Active mechanical expansion or contraction of the polymer begin immediately upon oxidation or reduction as the ions diffuse into the polymer and create a volumetric change. Once steady state is achieved, the polymer is fully doped with ions and cannot undergo a volumetric expansion unless there is an increase in the potential.

Equations of the Diffusive Elastic Model

Using the diffusive elastic model the volumetric strain of the polymer can be modeled analytically as a function of charge

$$\varepsilon = \frac{\sigma}{E} + \alpha \cdot \rho, \tag{1.1}$$

where ε is the induced strain, σ is the applied stress, E is polypyrrole's elastic modulus, α is an experimentally determined strain to charge ratio, and ρ is the applied charge per polymer unit volume. Relative time constants τ_D (ion diffusion), τ_{RC} (double layer charging) τ_{DDL} (double layer diffusion) for actuation of the polymer are derived from the admittance of a polymer strip in an electrolyte solution as given by

$$Y(s) = \frac{s}{R} \cdot \frac{\frac{1}{\sqrt{\tau_{DDL}}} \cdot \tanh(\sqrt{s \cdot \tau_D}) + \sqrt{s}}{\frac{\sqrt{s}}{\tau_{RC}} + s^{\frac{3}{2}} + \frac{s}{\sqrt{\tau_{DDL}}} \cdot \tanh(\sqrt{s \cdot \tau_D})}, \tag{1.2}$$

where

$$\tau_D = \frac{h^2}{4 \cdot D}, \tag{1.3}$$

$$\tau_{RC} = R \cdot C_{dl}, \tag{1.4}$$

$$\tau_{DDL} = \frac{\delta^2}{D}, \tag{1.5}$$

where *Y(s)* is the admittance as a function of the Laplace variable *s*, *h* is the thickness of the polymer strip, *D* is the diffusion coefficient of the ion within the polymer, *R* is the total series resistance, C_{dl} is the double layer capacitance, and δ is the thickness of the double layer.

The diffusive elastic model and its governing Equations accurately describe actuation in thin PF_6^- (TEAP ion) polypyrrole films over eight orders of magnitude of frequency. Figure 1-2 and Equations 1.1 through 1.5 govern the design considerations in the subsequent Chapters and provide a high level description of polypyrrole actuation

1.3 Goals

The ultimate goal of this research is to characterize and enhance macro-length polymer actuators for their incorporation into the development of a conducting polymer based rotary motor. Because of the scalability of EAPs down to micro- and potentially nanometer sizes without sacrificing efficiency or power, the research conducted in the following Chapters seeks to lay the groundwork for the feasibility of micro-scale conducting polymer rotary motors.

When researching the potential for a new actuator technology it is desirable to first understand the technology's benefits and shortcomings through experimentation and feasibility exercises. Enhancements to the technology can then be addressed through testing and characterization. Those enhancements and technological understandings can then be incorporated into the development of a mechanical system.

1.4 Chapter Descriptions

Chapter 2: This Chapter presents a reprint of a published journal article regarding the application and feasibility of polypyrrole as an actuator. Specifically, two different embodiments of the polypyrrole are investigated to manipulate the control surfaces of an underwater autonomous vehicle.

Chapter 3: The trimorph and linear actuators presented in Chapter 2 are limited by low forces and slow strain rates. This Chapter addresses both of those shortcomings with mechanical and material enhancements.

Chapter 4: An electrochemical dynamic mechanical analyzer (ECDMA) is developed and constructed to characterization and analysis of polymer films. The ECDMA provides a flexible platform capable of characterizing micro- and macro-length films with custom electrical and mechanical stimuli.

Chapter 5: This Chapter discusses the development of finite and infinite displacement rotary motors. In depth background and analysis are juxtapositioned with experimental results.

1.5 Chapter References

[1] Baughman, R.H.,. Shacklette, R.L., and Elsenbaumer, R.L., "Micro electromechanical actuators based on conducting polymers," *Topics in Molecular Organization and Engineering, Vol. 7: Molecular Electronics*, P.I. Lazarev, Ed., Dordrecht: Kluwer Academic Publishers, **V. 7** (1991): 267-289.

[2] Baughman, R.H., "Conducting polymer artificial muscles," *Synthetic Metals*, **V. 78** (1996): 339-353.

[3] Madden, J., Vandesteeg, N., Anquetil, P., Madden, P., Takshi, A, Pytel, R., Lafontaine, R., Wieringa, P., Hunter, I., "Artificial Muscle Technology: Pysical Principlces and Naval Prospects." *IEEE Journal of Oceanic Engineering*, **V. 29 No. 3** (2004): 706-728.

[4] Hunter, I. and Lafontaine, S., "A Comparison of Muscle with Artificial Actuators." *Technical Digest IEEE Solid State Sensors and Actuators Workshop*, IEEE (1992): 178-185.

[5] Bar-Cohen, Y., "Electro-active polymers: current capabilities and challenges," *Smart Structures and Materials 2002: Electroactive Polymer Actuators and Devices (EAPAD)*, Yoseph Bar-Cohen, Ed., *Proceedings of SPIE*, **V. 4695** (2002): 1-7.

[6] Caldwell, D.G., "Pseudomuscular actuator for use in dextrous manipulation," *Medical and Biological Engineering and Computing*, **V. 28** (1980): 595-600.

[7] Madden, J., Madden, P., Hunter, I., "Conducting polymer actuators as engineering materials," *Smart Structures and Materials 2002: Electroactive Polymer Actuators and Devices (EAPAD)*, Yoseph Bar-Cohen, Ed., *Proceedings of SPIE*, **V. 4695** (2002): 176-190.

[8] Madden, J., Cush, R., Kanigan, T., and Hunter, I., "Fast contracting polypyrrole actuators," *Synthetic Metals*, **V. 113** (2000): 185-192.

[9] Della Santa, A., D. De Rossi and A. Mazzoldi, "Performance and work capacity of a polypyrrole conducting polymer linear actuator," *Synthetic Metals*, **V. 90** (1997): 93-100.

[10] Madden, J., *Conducting Polymer Actuators*, Ph.D. Thesis, Massachusetts Institute of Technology, Cambridge, MA, 2000.

[11] Kuribayashi Kurosawa, M., Kodaira, O., Tsuchitoi, Y., and Higuchi, T., "Transducer for High Speed and Large Thrust Ultrasonic Linear Motor Using Two Sandwich-Type Vibrators", IEEE Transactions on Ultrasonics, Ferroelectrics, and Frequency Control. **V. 45 No. 5** (Sept. 1998): pp.1188-1195.

[12] http://www.mabuchi-motor.co.jp/english/

[13] Uchino, K., "Piezoelectric Ultrasonic Motors: Overview" *Smart Mater. Struct.* **V. 7** (1998): 273-285.

[14] Yu, H. and Swager, T., "Molecular Actuators – Designing Actuating Materials at the Molecular Level," *IEEE Journal of Oceanic Engineering*, **V. 29 No. 3** (2004): 692-695.

[15] Madden, P., *Development and Modeling of Conducting Polymer Actuators and the Fabrication of a Conducting Polymer Based Feedback Loop*, Ph.D. Thesis, Massachusetts Institute of Technology, Cambridge, MA, 2003.

Chapter 2

Application of Polypyrrole Actuators: Feasibility of Variable Camber Foils

The following section is a reprint of a published journal article regarding the application and feasibility of polypyrrole as an actuator. Understanding the capabilities and shortcomings of polypyrrole actuators in an actual mechanical system is invaluable to the engineering advancements of polypyrrole actuators. Specifically, two different embodiments of the polypyrrole are investigated to manipulate the control surfaces of an underwater autonomous vehicle.

Application of Polypyrrole Actuators: Feasibility of Variable Camber Foils

John D. W. Madden, *Member, IEEE*, Bryan Schmid, Martin Hechinger, Serge R. Lafontaine, Peter G. A. Madden, Franz S. Hover, *Associate Member, IEEE*, Richard Kimball, and Ian W. Hunter

***Abstract*—A decade of research into electroactive polymer actuators is leading to the exploration of applications. These technologies are not ready to compete with the internal combustion engine and electric motors in high power propulsion systems but are suitable for intermittent or aperiodic applications with moderate cycle life requirements, providing an alternative to solenoids and direct drive electric motors. Polypyrrole, an emerging actuator material, is applied to drive hydrodynamic control surfaces and in particular to change the camber of a foil. The foil is intended for use in the propeller blade of an autonomous underwater vehicle. A scaled prototype is constructed which employs polypyrrole actuators imbedded within the blade itself to vary camber. The kinematics required to generate camber change are demonstrated, with >30° deflections of the trailing edge being observed from both bending bilayer and linear actuator designs. Forces developed in still conditions are five times lower than the 3.5 N estimated to be required to implement variable camber. The observed 70 kJ/m^3 polypyrrole work density however is more than sufficient to produce the desired actuation from within the limited blade volume, enabling an application that is not feasible using direct drive electric motors. A key challenge with the polypyrrole actuators is to increase force without sacrificing speed of actuation.**

***Index Terms*—Actuator, artificial muscle, autonomous underwater vehicle, conducting polymer, control surface, hydrodynamics, electroactive, electroactive polymer (EAP).**

I. Introduction

ELECTROACTIVE polymer (EAP) research has reached a level of maturity such that applications are actively being sought and developed, as evidenced by the number of application related papers presented at the annual conference on EAPs [1]. Where new technologies are being introduced, it seems appropriate to seek applications in which distinct advantages over existing technology are offered. In this paper the feasibility of using conducting polymer actuators to vary the camber of propeller blades in autonomous underwater vehicles is investigated. Although the application is very specific, the experiments and analysis performed here will provide guidance in the general design issues and concerns encountered in applying EAPs. In combination with other papers in this issue—including a general review of artificial muscle technologies [2], and a specific look at operating conditions and limitations in polypyrrole actuators [3]—a comprehensive perspective on the application of artificial muscle technologies, and in particular conducting polymer actuators, is offered.

A. Application of Artificial Muscle Technologies: Where Are the Opportunities?

Established actuator technologies [4] for which artificial muscle technologies might offer an alternative include internal combustion engines, high-revving electric motors, direct drive electric motors, and piezoelectric actuators.

1) Propulsion Systems and Artificial Muscle: Competing with the internal combustion engine for propulsion of surface vehicles such as automobiles and ships is a challenge due to the high power to mass of these motors (1000 W/kg) [4] and the high energy density fuel (43 MJ/kg) employed. Fuel cells and hybrid engines can provide high energy density electrical energy sources, making the use of high revving electric motors feasible. Electric motors offer power densities similar to the internal combustion engine and efficiencies that can exceed 90% [4]. Only shape memory alloys and piezoceramic actuators can clearly surpass the power to mass of internal combustion engines and electric motors [5]. Piezoelectrics however generate very small strains (~0.1%) and thus it is a great challenge to use them to generate large displacements. Shape memory alloys are too low in electromechanical efficiency and cycle life to consider for continuous large scale propulsion [2], [5].

Underwater the energy equation changes substantially, as combustion engines and fuel cells rely on oxygen, which must be transported (unless dissolved oxygen or air bubbles are collected). Combustion of hydrocarbons is not particularly advantageous over battery power[1] undersea and battery driven electric motors are more practical for use in propulsion of submersibles.

Manuscript received October 23, 2003. This work was supported in part by the Office of Naval Research under the STTR Program.

J. D. W. Madden is with the University of British Columbia, Vancouver, V6T 1Z4 BC, Canada (e-mail: jmadden@ece.ubc.ca).

M. Hechinger is with the University of British Columbia, Vancouver, V6T 1Z4 BC, Canada

B. Schmid and S. R. Lafontaine are with the BioInstrumentation Laboratory, Massachusetts Institute of Technology, Cambridge, MA 02139 USA.

P. G. A. Madden is with the Department of Organismic and Evolutionary Biology, Harvard University, Cambridge, MA 02138 USA.

F. S. Hover is with the Department of Ocean Engineering, Massachusetts Institute of Technology, Cambridge, MA 02139 USA.

R. Kimball is with the Maine Maritime Academy, Castine, ME 04420 USA.

I. W. Hunter is with the BioInstrumentation Laboratory, Massachusetts Institute of Technology, Cambridge, MA 02139 USA.

Digital Object Identifier 10.1109/JOE.2004.833128

[1]http://www.panasonic.com/industrial/battery/oem/chem/lithion/ The combustion of hexane produces ~40 MJ/kg and requires 19 oxygen atoms. When the weight of oxygen is factored in, the energy per unit mass drops to ~4 MJ/kg. Lithium ion batteries have energy densities of ~0.6 MJ/kg, Given that combustion engines are typically one-third as efficient as high revving electric motors (30% versus >90%), the relative advantage of combustion is reduced to a factor of 2, not including the mass and bulk of the oxygen storage vessel and of the transmission system.

New actuator materials such as dielectric elastomers, ferroelectric polymers, conducting polymers and carbon nanotubes can offer power to mass ratios that are within a factor of four of the combustion engine [2]. The lower power densities of these materials may be compensated for by their "muscle-like" nature, making them more suitable for biomimetic propulsion [6], [7]. However, there are a number of challenges for system designers [8]. For example, dielectric elastomers and ferroelectric polymers operate at kilovolt level voltages, requiring dc–dc voltage conversion where battery power is employed. Lower voltage actuators based on conducting polymers, carbon nanotubes, and ionically conductive polymer metal composites currently suffer from poor electromechanical coupling [2]. Finally, none of the emerging actuator technologies has demonstrated cycle lifetimes of more than 10^7 [2] (in some cases the cycle life has yet to be properly measured). Continuous operation at 10 Hz may lead to failure after ten days or less. Although the new actuator technologies are expected to improve in many respects [2], at present they do not offer compelling alternatives to electric motors and combustion engines for high power, continuous propulsion.

2) Intermittent Actuation: Vehicular propulsion typically involves continuous rotation of wheels or screws, activities for which internal combustion engines and high revving electric motors are well suited. Discontinuous and aperiodic motions such as the grasping of parts by a robot arm, the opening of a valve, or the adjustment of a hydrodynamic control surface are not easily performed using rapidly spinning actuators with relatively narrow ranges of optimal rotation rates. In such cases direct drive electric motors are often employed. However the low force, torque, and work to mass ratios of these direct drive actuators means that they are relatively heavy and bulky [4]. For example, Honda's sophisticated humanoid Asimo robot, which relies on servo-motors for movement, does not have much torque to spare after lifting its own weight, thereby limiting the impact its legs can sustain, and in turn preventing walking speeds from exceeding 2 km/h.[2] A further disadvantage of the electromagnetic actuators is that they expend energy to hold a force, even when no mechanical work is being performed. Holding a fixed position under load is thus highly inefficient, unless a catch or lock can be implemented. Applications of a discontinuous nature occurring in situations where the space and or mass are at a premium, as in autonomous underwater vehicles (AUVs), could benefit from actuators with higher force and work densities that feature catch states. One such application which will be examined further is the positioning of hydrodynamic surfaces in order to change camber.

3) Anticipated Advantages of Variable Camber Propellers: Deflection of key areas of a propeller blade (such as the leading and trailing edges) leads to large changes in loading resulting from only small input forces [9]. Such a variable camber blade geometry is expected to offer many of the advantages of the controllable pitch propeller [10], which include:

- better off-design efficiency: efficient multimode operation;
- ability to adjust load to match engine or motor characteristic;
- cavitation mitigation under heavily loaded conditions (acceleration, towing etc.);
- ability to produce rudder flow at low vessel speeds to help low speed maneuvering;
- ability to operate in reverse thrust condition without changing shaft rotation direction;
- elimination of gearbox (though a reduction gear may still be required).

Distinct advantages of variable camber are:

- elimination of gearboxes;
- electronic actuation of the propeller blade geometry;
- no gears/shafting is required for the actuators;
- there is potential for individual blade control with minimal increase in system complexity;
- a simplified control driver is easily controlled by a computer.

These anticipated advantages are made possible by the voltage control, and by the relatively high energy densities and forces produced by artificial muscle materials [2], enabling these actuators to be incorporated into blades, and eliminating the need for transmission down the shaft.

The mechanical complexity and cost of pitch control mechanisms is the major disadvantage of such propellers. The mechanism requires gearing in the hub for each blade as well as control rods embedded in the propeller shaft and actuators inside the ship, thus requiring more complex sealing than a simple shaft [10]. Such systems are relatively expensive in comparison to fixed pitch propellers, and require more maintenance to ensure reliability [10]. For these reasons controlled pitch propellers have been primarily limited to large vessels where economies of scale are most attractive. An inexpensive mechanism that replaces variable pitch propeller mechanisms is potentially of great value in small vessels.

4) Illustration of the Efficiency Gained by Using Variable Camber Propellers: The following example illustrates the effect of load on the efficiency of a typical fixed propeller powered by a dc electric motor. Fig. 1(a) shows the motor performance curve of a typical dc motor along with the torque speed characteristics of a fixed propeller operating on a hull with quadratic resistance versus speed (i.e., a streamlined underwater hull). Under these conditions the propeller efficiency is roughly constant and if well designed will be near its maximum efficiency under typical operating conditions. However, as the speed of the vessel is changed the operating point moves off the motor's efficiency peak. By incorporating a variable geometry propeller, the operating point can be moved to better match the motor's performance as shown in Fig. 1(b). Such matching is not achievable with a fixed propeller system. The increase in efficiency is potentially very valuable in AUVs and related vehicles where energy and space are very restricted.

Efforts are under way to experimentally quantify the benefits of variable camber propulsion. The aim of this paper is to show the feasibility of employing new actuator materials [2], and in particular polypyrrole, to achieve variable camber, and to elucidate the advantages and challenges in employing this actu-

[2]Honda Motor Company, http://world.honda.com/ASIMO/P3/spec/

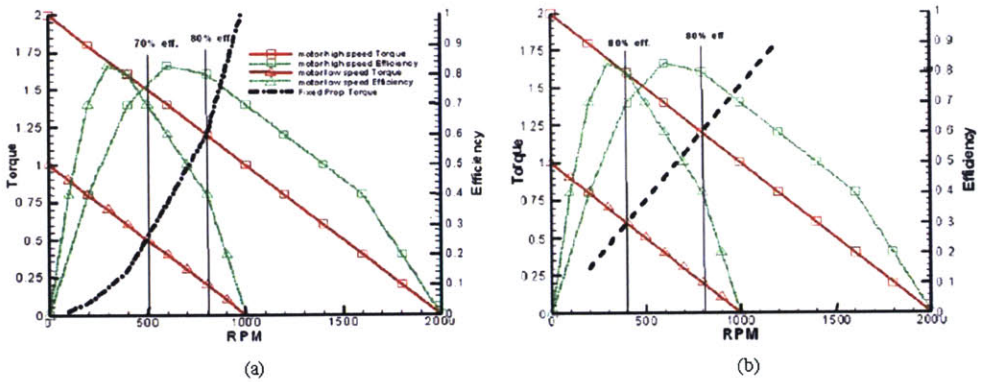

Fig. 1. (a) Operating curves of a motor/prop/hull with a fixed propeller. (b) Capabilities of a variable-geometry propeller with the same motor and hull as in (a). The propeller torque/speed relationship (dashed line) is shown to be modified in order to optimize efficiency.

ator technology in discontinuous and quasisteady applications. In particular the following questions are addressed: Is polypyrrole an appropriate actuator technology for such applications? What are polypyrrole's advantages and disadvantages compared to alternatives? How significant are the challenges in scaling up this technology from the laboratory scale (millijoule energy scale, millimeter displacements) to the device scale? What are the prospects for application in AUVs and other systems?

Before reporting on the experimental feasibility of employing polypyrrole actuators in variable camber systems, the desired performance is established, and the selection of polypyrrole is justified. After setting the specifications, two prototypes are described which were built with dimensions appropriate for ultimate testing in the Massachusetts Institute of Technology (MIT) water tunnel, and are thus larger in volume than required in the final vehicle. Scaling is used to estimate the feasibility of their use on the desired scale. The kinematics, force generation and water tightness are tested. It is shown that the devices meet the kinematic requirements. Forces need to be increased in order to achieve the performance targets. Time required to develop peak force is approximately 50 s in one device and tens of minutes in the other, and thus means of increasing speed will be required.

II. Specifications

The target vehicle for variable camber is the Expendable, Mobile Antisubmarine Warfare Training Target (EMATT) from Sippecan Inc, Marion, MA [13]. The vehicle is designed to act as a target for antisubmarine warfare exercises, and as such is expendable.

Minimum actuator/propulsor performance specifications are determined based on the EMATT speed and geometry.

1) Force: The streamlined EMATT vehicle is 100 mm in diameter and 900 mm length, and is geometrically similar to a Remus vehicle, whose specifications have been reported [11]. Remus requires 6.8 N of thrust to operate at 1.5 m/s (3 knots); it has a 165 mm diameter and fineness ratio (L/D) varying from six to 11. For a general idea of what forces are required in the EMATT vehicle, scaling is performed with the ratio of speeds squared, and the ratio of diameters squared. Operating at 1.5 m/s EMATT generates approximately 2.9 N of drag force. At the upper speed limit of 4 m/s, 21 N of drag force is expected.

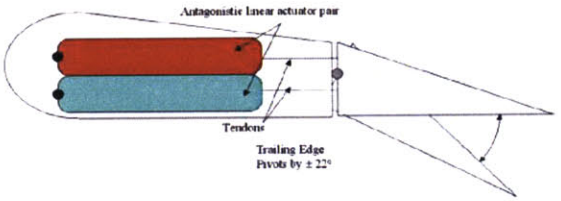

Fig. 2. Lever arm design for creating variable camber. The triangular tail section pivots about a joint (gray circle). Torque is applied to the trailing edge section via an antagonistic actuator pair coupled via tendons.

With three blades per propeller, the upper load limit is 7 N per blade acting over a span of about 50 mm (accounting for duct thickness and a small hub). Actuated trailing edges used for variable camber control will sustain less than half of the 7 N since the majority of the load is carried by the main solid core of the blade [9]. Thus less than 3.5 N per blade is born by the trailing edge and must be withstood by the actuator.

2) Implications of Force Estimates: Trailing Edge Designs: Based on Riegels' data [9] of blade pressures, as the flap is altered from its nominal position to $\pm 22°$ there is a large change in foil lift. The force on the trailing edge to achieve this lift change is small in comparison with the relative overall lift change [9] and therefore the controllable surface in this area of the foil will require only a relatively small actuation force to achieve a large change in overall lift. Riegels shows that pressures are very large near the leading edge of the foil—as a result, leading edge actuation requires substantially larger forces than at the trailing edge. Hence, in this work, camber is varied using the trailing edge only.

3) Displacement/Camber Change: The extent of displacement of the trailing edge has yet to be optimized. A trailing edge deflection of up to $\pm 22°$ occurring on the last 25–40% of the chord is chosen to emulate common high-lift flap geometries [12].

4) Mission Life: EMATT is a single use vehicle. The device must operate over a time period of 24 h without failure (the maximum mission duration). Assuming that camber variations are needed at most once every minute on average, the upper bound on number of cycles sustained by the moveable flap is 1500.

5) Environment: The EMATT performs shallow dives, attaining relative pressures of up to ~2 MPa. The vehicle must also be able to withstand a corrosive aqueous environment.

6) Cost: The cost limit remains to be determined, but current low-cost thruster assemblies of motors, shafting, and propellers are in the range of $100–$400 per vehicle [13]. Our objective is to minimize the additional cost resulting from the added degrees of freedom.

7) Aft Volume: The EMATT vehicle has a fairly large open area in the afterbody as the motor is situated well forward. The motor shaft is connected to the through-hull shaft with a flexible coupling. Suitably mounted, several electronic packages of >15 cm^3 each can easily be entrained, providing control and power to the propeller.

8) Power Connection: Fifteen DD size primary lithium-sulfur dioxide batteries with nominal voltages of 3 V provide a total energy total of 3 MJ [13].

9) Actuator Requirements: The next step is to calculate the forces, displacements, work densities, rates, and cycle life required of the actuators. Each EMATT propeller blade has an approximate span (length) of 50 mm, a chord (width) of 25 mm, and an average thickness of 6 mm. In our design the last 10 mm of the chord at the trailing edge will be pivoted so as to enable variable camber. Fig. 2 shows the approximate geometry. The angle of the trailing edge is to be adjusted by $\pm 22^\circ$ under a load of up to 3.5 N.

The unknown distribution of blade loading force is assumed to be applied at a single point 3 mm from the trailing edge, or, equivalently, 7 mm from the pivot point. The force of 1.75 N generates a torque of $T = 25$ mN·m about the pivot. If the total deflection is $\theta = 44^\circ$, the maximum work that must be done is $W = T \cdot \theta = (25 \text{ mN m}) \times (\pi/4) = 19$ mJ.

A key objective is to avoid the need for mechanical transmission down the shaft to reach the propeller. Ideally the mechanism employed will fit within a propeller blade. The nonpivoting portion of each blade has a volume of 6 mm × 15 mm × 50 mm = 4.5×10^{-6} m^3. Given the required work, the minimum work density in order to fit the actuator within the propeller volume is ~4.2 kJ· m^{-3}. In fact the work density will need to be at least double this value, or >8 kJ· m^{-3} as otherwise no space is allotted for structural elements, power delivery, encapsulation, electrodes, electrolyte, and sensors.

Assuming adjustment of the camber takes place over 1 to 10 s, the output power is 1.9 to 19 mW.

III. Actuator Selection & Challenges

The results presented here do not represent the first time artificial muscle technologies have been applied to fluid dynamic problems. Bandyopadhyay *et al.* employed ionically conductive polymer metal composites to show that oscillating the trailing edge "flap" of variable camber blades in a propeller appears to increase thrust, and thus should enable lower RPM operation of propellers, and reduced noise emission [14]. Reynaerts [15] and Beauchamp [16] have demonstrated the use of shape memory alloys to vary camber in wings and control surfaces in general. Given this history, why choose polypyrrole actuators over other emerging and established technologies? In this section the rationale for choosing polypyrrole actuators is presented [8].

The number of actuator technologies capable of meeting the work density and other requirements in order to fit within the propeller blade is limited. Candidate actuator technologies are now discussed.

1) DC Servo Motors: Direct drive electric motors are a well established, commercially available technology. These are powered by dc voltages readily obtained from a submersible's battery. There is a strong incentive to employ such established technology where possible. However these do not exhibit sufficient torque given the available volume for direct drive application.[3] Custom motors optimized for torque production have attained torque to mass ratios of 10 N·m/kg [17], about five times greater than are observed in conventional motors. However, as with the other direct drive electric motors a catch mechanism or servo control is needed to maintain position. The parallel disk geometry is even worse than the tetragonal shape of most motors for making effective use of the hydrofoil volume, they are not commercially available, and are challenging to build due to their magnetically unstable configuration [17]. For these reasons alternative actuator technologies are considered.

2) Emerging Actuator Materials: Recently a number of new actuating materials have emerged that generate sufficient force and energy to make them promising candidates for enabling in situ propeller shape changes [2]. Of these, dielectric elastomers, ferroelectric polymers, and conducting polymers have sufficient work density to fit within the blade dimensions, and appear to offer the necessary degree of position control [2], [8]. Furthermore, unlike electric motors they can work against a constant force without requiring energy input. Finally, the magnitude of the applied potential and the extent of charge transfer can be used to predictably set the stress-strain state of these actuators. Thus these materials are readily controllable (unlike shape memory alloys [2]).

Dielectric elastomers are rubbery materials (silicones and acrylics) which, when used as the dielectric in a capacitor, deform when fields are applied due to the attraction between capacitor electrodes [2], [8]. Relaxor ferroelectric polymers feature polar groups on the polymer backbone which are realigned by applied fields, leading to dimensional changes [2]. Dielectric elastomers and ferroelectric polymers typically require activation potentials on the order of several kilovolts.

Conducting polymer actuators are composed of conjugated polymers that are electronically conductive. Dimensional changes are observed in response to changes to electrochemically induced changes oxidation state [2]. Applied potentials are in the range of 1 to 10 V.

Each of these emerging actuator technologies has significant advantages and challenges associated with it. Both dielectric elastomers and ferroelectric polymers feature high electromagnetic coupling, suggesting that efficient operation is possible. Furthermore they are relatively fast (bandwidths of 10 Hz up to

[3]http://www.futaba-rc.com/servos/futm0029.html For example, the Futaba S3101 micro servo has dimensions of 28 mm × 12.7 mm × 30 mm and a mass of 17 g, and generates a torque of 25 mN·m at 4.8 V or 32 mN·m at 6 V. The volume is twice as large as the maximum available, The torque to volume ratio is 3000 N·m/m^3 and the torque to mass ratio is ~2N·m/kg.

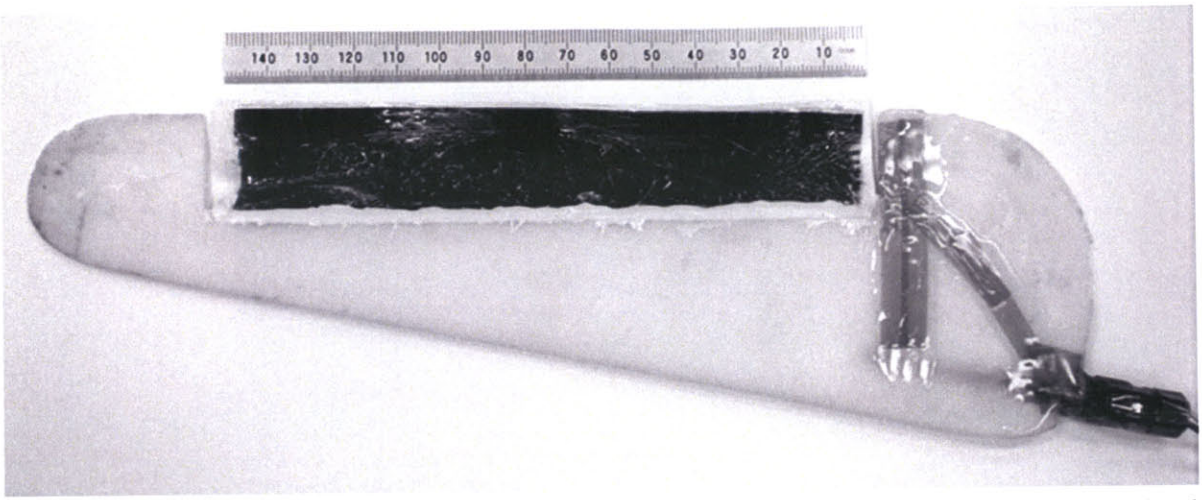

Fig. 3. A 240 mm long foil with trailing edge at top. The black rectangle is a 150 mm long, 30 mm wide active section that bends under applied potential, resulting in a change in foil camber.

tens of kilohertz). Dielectric elastomers have the further advantage of achieving large strains, which can exceed 100%. A technical challenge encountered with dielectric elastomers and ferroelectric polymers is that they require high voltages, whereas only low battery voltages are available in most autonomous underwater vehicles.

The need for high voltages to drive dielectric elastomers and ferroelectric polymers can be resolved by employing compact dc–dc converters (e.g., EMCO high voltage).[4] These would likely be placed in the afterbody, where substantial space is available. High voltages would then be transmitted down the shaft to the propeller. At present the cost of the dc–dc converters and the continuous drain on power are too high to be practical for application in EMATT.

3) Conducting Polymer Actuators: Conducting polymer actuators that employ polypyrrole as the active material feature work densities in the range of 85 to 100 J/m^3 [18], [19], an order of magnitude larger than the minimum required. They also operate at low voltages and feature a catch state in which virtually no current is drawn. These actuators are electrochemical in nature, requiring two electrodes separated by an electrolyte. Application of a voltage between the electrodes, one or both of which are polymer, leads to changes in polymer dimension as charges are added or removed from the polymer and ions are inserted or removed in order to maintain charge balance.

Three principal challenges are encountered in using polypyrrole actuation. The first is that the strains are typically ~2% [2], requiring mechanical amplification, and the second is that lamination of thin films or fibers will be required in order to produce acceptable actuation rates. Finally, although polypyrrole actuators can be run in salt water,[5] the lack of control over the solute concentration and content will likely lead to unreliable performance and a method of encapsulation is required.

4) Mechanical Amplification: Polypyrrole actuators are capable of producing 2% strains at 5 MPa. Since the force needed to deflect the trailing edge flap, divided by the cross-sectional area of the blade and multiplied by the relative moment arms ($3.5\text{N}/(50\text{ mm} \times 6\text{ mm}) \times 7\text{ mm}/3\text{ mm} = 28$ kPa) is much less than the stress that the actuator is capable of generating, no amplification of the force is required. In fact the force per cross-sectional area can be reduced by two orders of magnitude if needed to magnify the displacement.

If the strain multiplied by the length of the actuator is roughly equal to the required displacement required at the tendon attachment point on the trailing edge then little or no amplification of the strain is required, simplifying design and fabrication. The strain required to directly drive the actuator without mechanical amplification is the displacement needed divided by the actuator length. The actuator length is constrained by the 15 mm length of the leading edge (Fig. 2). The displacement is determined by the attachment point to the trailing edge and the angular deflection. Assuming that the attachment point is 3 mm above the joint and that a total angular deflection of at most 22° is needed, then the "ideal" strain is 15%. Clearly there is a need to amplify the 2% strains that are typically observed in polypyrrole actuators.

One possibility is to employ a recently reported method for obtaining 12% strain in polypyrrole [20]. Although this approach is promising, the relatively large creep observed at reduced stresses and the lack of multicycle response data make it risky at present. Two methods of amplification are instead proposed and demonstrated on scaled prototypes.

5) Actuation Rate: In changing camber, a 1 to 10 s response time is sufficiently short for blade optimization during long periods of steady cruising. The actuator material thickness cannot exceed tens of micrometers if the actuator is to respond within ~10 s, due to mass transport limitations, as discussed by P. Madden in this issue [3], [21]. In cases where high forces are required and width of the actuator is restricted, layering or folding

[4]http://www.emcohighvoltage.com/

[5]A polypyrrole actuator was operated by Patrick Anquetil, MIT, using water collected at Revere Beach, MA, for a period of 1 h at a rate of approximately ~0.1 Hz and applied voltage amplitudes of 2 to 3 V versus a stainless steel counter electrode, Significant deposits formed on the polypyrrole, which could lead to degradation in response over longer time periods. Oxidation of the stainless steel also occurred, leading to strong discoloration of the electrolyte.

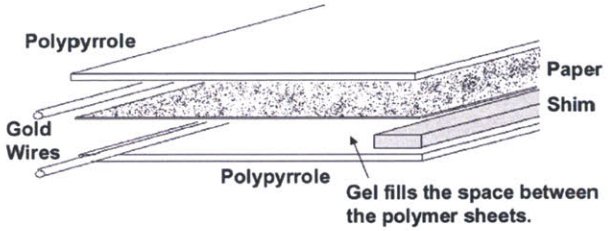

Fig. 4. Layered structure of the active section (not to scale). The 30 μm thick PPy sheets (top and bottom), are separated by a paper spacer. A 350 μm thick mica shim (bottom right) provides spanwise rigidity at the trailing edge, and 75 μm diameter gold wires (left) form electrical contacts. The space between the PPy sheets is filled with gel electrolyte. The total thickness is approximately 120 μm, except at the shim. An encapsulating layer of very thin mylar film covers the entire structure (not shown).

of thin actuator sheets may be necessary so that the force and speed specifications can both be met. Such lamination will be needed in order to meet the force and displacement specifications set out for the EMATT vehicle, as will be discussed, and represents a design and fabrication challenge.

6) Electrical Connections: The polypyrrole actuators employed in this study behave electrically as enormous capacitors and feature a capacitance per unit volume of 10^8 F/m^3. As a result the resistance must also be limited in order to minimize RC charging times [3], [21]. Thus multiple electrical contacts with the polymer and minimal separation between electrodes are essential [19].

IV. Design Approach and Results

Two mechanical amplification methods are used. One is a bending trilayer [22]–[24] which operates like a bimetallic strip. Two thin sheets of polypyrrole are laminated together, separated by a thin layer of gel electrolyte, forming a trilayer structure. Application of a potential difference between them causes one sheet to expand and the other to contract, producing bending. In the second approach linear contraction of the polypyrrole is amplified by two sequential cantilevers to generate the required displacement.

The initial objective is to demonstrate the operation of a variable camber foil in air and in pure water. Geometry and flow conditions are chosen to be consistent with those of the MIT water tunnel. A deformable portion at the trailing edge of the wing is designed to act as an aileron, generating torques consistent with flow rates of up to 1 m/s and a 44° bending angle.

A. Bending Trilayer

The foil geometry, shown in Fig. 3, is approximately NACA 0014 (no camber, thickness is 14% of chord). The span is 240 mm, the average chord length is 70 mm, and the maximum thickness is 34 mm. Camber is varied by deforming a rectangular polypyrrole actuated section that is 150 mm long, 30 mm wide, and ~0.12 mm thick. The actuating section is inserted into a groove in the foil and fixed in place using polyurethane adhesive. In this actuation mechanism, the application of potential between two polymer layers separated by a gel electrolyte causes one to swell and the other to contract, leading to bending. Equations of a bimetallic strip were adapted for a three layer

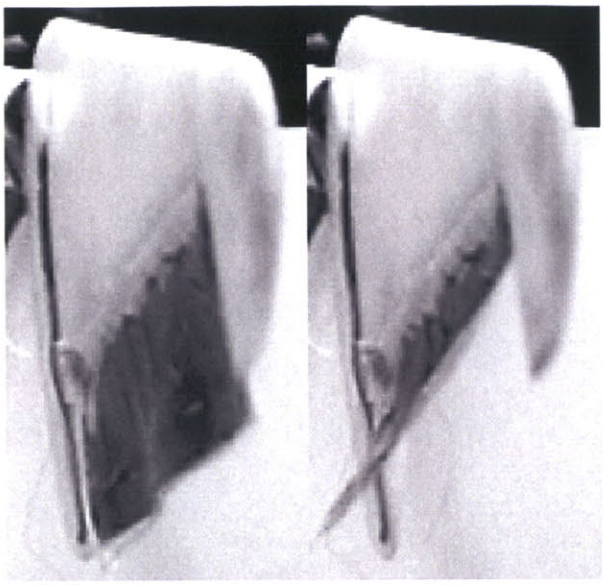

(a) (b)

Fig. 5. Spanwise view of foil (looking from the blade tip), showing the (a) neutral and (b) deflected states during actuation in air.

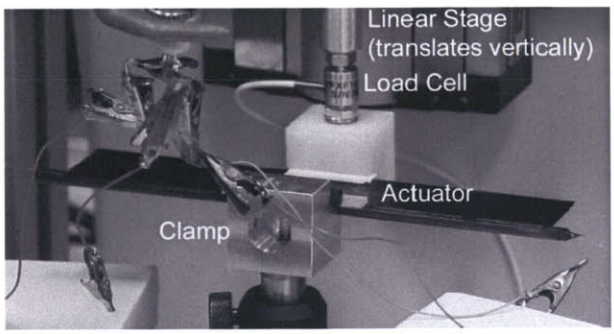

Fig. 6. Force measurement apparatus. The bending actuator (black) is held horizontally and clamped on each of its long sides to prevent motion. Electrical activation produces a vertical force, as measured by a load cell.

structure to determine the layer thicknesses necessary to produce the desired ±22° deflection [25]. The forces required to maintain the deflection given a flow speed of ~1 m/s (for water tunnel testing) were also considered in designing the structure. Calculations based on the flow speed and geometry predict that a force of 0.15 N needs to be maintained on the trailing edge. The actuator is designed to achieve this force.

1) Synthesis and Fabrication: The active portion of the foil consists of five main components as depicted in Fig. 4: two layers of polypyrrole (PPy), a paper separator (Kodak EK1 546 027) which prevents electrical shorting, gold wire providing electrical contact (75 μm diameter), laminated muscovite mica shims which prevent spanwise bending, and gel electrolyte. Construction of the trilayer begins with electro-deposition of 30 μm thick films of hexafluorophosphate-doped PPy onto a glassy carbon crucible following a previously described procedure [26]. Once removed from the glassy carbon, two pieces of PPy are cut to the desired geometry (150 mm × 30 mm). Two 150 mm long, 5 mm wide muscovite mica

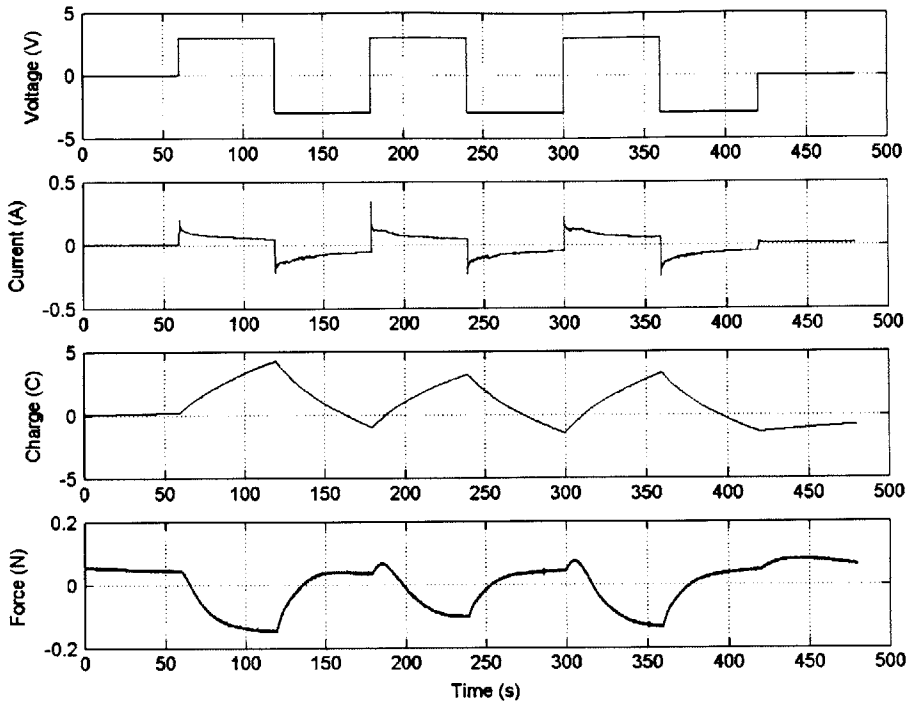

Fig. 7. Force generated at the tip of the laminated actuator in the chordwise direction in response to ±3 V steps. The asymmetries in the force response observed at 180 and 300 s are associated highly oxidized states [29].

shims (~350 μm thick) are laminated together to serve as a mechanical restraint to span-wise bending. These form the trailing edge of the active portion of the foil.

Synthesis of the gel electrolyte is based on a procedure described by Noda and Watanabe [27]. The gel is prepared from a mixture of 10 g (40 mol·%) of 1-butyl-3-methylimidazolium tetrafluoroborate, 8.41 g (58.4 mol·%) of 2-hydroxyethyl methacrylate, 0.175 g (0.8 mol·%) of ethylene glycol dimethacrylate, and 0.8 g (0.145 mol·%) of azobisisobutyronitrile. All ingredients are stirred together. The starting substances are obtained from Sigma-Aldrich.com.

During fabrication, one sheet of PPy is placed on a Teflon surface. Gold wire is placed along one side of the sheet's major axis to provide electrical contact. Next, a sheet of lens paper is laid down. Laminated muscovite mica is placed along the major axis. The electrolyte gel is then spread evenly over the paper and a second gold wire in put down. The second PPy sheet is placed over the sample. A sheet of Teflon is temporarily placed over the entire trilayer and the layers are clamped between two metal plates. The trilayer is placed in an oven and baked at 80 °C for 12 h. Encapsulation is achieved using a 3.5 μm thick polyethylene terephthalate film (www.goodfellow.com) which is folded over the trilayer and sealed with flexible polyurethane (Kalex D-50, www.elementis-specialties.com). A syringe and needle are used to remove excess air as the urethane seal is compressed.

2) Results: Step potentials of ±2.5 V are applied to the polymer actuator in air to actively and reversibly change camber. Fig. 5 depicts the foil with the span almost perpendicular to the camera and the chord oriented vertically and demonstrating a 35° orientation change of the active member (black). The deflection shown is achieved in 4 s.

Force testing is performed by fixing both ends of the active member and applying ±3 V potential steps. A ±2 N range load cell (XFTC-101, www.GSSensors.com) was used to measure forces, in combination with a Vishay 2311 signal conditioning amplifier (www.vishay.com). A photograph of the force measuring apparatus is shown in Fig. 6. The recorded potential, current, and force are plotted in Fig. 7. Generated forces exceed the minimum 0.15 N with the actuator held in the undeflected position. It takes 25 s or more for most of the force change to occur, significantly slower than the 4 s observed in the unloaded films. This slower response results at least in part from the fact that after 4 s the bilayer has not achieved full deflection, whereas the actuation over 25 s is nearly complete, as demonstrated by the saturation in force.

Stiffness is tested by recording force as a function of trailing edge deflection. Fig. 8 shows the force in response to ±1 mm deflections. The deflections are induced via a stepper motor and linear stage (Zeta drive, www.compumotor.com), to which the load cell is attached. The trailing edge deflects by less than 1 mm under a normal force of >0.15 N. This is a very important result, as it indicates that the actuator is capable of withstanding the design forces without significant deflection.

Experimentation in water is at an early stage. Actuation is observed in shallow water. The encapsulation is breached when submerged to depths of greater than ~1 m. This leakage has prevented water tunnel testing.

3) Scaling: Tests to date have been performed on a larger foil to enable characterization in the MIT water tunnel. In order to apply this technology to EMATT forces need to be scaled up from 0.15 to 3.5 N, while angular deflections need to be maintained. Geometrical relationships are used to determine the

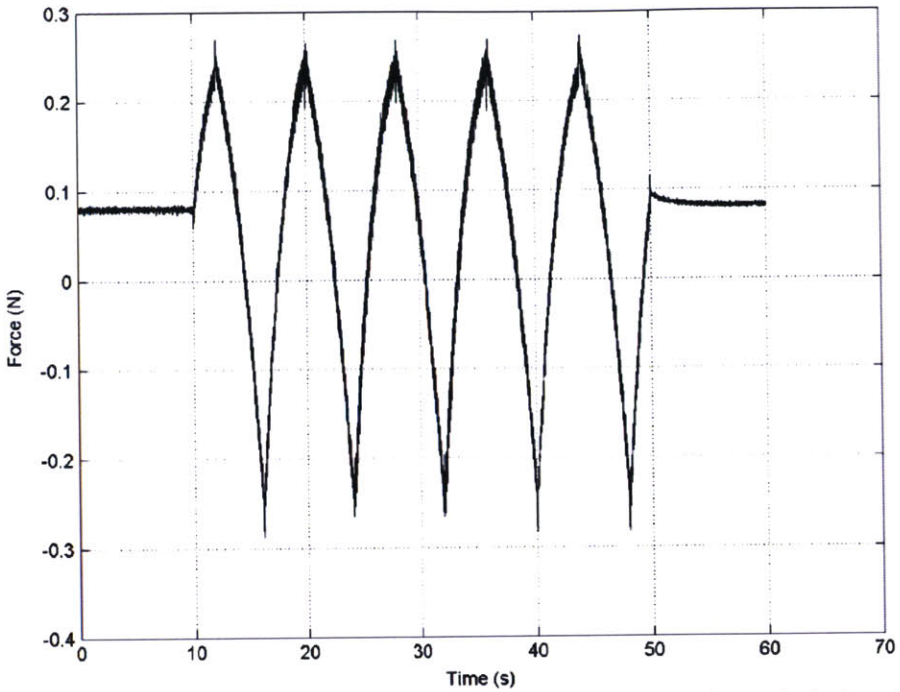

Fig. 8. Stiffness of the variable camber trailing edge. A 1 mm amplitude triangular wave displacement is applied, generating the forces shown.

thicknesses of the polymer layers that will enable the same angular displacements to be achieved in the EMATT propeller as are achieved in the foil geometry shown in Fig. 3.

Two bending structures achieve the same angular deflection if their ratios of segment length to radius of curvature are identical. Therefore the ratio of the curvatures must equal the ratio of segment lengths. The trailing edge segment of the structure in Figs. 3 and 5 is 30 mm long, whereas 10 mm is desired in the final EMATT design. The radius of curvature on the EMATT trailing edge must then be one-third that of the flap demonstrated here. In both bilayer and trilayer actuators, in which displacement is achieved by contracting one layer of a laminated structure relative to the other, the ratio of the total thickness of the structure to the radius of curvature is given by a constant multiplied by the relative difference in strain [25], [28], providing in the trilayer case that the relative thicknesses of the central layer and the outer layers remains constant. These relationships also assume the same relative change in oxidation state is induced in both cases. Thus in order to achieve the same angular displacement in the EMATT propeller as has been achieved in the polymer actuated foil, the trilayer used in the EMATT propeller must be one-third as thick, or approximately 40 μm total. The two polypyrrole layers, which are 30 μm thick in the experiments presented here, must now be 10 μm thick, and the gel layer that was previously 60 μm thick is now reduced to 20 μm.

The ratio of forces F_2/F_1 is determined using the relationship [25], [28]

$$\frac{F_2}{F_1} = \frac{W_2 \cdot t_2^2}{W_1 \cdot t_1^2} \cdot \frac{L_1}{L_2} \tag{1}$$

where W represents trilayer width (spanwise), t represents thickness, and L is the length (chordwise). Once again (1) is only valid if the two trilayers have the same ratios of polymer to gel thicknesses, and consist of the same materials. The ratio of forces is known (3.5 N/0.15 N), as are the lengths ($L_1 = 30$ mm, $L_2 = 10$ mm) and thicknesses (from the geometrical arguments above, $t_2/t_1 = 1/3$). The width W_1 is 150 mm, enabling W_2 to be evaluated. The resulting width W_2 is 2.1 m. The actual width W_2 is 50 mm at best, or 42 times shorter. This deficiency can be rectified by creating 42 layers, with a minimum total thickness of 1.7 mm.

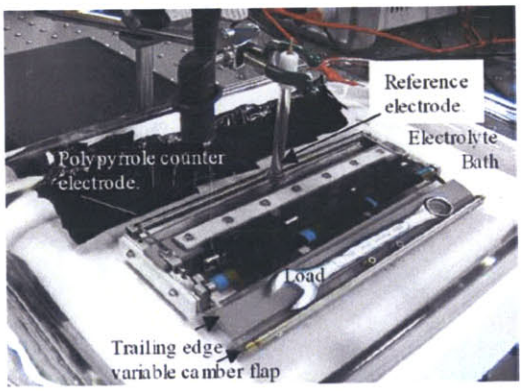

Fig. 9. The linear actuator test cell, showing the 1.2 l 0.05 M tetraethylammonium hexafluorophosphate in propylene carbonate filled bath. The trailing edge is at the bottom. The three black strips are each 38 mm wide, 70 mm long, and 46 μm thick polypyrrole films. These are held at one end by a nylon plate, wrapped around the blue roller, and are fixed on the bottom surface of the structure. The actuators contract, tensioning lines that in turn deflect the trailing edge in a direction in and out of the page (see Fig. 10).The polypyrrole counter electrode, the reference electrode, and a load applied to the trailing edge are also shown.

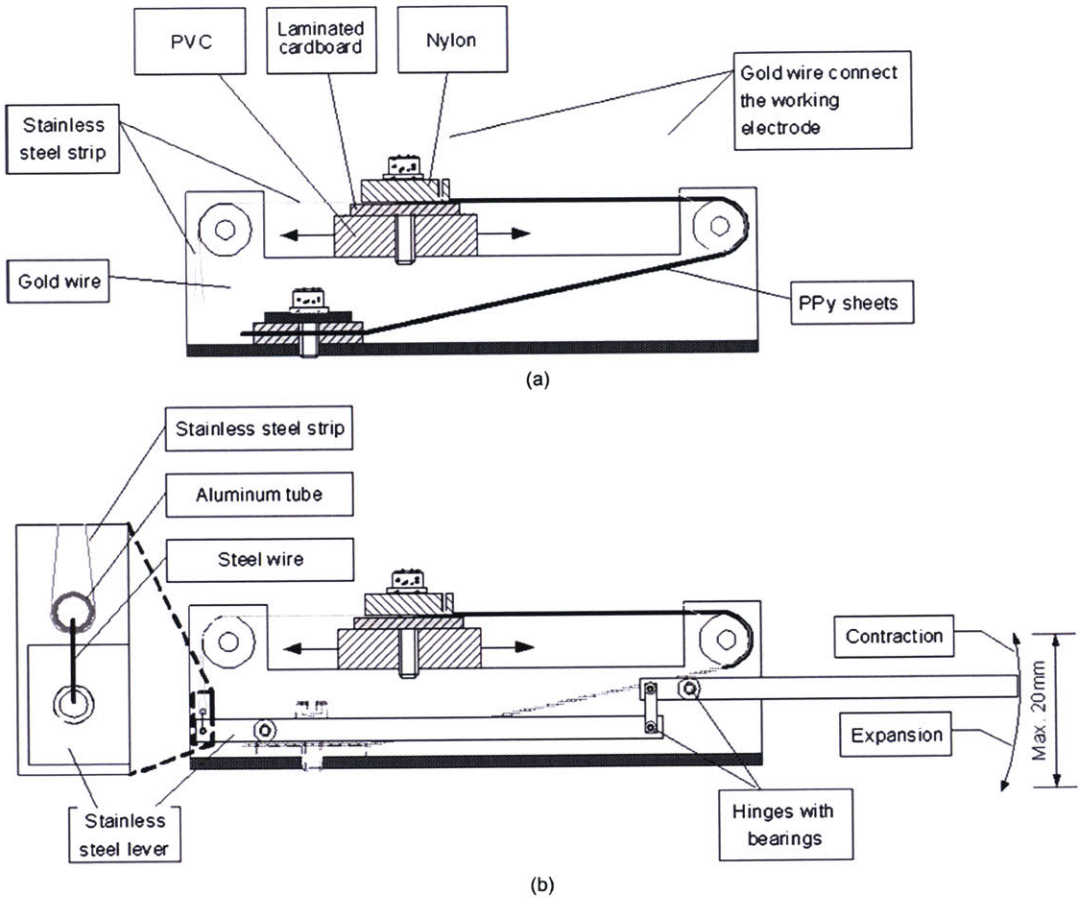

Fig. 10. Side view diagram of the linear actuator driven foil. The top diagram shows how polypyrrole sheets (black in Fig. 9) are fixed to the base at one end. From the base, the strips cross diagonally up to a cylinder (blue in Fig. 9) that rolls on two bearings (at either end). The strips are then clamped to a moveable truck. Two thin stainless steel ribbons (50 μm thick, 2 mm wide) extend from the far side of the trucks, one on each side of the device, and are wound around another roller (left side in this figure, top cylinder in Fig. 9). The ribbons are each attached to a beam. As polypyrrole contracts, the left ends of the beams are pulled upwards, rotating them about their bearings. The far ends of the beams displace downwards, with 5× greater displacement than the left ends, due to the placements of the bearings. The beams each pull a second cantilever, which again has a 5× amplification factor, with the result that the right hand tip of the second cantilever deflects upwards by 25× the initial displacement of the polymer. The cantilevers in Fig. 8 move out of the page. Gold wires make electrical connections to the polypyrrole films.

The results suggest that stacking 42 trilayers will generate 42× more force. However, the stacking is not trivial because adjacent trilayers must not mechanically interfere with one another. The calculations demonstrate that trilayer actuation is possible, but the practical challenge of stacking such a large number of actuators without interference led to the creation of a linear actuator design, in which cantilevers are used to amplify small displacements generated by linear actuators.

V. Linear Actuator

An advantage of employing a linear actuator, as opposed to the bending trilayer, is that the linear actuator may sit within the rigid portion of the blade, or even on the shaft, providing larger volume and thereby enabling larger forces to be contemplated for a given deflection. The primary drawback of a linear approach is that it requires a mechanical amplification mechanism, adding complexity to the design. Also, unlike the trilayer approach, the actuator only generates work when operating in tension (otherwise it buckles). Where two-way actuation is desired, twice the volume of polymer is required, as compared with trilayers, in which actuation can occur both in expansion and compression.

The same angular displacement and force is sought with the linear actuator as is obtained with the trilayer.

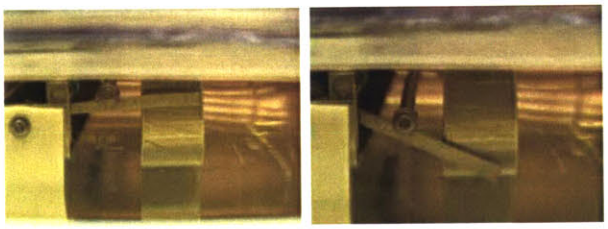

Fig. 11. Deflection of the linear actuator driven trailing edge by >30°. The deflection takes place in electrolyte, and only the trailing edge segment is shown. A graduated plate is used for assisting in angle measurement.

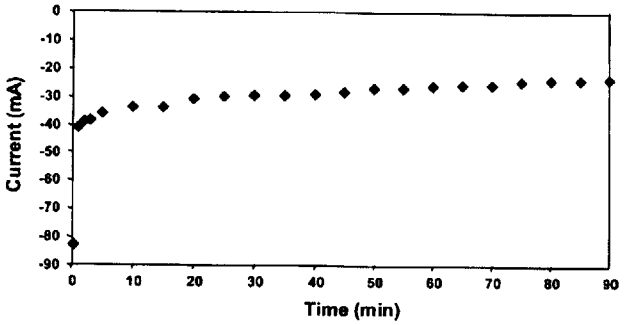

Fig. 12. Current induced by the application of a step input of −3.5 V to the linear actuator. The current is accompanied by contraction of the polypyrrole and lifting of a 0.65 N weight.

A. Design

Two cantilevers placed in series produce a 25× amplification of the displacement of polypyrrole linear actuators. The apparatus is shown in Fig. 9 and its operation is described in Fig. 10. The geometry is designed to match that of the trilayer actuated configuration, with the 150 mm between cantilevers, and the 30 mm protruding length (bottom of Fig. 9) matching the dimensions of the trilayer flap in Fig. 3. Polypyrrole actuation is achieved by placing the entire apparatus into an organic solvent salt bath and applying potential between the polypyrrole films and a counter electrode. (In the final version, the electrolyte and counter electrode will be encapsulated within the foil structure.) Synthesis of the polymer films follows the procedure described above. A potentiostat is employed in order to set an applied voltage [29]. Load is varied by applying weights to the cantilevers (e.g., the wrench shown in Fig. 9). The force exerted on the foil is calculated based on the applied mass and the buoyancy of the electrolyte. Displacements are recorded by video camera, and currents and voltages are recorded via an analog to digital converter.

1) Results: Fig. 11 depicts the extent of deflection obtained by driving the mechanism using a voltage range of 3.5 V. A 33° displacement occurred in 12 min under a load of 0.65 N. Stresses produced by the polypyrrole actuator are estimated to reach 7 MPa, and strains are just over 1%, based on observed changes in position of the trailing edge. The work density achieved is 70 MJ/m^3. Initial currents observed upon the application of a step change in potential reach ~80 mA, and drop to <30 mA within 15 minutes, as shown in Fig. 12. Substantial parasitic current is observed, and is likely due to parasitic reactions at the surface of the steel frame (which can be eliminated by coating or encapsulation).

2) Rate: The 12 min time to vary camber is much too slow to be practical. What limits the actuation rate and what are the opportunities for substantially reducing the actuation time? The initial current shown in Fig. 12 suggests that series resistance of the cell is 40 Ω. Given the capacitance of conducting polymers, which can reach 10^8 F/m^3, and the available volume, the effective capacitance of the actuator film is 13 Farads. The RC time constant is calculated to be 500 s, or nearly 10 min, explaining the slow response. The rate will need to be improved by two orders of magnitude to make this approach feasible.

3) Scaling: In order to apply this technology to the EMATT, forces need to be scaled up from 0.65 to 3.5 N while maintaining angular deflections. Furthermore the dimensions of the foil need to be reduced from 150 mm long in the active region and 70 mm wide, to 50 mm long and a total blade chord of 35 mm.

Desired displacements and strains can readily be scaled by reducing the size of the mechanism while maintaining mechanical advantage. The force can be increased by using more cross-sectional area of polymer. At present the cross-sectional area of polymer employed is 5×10^{-6} m^2. This will need to increase by a factor of 5.4 in order to produce 3.5 N, corresponding to a cross-sectional area of 27×10^{-6} m^2. The available width is reduced from 150 to 50 mm, and thus the total polymer thickness must be 540 μm. This thickness corresponds to approximately 12 layers of polymer assuming actuator films are 43 μm thick. Thus the burden of mechanical amplification, in terms of needed layers of polypyrrole film, is not as severe as it is in the trilayer design.

Achieving the necessary improvement in rate is a real challenge in the linear actuator design. Scaling to the EMATT blade specifications will result in a need for more than double the volume of polymer, resulting in a corresponding increase in capacitance, and necessitating an overall reduction in cell resistance of more than 100×, to less than 0.4 Ω. Achieving this reduction in resistance can be achieved by interleaving the 12 layers with polymer counter electrodes, thereby minimizing the solution resistance. The current required to achieve fast actuation will also be correspondingly higher.

4) Cycle Life: Cycle life has not been addressed. Close to a million cycles are possible [30] using appropriate electrolytes similar to those used in this experiment.

VI. Discussion

Polypyrrole actuators are employed to generate variable camber foils. These foils achieve the appropriate range of deflection, but forces are as yet too small for the desired application. In order to increase force, parallel actuating films will be required, in which the placement of the counter electrodes must be carefully considered so that specified rates can be achieved. Encapsulation will also need to be improved. Given the increased forces in the final prototype tougher coatings can be used, increasing the chances of success.

References

[1] "Smart structure and materials 2003, electroactive polymer actuators and devices," in *Proc. SPIE*, vol. 5051, Y. Bar-Cohen, Ed., 2003.

[2] J. D. Madden, N. Vandesteeg, P. A. Anquetil, P. G. Madden, A. Takshi, R. R. Pytel, S. R. Lafontaine, P. A. Wieringa, and I. W. Hunter, "Artificial muscle technology: Physical principles and naval prospects," *IEEE J. Oceanic Eng.*, vol. 29, pp. 706–728, July 2004.

[3] P. G. Madden, J. D. Madden, P. A. Anquetil, N. A. Vandesteeg, and I. W. Hunter, "The relationship between conducting polymer actuator material properties and performance," *IEEE J. Oceanic Eng.*, vol. 29, pp. 696–705, July 2004.

[4] J. Hollerbach, I. Hunter, and J. Ballantyne, "A comparative analysis of actuator technologies for robotics," in *The Robotics Review 2*, O. Khatib, J. Craig, and T. Lozano-Perez, Eds. Cambridge, MA: MIT Press, 1992, pp. 299–342.

[5] I. Hunter and S. Lafontaine, "A comparison of muscle with artificial actuators," in *Tech. Dig. IEEE Solid State Sensors & Actuators Workshop*, 1992, pp. 178–185.

[6] M. S. Triantafyllou, A. H. Techet, and F. S. Hover, "Review of experimental work in biomimetic foils," *IEEE J. Oceanic Eng.*, vol. 29, pp. 585–594, July 2004.
[7] G. S. Triantafyllou, M. S. Triantafyllou, and M. A. Grosenbaugh, "Optimal thrust development in oscillating foils with application to fish propulsion," *J. Fluids Structures*, vol. 7, no. 2, pp. 205–224, 1993.
[8] J. D. Madden, "Actuator selection," in *Proc. SPIE Smart Structures and Materials: Electroactive Polymer Actuators and Devices*, Y. Bar-Cohen, Ed., Bellingham, WA, 2004, to be published.
[9] F. W. Riegels, *Aerofoil Sections*. London, U.K.: Butterworths, 1961.
[10] K. Brownlie, *Controllable Pitch Propellers*. London, U.K.: Witherbys, 1998.
[11] B. Allen, W. S. Vorus, and T. Prestero, "Propulsion system performance enhancements on REMUS AUVs," in *Proc. MTS/IEEE Oceans 2000*, 2000.
[12] I. H. Abbott and A. E. von Doenhoff, *Theory of Wing Sections*. New York: Dover, 1959.
[13] Sippican, BAE Systems, private communication, 2003.
[14] P. R. Bandyopadhyay, "A biomimetic propulsion for active noise control: Experiments, NUWC-NPT," Naval Undersea Warfare Center, Tech. Rep. 11 351, Mar. 2002.
[15] D. Reynaerts, W. Van Moorleghem, and H. Van Brussel, "Design and construction of a stepping shape memory actuator for driving a variable camber aircraft wing," in *Proc. 10th IEEE Conf. Advanced Robotics*, 2001.
[16] C. H. Beauchamp, R. H Nadolink, S. C. Dickinson, and L. M. Dean, "Shape memory alloy adjustable camber (SMAAC) control surfaces," in *Eur. Conf. Smart Structures and Materials*, 1992, p. 189.
[17] J. M. Hollerbach, J. Lang, E. Vaaler, I. Garabieta, R. Sepe, S. Umans, and I. W. Hunter, "The McGill/MIT direct drive motor project," in *Proc. IEEE Int. Conf. Robotics and Automation*, vol. 2, Atlanta, GA, May 2–7, 1993, pp. 611–617.
[18] G. M. Spinks, D. Z. Zhou, L. Liu, and G. G. Wallace, "The amounts per cycle of polypyrrole electromechanical actuators," *Smart Mater. Structures*, vol. 12, no. 3, pp. 468–472, 2003.
[19] J. D. Madden, P. G. Madden, and I. W. Hunter, "Conducting polymer actuators as engineering materials," in *Proc. SPIE Smart Structures and Materials 2002: Electroactive Polymer Actuators and Devices*, Y. Bar-Cohen, Ed., Bellingham, WA, 2002, pp. 176–190.
[20] L. Bay, K. West, P. Sommer-Larsen, S. Skaarup, and M. Benslimane, "A conducting polymer artificial muscle with 12% linear strain," *Adv. Mater.*, vol. 15, pp. 310–313, 2003.
[21] J. D. Madden, P. G. Madden, and I. W. Hunter, "Characterization of polypyrrole actuators: Modeling and performance," in *Proc. SPIE 8th Annu. Symp. Smart Structures and Materials: Electroactive Polymer Actuators and Devices*, Y. Bar-Cohen, Ed., Bellingham, WA, 2001, pp. 72–83.
[22] T. F. Otero, J. Rodriguez, E. Angulo, and C. Santamaria, "Artificial muscles from bilayer structures," *Synth. Metals*, vol. 55–57, pp. 3713–3717, 1993.
[23] Q. Pei and O. Inganas, "Electrochemical application of bending beam method," *J. Phys. Chem.*, vol. 96, no. 25, pp. 10507–10 514, 1992.
[24] D. Z. Zhou, G. M. Spinks, G. G. Wallace, C. Tiyapiboonchaiya, D. R. MacFarlane, M. Forsyth, and J. Z. Sun, "Solid state actuators based on polypyrrole and polymer-in-ionic liquid electrolytes," *Electrochimica Acta*, vol. 48, no. 14–16, pp. 2355–2359, 2003.
[25] P. G. Madden, "Development and modeling of conducting polymer actuators," Ph.D. disseration, MIT Mechanical Engineering Dept., Cambridge, MA, 2003.
[26] M. Yamaura, T. Hagiwara, and K. Iwata, "Enhancement of electrical conductivity of polypyrrole film by stretching: Counter ion effect," *Synth. Metals*, vol. 26, pp. 209–224, 1988.
[27] A. Noda and M. Watanabe, "Highly conductive polymer electrolytes prepared by *in situ* polymerization of vinyl monomers in room temperature motten salts," *Electrochimica Acta*, vol. 45, pp. 1265–1270, 2000.
[28] J. D. Madden and C. J. Brenan. (1997, Nov.) Progress toward an automatic microfabricated polymer air-fluid sampling inlet. U.S. Department of Defense, National Technical Information Service Order AD-A332 030/6. [Online]. Available: www.ntis.gov
[29] J. D. Madden, R. A. Cush, T. S Kanigan, and I. W. Hunter, "Fast contracting polypyrrole actuators," *Synth. Metals*, vol. 113, pp. 185–193, May 2000.
[30] W. Lu, A. G. Fadeev, B. H. Qi, E. Smela, B. R. Mattes, J. Ding, G. M. Spinks, J. Mazurkiewicz, D. Z. Zhou, G. G. Wallace, D. R. MacFarlane, S. A. Forsyth, and M. Forsyth, "Use of ionic liquids for pi-conjugated polymer electrochemical devices," *Science*, vol. 297, no. 5583, pp. 983–987, 2002.

John D. W. Madden (M'95) was born in Ottawa, ON, Canada in 1968. He received the B.Sc. degree in physics from the University of British Columbia (UBC), Vancouver, BC, Canada, in 1991, the M.Eng. degree in biomedical engineering from McGill University, Montreal, PQ, Canada, in 1995, and the Ph.D. degree from the BioInstrumentation Laboratory, Massachusetts Institute of Technology, Cambridge, in 2000.

He joined UBC in 2002 and is currently an Assistant Professor of electrical and computer engineering. His research involves fundamental studies and applications of polymer and nanotube actuators and electronic devices.

Bryan Schmid was born in Buffalo, NY, in 1981. He received the B.Sc. degree in mechanical engineering from the Massachusetts Institute of Technology, Cambridge, in 2003, where he is currently pursuing the M.Sc. degree.

He has performed research for Molecular Mechanisms, LLC. His current studies pertain to the Army's Institute of Soldier Nanotechnologies (ISN), Cambridge. His research interests include mechanical design and conducting polymer technologies.

Mr. Schmid is a member of Pi Tau Sigma. He received the Padmakar P. Lee Student Award and was a representative of the United States for the International Design Competition in 2002.

Martin Hechinger was born in Herbolzheim, Germany in 1977. He is working toward the Dipl. Ing. (FH) degree in electrical engineering at the Offenburg University of Applied Sciences, Offenburg, Germany.

He was an Electronics Installer with Energy BW AG from 1994 to 1999 and then for EHT Werkzeugmaschinen GmbH from 2000 until 2001. He performed research for Molecular Mechanisms, LLC, during an internship at the University of British Columbia (UBC), Vancouver, Canada, in 2003. He developed a low-noise measurement system for organic transistor characterization at UBC as his thesis project.

Serge R. Lafontaine received the B.Sc. degree in physics from the University of Montreal, Montreal, PQ, Canada, and the Ph.D. degree from the Department of Biomedical Engineering, McGill University, Montreal.

He is a scientific consultant whose interest is the development of medical and biomedical instrumentation. He spent two years as Postdoctoral Fellow at the BioInstrumentation Laboratory in mechanical engineering at the Massachusetts Institute of Technology. His main research interests include sensors and actuators including conducting polymers and shape memory alloys, data acquisition and control mainly applied to the development of new devices for the characterization of materials and systems, optics, electronics, and software algorithms. He has developed a wide-field optical imaging system for the quantitative detection of fluorescence in high-throughput massively parallel drug discovery, genetic engineering and diagnostic system and a fully digital imaging and beam control system of an electron microscope. He has participated in the creation of several new businesses including Biotrove, Inc., and LifeFX Technologies, Inc. As Chief Technology Officer of LifeFX, Inc., he led the research and development of the company's software products. His interest in the future will remain in the startup of new companies and development of commercial products.

Peter G. A. Madden was born in Ottawa, ON, Canada, in 1971. He received the B.A.Sc. degree in engineering physics from the University of British Columbia (UBC), Vancouver, BC, Canada, in 1993, the M.Eng. degree in biomedical engineering from McGill University, Montreal, PQ, Canada, in 1996, and the Ph.D. degree in mechanical engineering from the Massachusetts Institute of Technology, Cambridge, in 2003.

He is currently a Postdoctoral Associate in the Department of Organismic and Evolutionary Biology, Harvard University, Cambridge, MA. His current research is in the area of fish pectoral fin propulsion and maneuvering.

Franz S. Hover (A'93) received the B.S. degree in mechanical engineering from Ohio Northern University, Ada, in 1987 and the S.M. and Sc.D. degrees in oceanographic and mechanical engineering from the Woods Hole Oceanographic Institution/Massachusetts Institute of Technology (MIT), Cambridge, in 1989 and 1993, respectively.

He was a Postdoctoral Fellow with the Monterey Bay Aquarium Research Institute. He has been a regular consultant to industry. He is currently a Principal Research Engineer in the Department of Ocean Engineering, MIT. His areas of research interest include design and applied control of marine systems.

Dr. Hover is a member of the American Society of Mechanical Engineers.

Richard Kimball, photograph and biography not available at the time of publication.

Ian W. Hunter was born in New Zealand in 1953. He received the B.Sc., M.Sc., D.C.P., and Ph.D. degrees in science from the University of Auckland, Auckland, New Zealand in 1974, 1975, 1976, and 1980, respectively.

He was with McGill University, Montreal, PQ, Canada, from 1980 to 1994. He then joined the Faculty of the Massachusetts Institute of Technology, Cambridge, where he presently is the Hatsopoulos Professor of Mechanical Engineering, a Professor of biological engineering, and Head of the BioInstrumentation Lab. His current research interests are microinstrumentation, microfabrication, microrobotics, microsurgical robotics, artificial muscle fibers, laser imaging systems, and instrumentation physics.

Chapter 3

Mechanical Enhancements of Conducting Polymers

The reprinted journal article in Chapter 2 reveals shortcomings in the trimorph's capability to achieve high forces and the linear actuator's ability to undergo large strains and strain rates. The subsequent Sections will address these shortcomings with enhancements to the polymer actuator.

3.1 Introduction

The potential for conducting polymer actuators as a linear motion solution would increase tremendously with advancements in achievable strain and strain rates. Conducting polymers currently exhibit 2 to 4% repeatable strain [1,2] under normal actuation conditions of ± 1.5 V and strain rates of 3%/s under increased potential actuation conditions. In the absence of new conducting polymers capable of achieving both large active strains and stresses, mechanical enhancements to existing polymer films must be investigated. Investigating possible mechanical enhancements to the conducting polymer film provides a tool box for device design employing conducting polymer actuators. The following Sections describe two different methods of enhancing the active displacement properties of conducting polymers for bending and linear actuation.

3.2 Trimorph Bending Actuator

A trimorph configuration, representing one of the mechanically enhanced embodiments, creates a mechanical advantage through the juxtaposition of multiple films (active or passive) to enhance small active polymer strains into bending displacements as pictured in Figure 3-1. The trimorph is composed of two conducting polymer films that

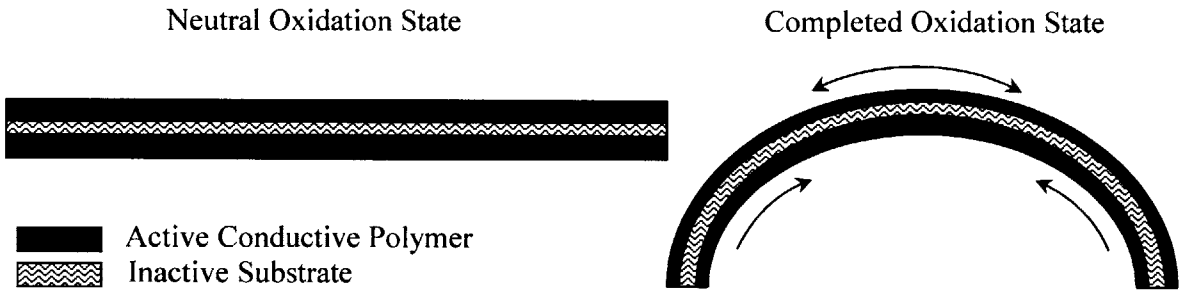

Figure 3-1: Schematic structure of a trimorph and its actuation

sandwich an electrically inert and inactive substrate. The inactive substrate is comprised of an ionically conducting gel as an electrolyte source for the opposing conducting polymer films during actuation [2]. The union of the polymer films and electrolyte gel encompass an elegant device package that does not require additional electrodes or electrolyte sources for actuation. Rather each polymer film acts as the opposing working and reference electrode during oxidation and reduction as the polymer gleans ions from the electrolyte gel.

Bending displacements are achieved in a manner analogous to the bending displacement in a bimetallic strip used for temperature measurements in some thermostats. Rather than a thermal expansion, conducting polymer films undergo an active expansion (contraction) during electrochemical oxidation (reduction) as ions diffuse in and out of the polymer. The active linear polymer displacement is then mechanically enhanced into a large bending deformation due to the constraints from the adhesion of the two dissimilar films. [3-6]. Assuming that the polymer actuation occurs due to a linear ion diffusion into the polymer film as a function of charge [7], the trimorph's force and curvature can be modeled.

The trimorph Equations of motion [8,9] model the curvature (3.1) and force (3.2) as a function of the charge density ratio

$$\frac{K}{\Delta\rho} = \frac{3\alpha}{2h_g}\left[\frac{(1+\gamma)^2 - 1}{(1+\gamma)^3 + \left(\frac{1}{e} - 1\right)}\right], \tag{3.1}$$

$$\frac{F}{\Delta\rho} = \frac{E_p \alpha}{L} W h_g^2 \left[(1+\gamma)^2 - 1\right], \tag{3.2}$$

where K is the trimorph curvature, F is the force, $\Delta\rho$ is the charge per unit volume in the polymer, α is the polymer's strain to charge coefficient, $2\ h_g$ is the inactive layer thickness, $\gamma = \frac{h_p}{h_g}$ is the ratio of the polymer thickness to the ½ thickness of the inactive substrate and $e = \frac{E_p}{E_g}$ is the respective ratio of the polymer's elastic modulus to the substrate's elastic modulus, W is the width of the trimorph (into the page in Figure 3-1), and L is the trimorph's length.

The trimorph schematic in Figure 3-1 and Equations of motion provide a visual and analytical picture of the operating principles behind a trimorph and its mechanical enhancements. As previously mentioned, the mechanical advantage resulting in a large bending displacement comes at the cost of high forces. To address the loss of large active stresses in trimorphs, a stacked trimorph configuration is investigated as a method of increasing the active tip force in a trimorph.

3.2.1 Trimorph Stacking

The concept of stacking trimorphs entails the placement of multiple trimorphs on top of one another to enhance the bending tip force [3,4,8]. An interesting phenomenon of stacked trimorphs is that the amplification of force is not linearly proportional to the

number of trimorphs stacked in series. Rather the force decreases exponentially due to mechanical impedance between films. The following research addresses a technique to reduce the mechanical impedance within trimorph actuators. The construction of trimorphs, incorporation of a slip surface into a stacked actuator device, and experimental results are presented in this Section.

The construction of each modular trimorph begins by electrochemically depositing 0.05 M tertraethylammonium hexafluorophosphate, 0.05 M distilled pyrrole, and 1% volume distilled H_2O onto a glassy carbon crucible. Films are galvanostatically grown at 0.8 A/m^2 at - 40 °C for approximately 14 hours to achieve an approximate thickness of 25 to 30 μm. The PPy films are then removed from the crucible with a razor blade and cut to size for the trimorph construction.

Table 3.1: Gel Electrolyte Synthesis Ingredients

	Mol%	**Mass (g)**
1-Butyl-3-methylimidazolium tetrafluoroborate (226.03 g/mol)	40	10.0
2-Hydroxyethyl methacrylate (130.14 g.mol)	58.4	8.41
Ethylene glycol dimethacrylate (198.22 g/mol)	0.8	0.175
Azobisisobutyronitrile (164.21 g/mol)	0.8	0.145
Note: Cross-linking of the acrylate occurs after mixing and heating at 80 °C for 12 hours.		

For the next step in trimorph fabrication, one sheet of PPy is placed on a Teflon surface. Next, a sheet of Kodak lens paper is laid down on top of the PPy film. The electrolyte gel [9,10], described in Table 3.1, is then poured evenly over the lens paper. A second PPy sheet is placed over the entire sample. A sheet of Teflon is then placed over the entire trimorph and clamped between two metal plates. The trimorph is then placed in an oven and heated to 80 °C for 12 hours to complete its construction.

For characterization of the constructed trimorph actuators, a custom electrochemical dynamic mechanical analyzer (ECDMA) was constructed by Peter Madden as pictured in Figure 3-2. The ECDMA recorded the electrochemical input to the trimorph and the corresponding tip force into a MATLAB file for analysis.

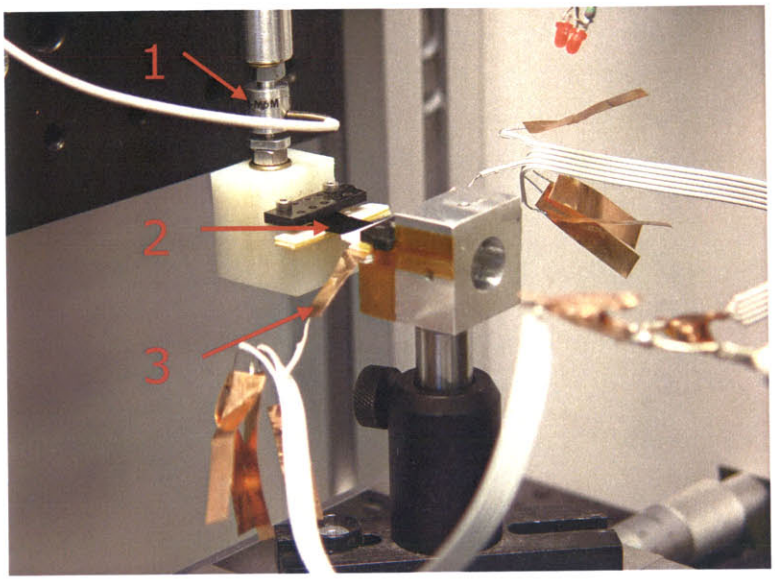

Figure 3-2: The trimorph ECDMA setup. 1) Load cell for tip force measurements. 2) Stacked trimorphs. 3) Electrical contacts from potentiostat.

For characterizing the stacked setup, a constant geometry was established for continuity across the trimorph films. Each trimorph comprising the stacked setup measures 12 mm wide by 25 mm long and averaged 120 μm in thickness. Trimorphs were then stacked and characterized as each trimorph was added until a stacking of four trimorphs was achieved.

During stacking great care was taken to avoid mechanical impedance from stiction between trimorph layers as noted by Madden [8]. In between each trimorph, a piece of 9 μm thick condenser paper was inserted as a slip surface. The careful addition of a slip surface proves to be a simple solution that adequately corrects for the interference

between trimorphs as shown in Section 3.1.2. When using the condenser paper, mechanical impedance is further addressed by the method of clamping. Only the end of the stacked trimorph device receiving electrical contact was rigidly constrained. The opposing end was loosely constrained at the load cell to allow for the trimorphs to slip past one another during actuation. Although the loose constraint helps improve tip force measurements, the following tip force results are inaccurate when the trimorph stack is near zero curvature and not providing a coupled tension or compression on the load cell.

3.2.2 Trimorph Stacking Results

An electrical stimulus of ± 1.5 V from the trimorph open circuit potential was applied to each trimorph during experimentation. When actuated, each trimorph exerted an individual tip force of approximately 5 mN. In Figure 3-3, the tip force is plotted against time as a square wave potential of ± 1.5 V per trimorph is input to the trimorph device. Results from Figure 3-3 are representative of repeated experimentation which showed a

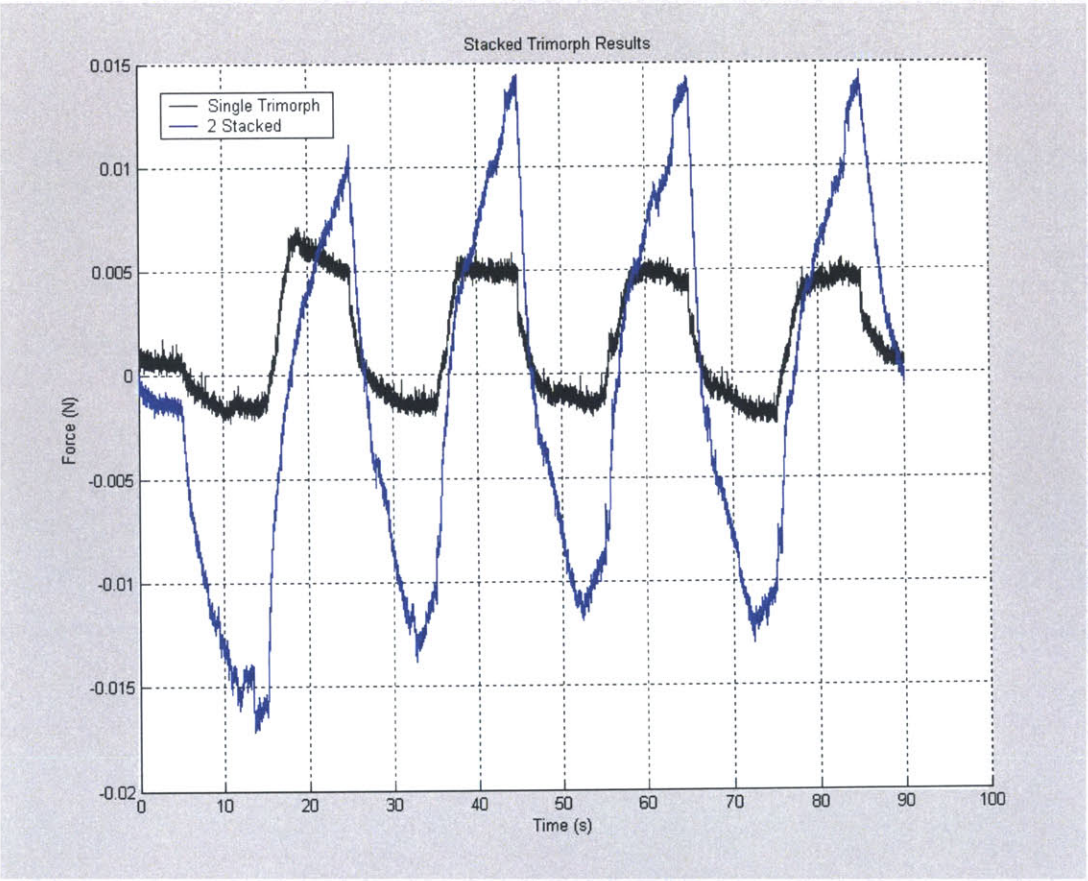

Figure 3-3: Tip force of a single and two stack trimorph device driven by ± 1.5 V per trimorph.

drastic increase in trimorph tip force with two stacked trimorphs. It is intriguing to note that the effective tip force for the stacked configuration of two trimophs increased the

force by approximately 350%. Whereas the stacked trimorph experiments without the slip surface failed to produce tip forces greater than the individual sum of all trimorph forces in the stack. Intuitively, the expected force from two stacked trilayers would not exceed twice the tip force of a single trilayer. However, repeated experiments demonstrated a tip force of more than twice the combined individual tip force from each trimorph with the condenser paper slip surface. One possible explanation assumes that the trimorph applying the coupled pressure to the second trimorph reduces the elastic modulus impedance of the second trimorph. Equation 3.1 shows a relationship between the achievable curvature of a trimorph and its young's modulus. If all other variables remain constant and the elastic modulus, e, is decreased, the active curvature increases exponentially. The tip force derivation, which is based upon a summation of the torques generated by the trimorph. [3,4,8,9], is therefore also effected by a reduction in the effective Young's modulus. A decrease in the effective elastic modulus increases the achievable curvature exponentially. If the effective elastic modulus reduction in the stacked trimorph configuration is less than the sum of the individual trimorphs, a tip force greater than twice the individual trimorph tip forces can be achieved.

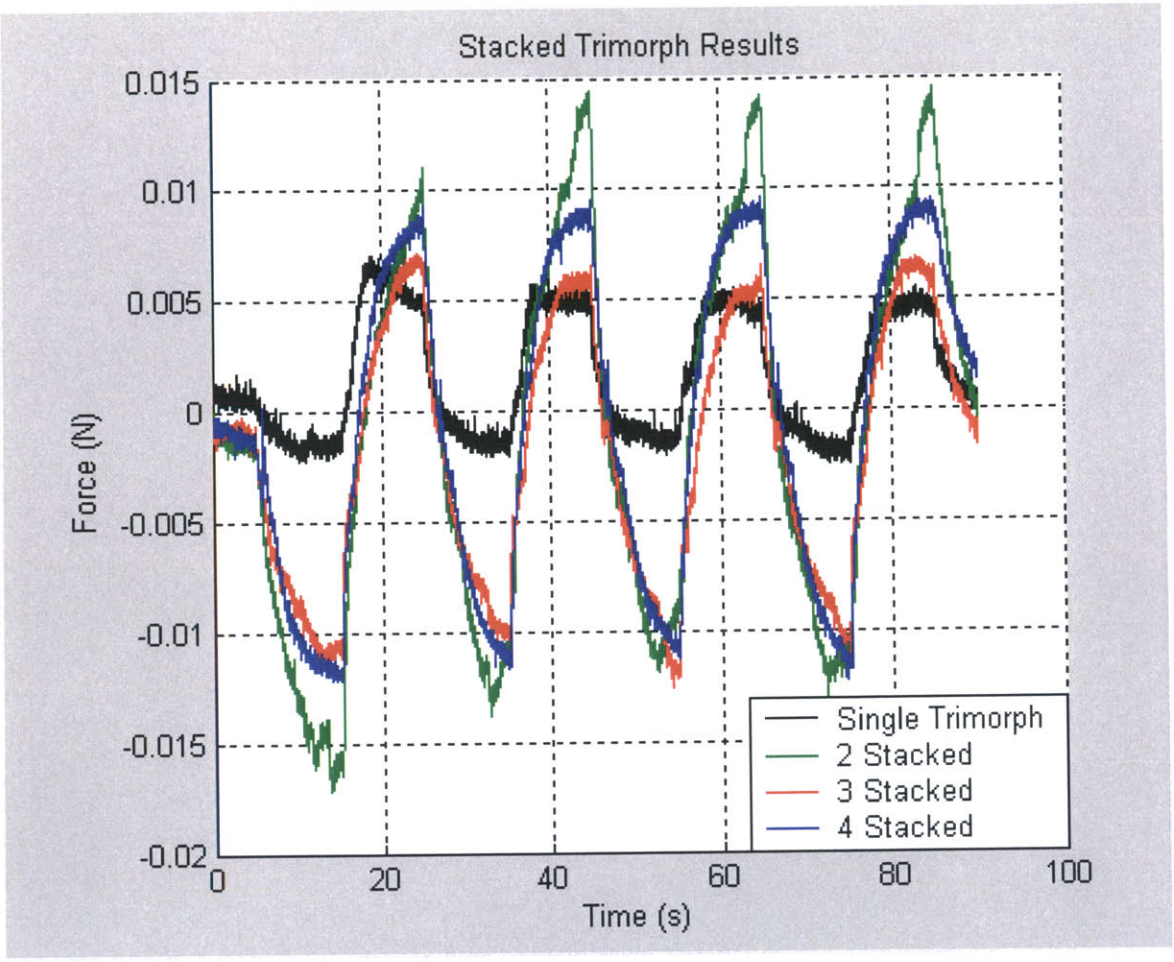

Figure 3-4: Tip force of one to four trimorph stacks driven by ± 1.5 V per trimorph.

In Figure 2-4, the number stacking layers in the configuration increases from one to four. As the stacked device increases in layers, the condenser paper's ability to mitigate mechanical impedance from stiction decreases. Upon reaching a stack of four trilayers, the effective tip force multiplication factor becomes minimal yet is still superior to the stacking of four trimorphs without slip surfaces.

3.3 *Mechanically Enhanced Linear Conducting Polymer*

The second mechanical enhancement explored aims to improve the active linear strain in conducting polymers by embedding conductive materials into the film during electrochemical deposition. Implanting conductive materials within conducting polymer films addresses the polymer's inherent limitations distributing an applied charge. When embedding conductive electrodes onto conducting polymer electrodes, the adverse affect of impeding either the ion transfer or mechanical compliance [11,12] must be addressed as design constraints.

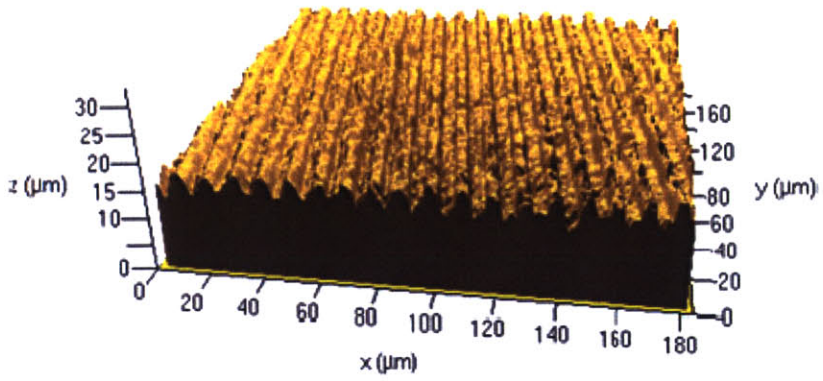

Figure 3-5: 500 to 1000 nm gold coating on polypyrrole actuator. (Copied from [13])

One such example of an embedded conducting material by Bay [13] in Figure 3-5 depicts a thin coating of gold onto a PPy-DBS foil which was porous enough to allow ion transport. As shown by Bay, the addition of a conductive material improves the polymer's ability to propagate a charge thus increasing the charge dependant active strain.

The intuitive notion that improving the polymer's conductivity is necessary is also validated by Madden's multiple tap experiment [8] pictured in Figure 3-6.

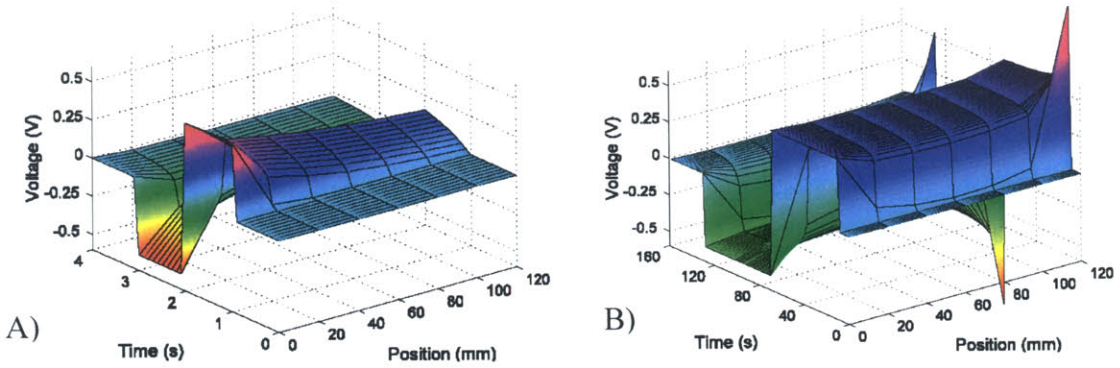

Figure 3-6: Measured voltage drop along the length of a polypyrrole film. A) Depicts a single ended charge injection point and B) depicts double ended injection points. (Copied from [8])

Madden's experiment clearly shows the manner in which a single ended voltage drops as it propagates along a film. By simply adding multiple points of applied voltage, the voltage drop across the film is quickly reduced allowing for improved charge delivery and active strains.

To adequately address the need for improved charge delivery within a conducting polymer film, the following device was constructed as a means to enhance linear actuation by embedding electrical contacts into the polymer film during electrochemical deposition.

3.3.1 Design and Construction

The design of the mechanically enhanced linear actuator is depicted in Figure 3-7 where a gold wire is embedded into a polymer film in a sinusoidal pattern. The sinusoidal shape of the gold wire embedded in the film is chosen so that the embedded Sections of the wire lie perpendicular to the major axis of contraction during actuation.

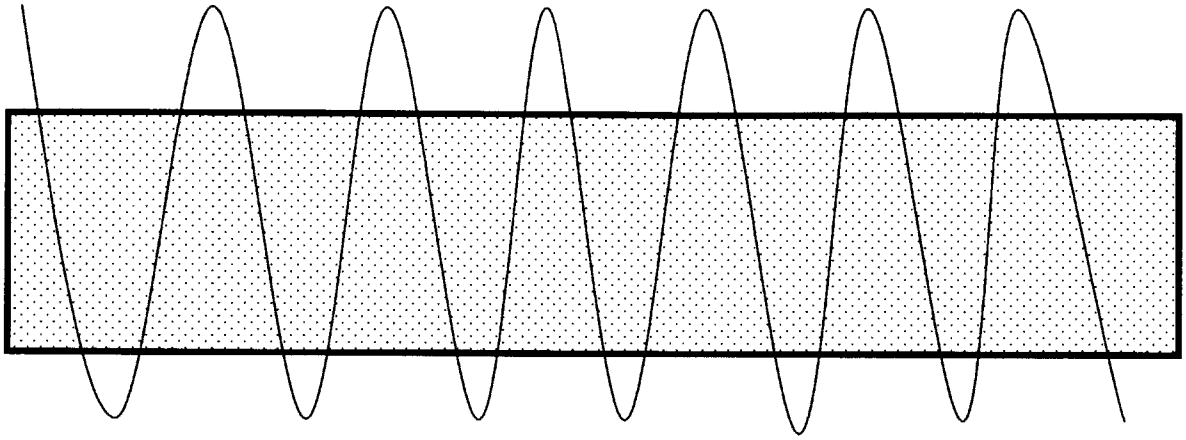

Figure 3-7: The mechanically enhanced linear film actuator embodiment.

The perpendicular layout of the wire reduces the mechanically enhanced impedance from the gold wire. A parallel construction along the major axis of contraction would resist the actuation. Additionally, the single sinusoidal shaped gold wire allows for the enhanced linear actuator to be electrically stimulated by every point of contact along the wire mimicking a multiple point charge injection.

Construction of the enhanced PPy linear actuator follows the described method of electrochemical deposition in Section 3.2.1 following a trace layout of gold wire. Rather than depositing the film onto a clean carbon crucible, the gold wire pattern described in Figure 3-7 is applied to the crucible as pictured in Figure 3-8. The gold bonding wire [14] is masked on to the carbon crucible with 25 μm Kapton® tape [15].

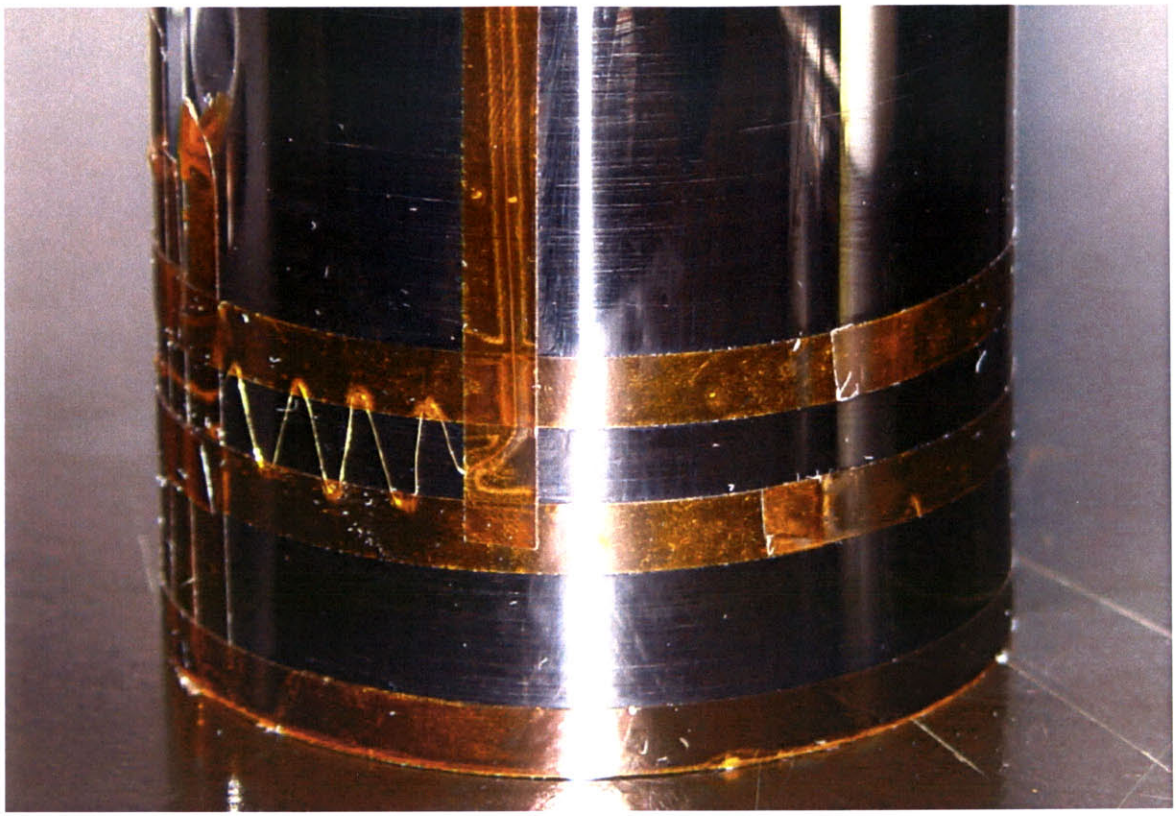

Figure 3-8: A 75 µm gold bonding wire masked onto a carbon crucible.

The polymer was then electrochemically deposited onto the crucible galvanostatically at 0.8 A/m^2 in - 40 °C for 14 hours to achieve a thickness of 25 to 30 µm. The resulting film after removal of the Kapton® tape is pictured in Figure 3-9.

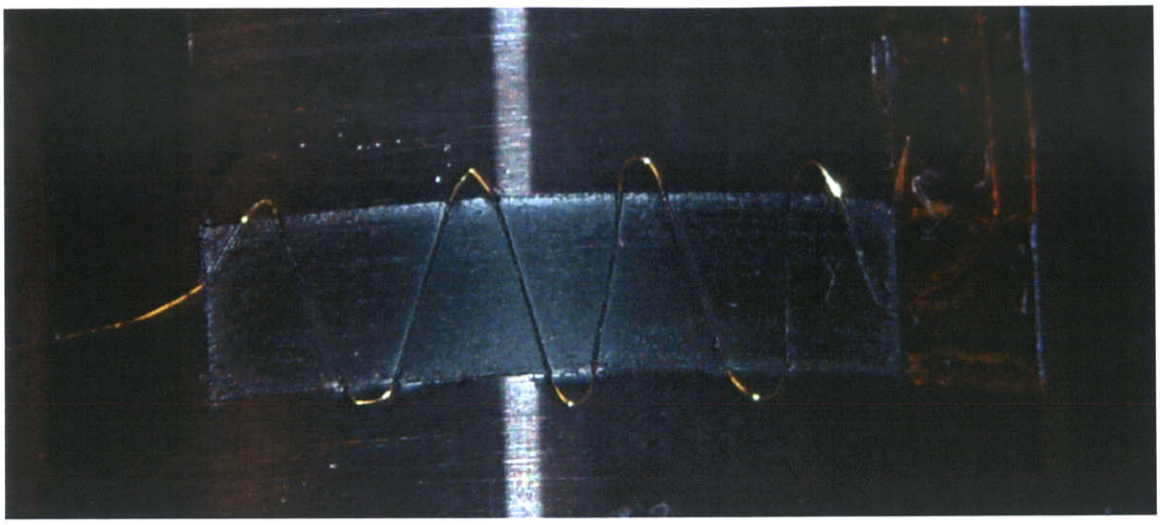

Figure 3-9: The enhanced linear actuator prior to removal from the crucible.

The enhanced linear actuator was then removed from the crucible with a razor blade for testing in an ECDMA constructed by Rinderknecht [16].

3.3.2 Results

Enhanced linear contracting films were mounted into Rinderknecht's ECDMA for characterization of the electrochemical and mechanical response. A control film deposited on the same crucible without the embedded gold wire was also tested. In each experiment, identical electrochemical and mechanical conditions were applied to the control and enhanced films. In Figure 3-10, a typical electrochemical response is depicted for an enhanced linear actuator.

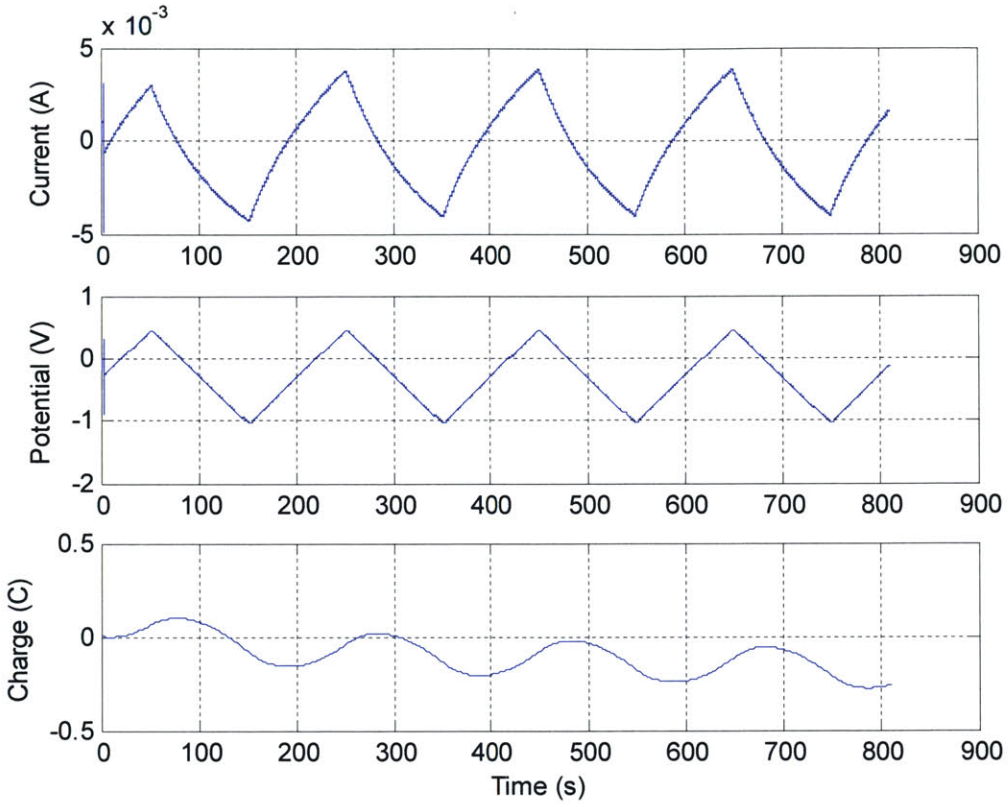

Figure 3-10: A characteristic electrochemical response in the linear actuator

Isotonic conditions were imposed as the mechanical environment for testing. A constant stress of 1 MPa was applied to the enhanced and control polymers.

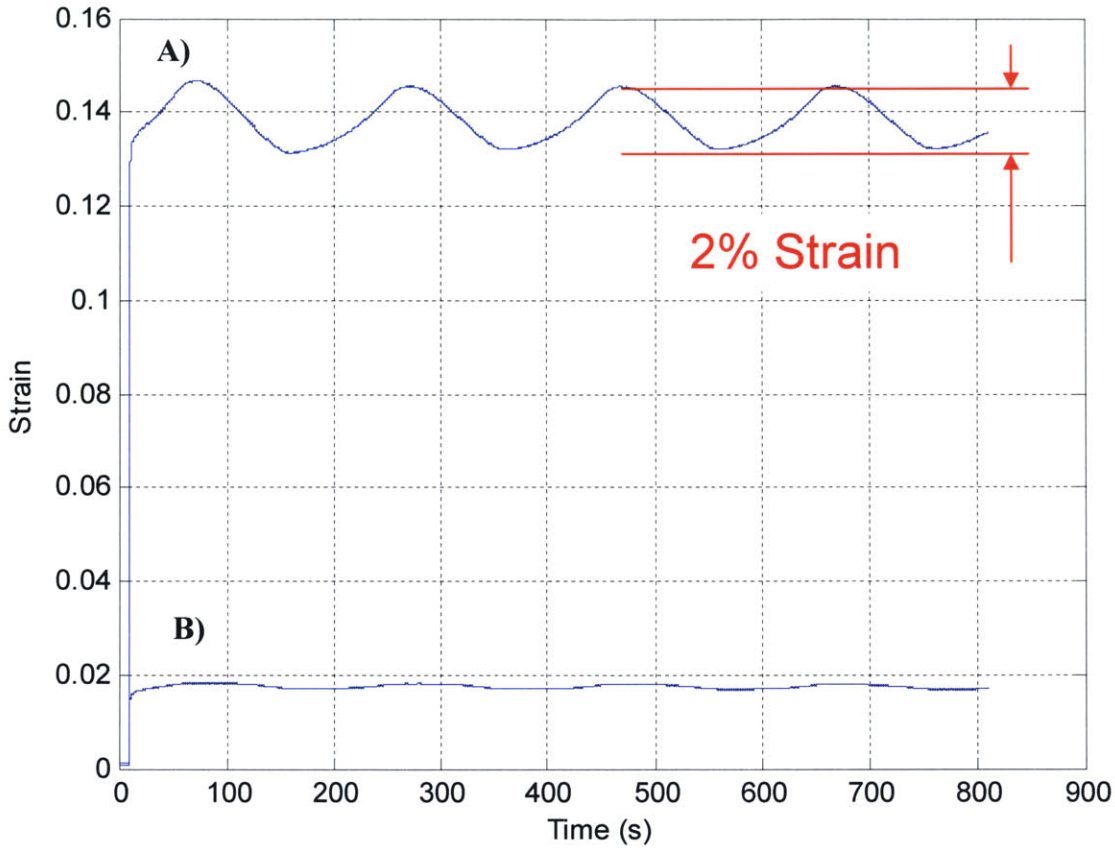

Figure 3-11: Isotonic comparison between A) an enhanced film and B) control film.

After overcoming the initial passive strain as the ECDMA achieves the 1 MPa isotonic stress, the resulting active strain results are depicted in Figure 3-11. The large difference in the passive strain is due to the enhanced film being placed at a far lower stress than the control film prior to the experiment.

The active strain of the enhanced linear actuator is 7.22 times greater than the control film. A comparison between strain rates also illustrates the gold wire embedded film's ability to actuate 8.38 times faster than the control film. The rapid strain rate and increase in total active strain are attributed to the propagation of charge through the enhanced polymer. As shown by Madden's multiple point charge injection model in

Figure 3-6, the embedded gold wire mimics Madden's multiple point charge injection to deliver a charge to the polymer rapidly. The need to rapidly deliver a charge to enhance the active strain of the film is further emphasized by Equations 1.1 and 1.2.

3.4 Conclusions

The results from the novel mechanical enhancements presented in this Chapter provide proven methods for increasing the polymer's active mechanical properties. Adjustments to the constraints imposed on stacked polymer trimorphs and the addition of slip surfaces between each layer reduces the mechanical impedance between layers. The reduced mechanical impedance resulted in an increased tip force of 350 % and reduced the effective stiffness of the stacked trimorph device. Future research efforts should continue to address the mechanical interference for stacked trimorphs in excess of two layers.

The results from the linear enhanced polypyrrole film provide a simple solution to increasing the achievable strain and strain rate. Results yield a seven fold increase in strain from a simple mechanical enhancement that does not involve difficult processing techniques.

The tools presented in this Chapter will advance the potential application of EAPs as an actuator solution by circumventing science's dependence on material advances on the chemical level.

3.5 Chapter References

[1] Madden, J., Vandesteeg, N., Anquetil, P., Madden, P., Takshi, A, Pytel, R., Lafontaine, R., Wieringa, P., Hunter, I., "Artificial Muscle Technology: Pysical Principlces and Naval Prospects." *IEEE Journal of Oceanic Engineering*, **V. 29 No. 3** (2004): 706-728.

[2] Madden, J., Cush, R., Kanigan, T., and Hunter, I., "Fast contracting polypyrrole actuators," *Synthetic Metals*, **V. 113** (2000): 185-192.

[3] Pei, Q. and Inganas, O., "Conjugated Polymers and the Bending Cantilever Method: Electrical Muscles and Smart Devices." *Advanced Materials,* **V. 4 No. 4**, (1992): 277 – 278.

[4] Pei, Q. and Inganas, O., "Electrochemical Application of the Bending Beam Method: Mass Transport and Volume Changes in Polypyrrole During Redox." *Journal of Physical Chemistry.* **V. 96 No. 25**, (1992): 10507 – 10514.

[5] Smela, E., Inganas, O., Pei, Q., and Lnudstrom, I., "Electrochemical Muscles: Micromachining Fingers and Corkscrews." *Advanced Materials.* **V. 5 No. 9**, (1993): 630 – 632.

[6] Smela, E., Inganas, O., and Lnudstrom, I., "Controlled Folding of micrometer-Size Structures." *Science.* **V. 268**, (1995 Jun 23): 1735 – 1738.

[7] Madden, J.D., Madden, P.G., Hunter, I.W. "Conducting Polymer Actuators as Engineering Materials." *Proceedings of SPIE 9th Annual Symposium on Smart Structures and Materials: Electroactive Polymer Actuators and Devices*, Yoseph Bar-Cohen, Ed., **V. 4695**, SPIE, San Jose CA, (2002): 176-190.

[8] Madden, P., *Development and Modeling of Conducting Polymer Actuators and the Fabrication of a Conducting Polymer Based Feedback Loop*, Ph.D. Thesis, Massachusetts Institute of Technology, Cambridge, MA, **2003**.

[9] Schmid, B., *Device Design and Mechanical Modeling of Conducting Polymer Actuators*, S.B. Thesis, Massachusetts Institute of Technology, Cambridge, MA **2003**.

[10] Wallace, G. G., Ding, J., Zhou, D, and Spinks, G. M., "Ionic Liquids: An Elixir for Inherently Conducting Polymer Based Artificial Muscles." *World Congress on Bioartificial Muscles*. Albuquerque, New Mexico (2002).

[11] P. Graveson, M. Y. Benslimane, *WO Patent 0237 660*, **2002**.

[12] Benslimane, M., Gravensen, P., Sommer-Larsen, P., *SPIE 9th Ann. Int. Symp. On Smart Structures & Materials 2001* (Ed: Y. Bar-Cohen), SPIE Press, Bellingham, WA (2002): 150.

[13] Bay, L., West, K., Sommer-Larsen, P., Skaarup, S., Benseliane, M., "A Conducting Polymer Artificial Muscle with 12% Linear Strain." *Adv. Mater.*, February **V. 15, No. 3**, (2003): 310 - 313.

[14] Kulicke and Soffe ID#: ZS5550534115A003. http://www.kns.com

[15] CS Hyde Company Product 18-1S with Silicone Adhesive

[16] Rinderknecht, D., *Design of a Dynamic Mechanical Analyzer for the Active Characterization of Conducting Polymer Actuators*, S.B. Thesis, Massachusetts Institute of Technology, Cambridge, MA, **2002**.

Chapter 4

Development of an Electrochemical Dynamic Mechanical Analyzer for Characterization of Macro-Length Conducting Polymers

4.1 Background

An electrochemical dynamic mechanical analyzer (ECDMA) is an instrument used to characterize the active mechanical and electrochemical properties of conducting polymers. The ECDMA is typically able to perform both constant strain (isometric) and constant stress (isotonic) active testing on films in either frequency controlled galvanostat or potentiostat conditions.

Active and passive ECDMA characterization of electroactive polymer performance has been limited to the investigation films of ~ 0.1 mm to 10 mm in length because commercial instruments available do not allow for long film length testing. Recent research initiatives, such as The Institute of Soldier Nanotechnologies at the Massachusetts Institute of Technology, have begun to explore the development of devices implementing conducting polymer actuators of various lengths and sizes beyond the capacities of available instruments.

Although a plethora of literature exists on the characterization of EAPs, no literature to date describes macro-length (> 80 mm) characterization of conducting polymers. The development of a macro-length conducting polymer ECDMA will allow for an

investigation of the experimental characterization of macro-length films versus an accepted strain to charge model. Equation 4.1 below relates the strain ε as a function of the applied charge per unit volume ρ and the strain to charge ratio

$$\varepsilon = \frac{\sigma}{E} + \alpha \cdot \rho \ , \tag{4.1}$$

where σ is the stress in the system and E is the polymer's elastic modulus [1]. When using an electrochemical DMA to characterize a polymer and the strain to charge ratio, two distinguishable embodiments of an ECDMA exist. One variation employs a passive load for active testing and another utilizes an actuator (such as a voice coil motor or linear stage) for active testing through force feedback from a load cell.

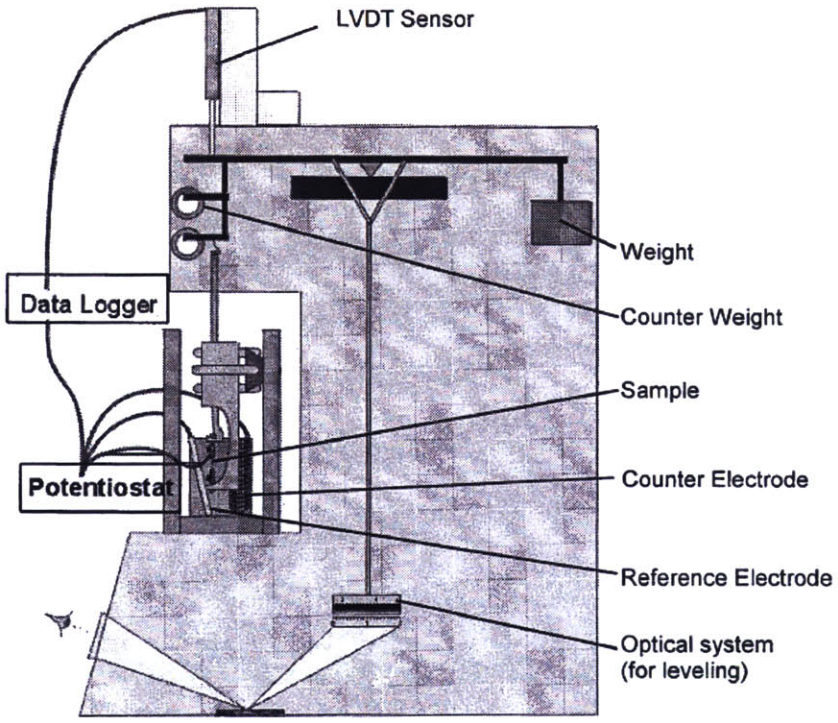

Figure 4-1: Passive balance beam dynamic mechanical analyzer employing a weighted balance beam and linear variable distance transducer in conjunction with a potentiostat. (Figure reprinted from Spinks et al [2])

Passive ECDMAs, such as the example [2] pictured in Figure 4-1, provide an attractive and cost effective solution to conducting polymer characterization. However a passive DMA is hindered by inflexible isotonic testing conditions due to the limited available weight options needed to generate a stress, the dampening of the isotonic response within the system components, the inability to measure active stresses during isometric testing, and the large physical size needed for the instrument.

Active ECDMAs, such as Rinderknecht's [3] ECDMA developed in the MIT BioInstreumentation Lab in Figure 4-2, employ actuators for isotonic and isometric

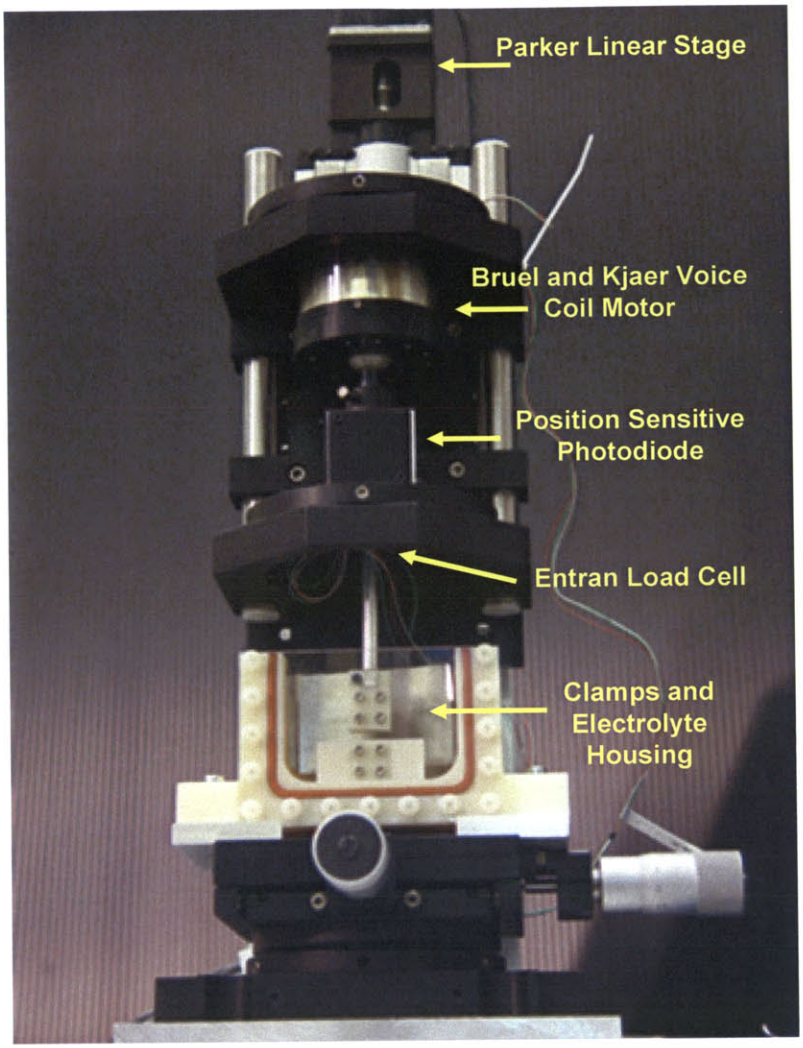

Figure 4-2: Rinderknecht's voice coil actuated ECDMA is able to both apply and measure force and displacement. (Adapted from [3])

testing. Rinderknecht's ECDMA enables the user to perform characterization at up to 100 Hz bandwidth with a minimum resolvable displacement of 1 μm and minimum resolvable force of 1 mN. Rinderknecht's ECDMA is able to characterize films of ~ 1 mm to 10 mm with a maximum active voice coil displacement of 3 mm and maximum applied force of 1 N.

No commercial electrochemical isotonic testing device exists today with the capacity for high resolution electrochemical and mechanical property monitoring. The following Sections describe the development of an ECDMA instrument capable of high resolution conducting polymer characterization for polymer lengths from 1 mm to 1250 mm long (assuming 4% active strain).

4.2 Design Description and Considerations for an Electrochemical Dynamic Mechanical Analyzer

Active electrochemical characterization of a conducting polymer typically involves the following main components: an electrochemical cell where the polymer is actuated, the conducting polymer film, a liquid electrolyte, electromechanical contacts for actuation, a data acquisition unit, a force sensor, an actuator, and a software interface. The embodiment of these components into an instrument must succumb to the design constraints of the system's dynamics, the electrolyte's chemical properties, and the simplicity of the human interface. In particular the mass and stiffness of each component should be optimized to reduce the resonance of the instrument and enhance its effective bandwidth. Additionally, the electrolyte for conducting polymers typically consists of a solvent, such as propylene carbonate, which because of a low surface energy, quickly coats the instrument and destroys electrical sensors. Yet these design constraints cannot supersede the user interface when a sample is loaded and characterized.

The electrochemical dynamic mechanical analyzer described in the following Sections utilizes a low-profile, high resolution linear stage with a large displacement for isotonic and isometric testing. With the design constraints in mind, the design goals for the advanced ECDMA included the following:

- High resolution position sensing
- Flexible platform for traditional and macro-length EAP samples
- Compact instrument with few hardware components
- Easy loading and setup of samples
- Flexible software program allowing for classical isotonic and isometric testing along with custom isotonic, isometric, and voltammetry profiles
- Tight PID control of the isotonic conditions
- Minimal buoyancy effects from the electrolyte solution on stress and strain readings
- Minimal momentum effects on the load cell from the linear stage actuator

4.2.1 Hardware Components

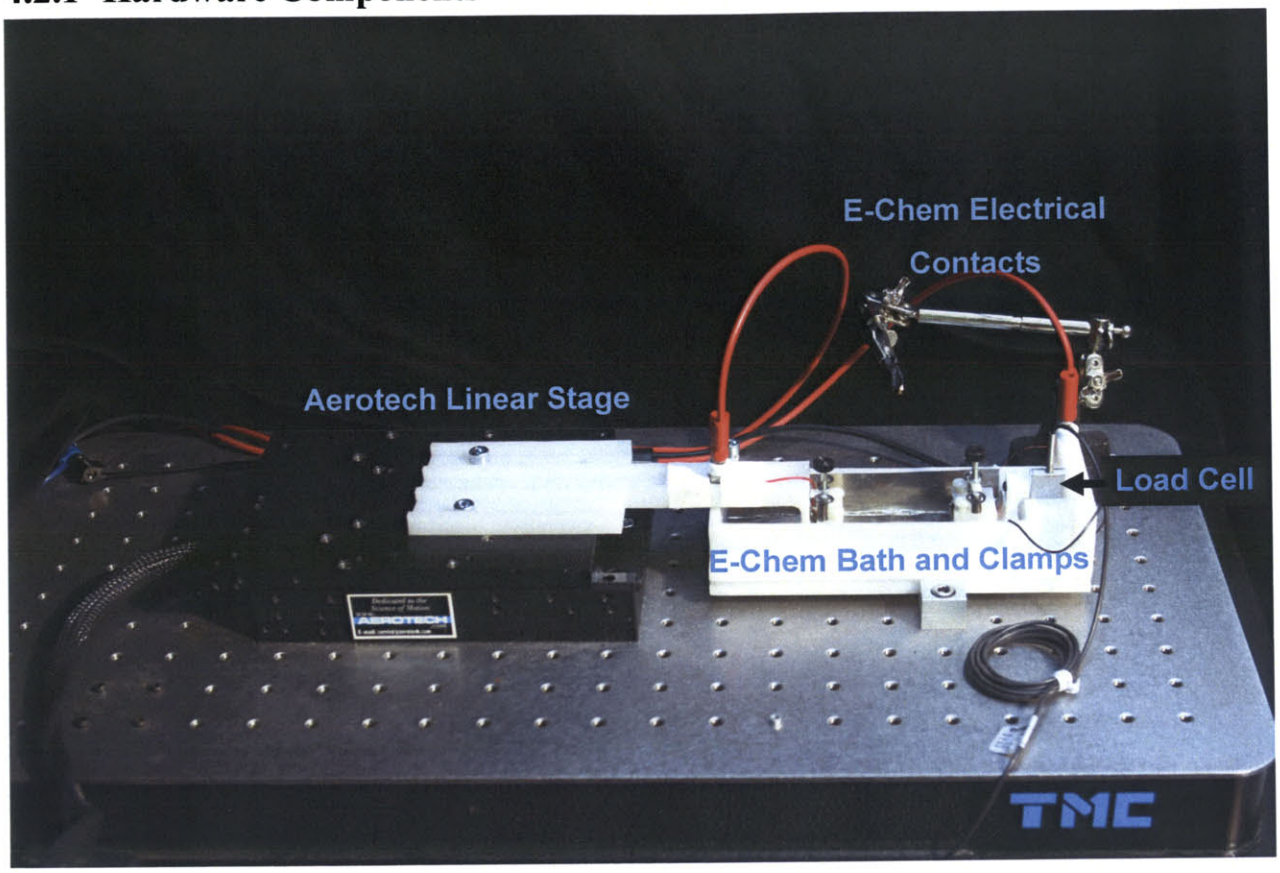

Figure 4-3: The assembled ECDMA instrument

The ECDMA consists of an Aerotech© ALS130-050 brushless linear motor stage with high accuracy HALAR (http://www.aerotech.com/products/stages/als130.html) specifications to control the isotonic and isometric testing conditions as pictured in Figure 4-4 (See Appendix A for detailed drawings).

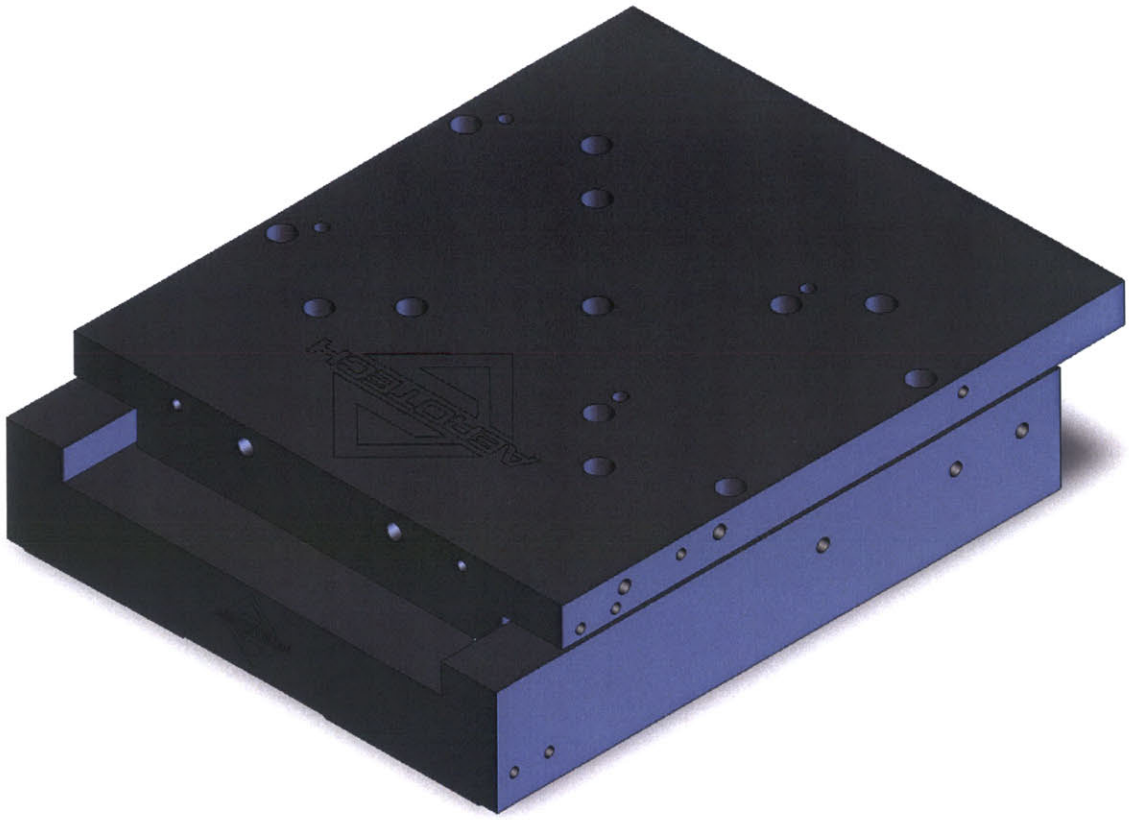

Figure 4-4: The Aerotech ALS130-050 linear stage

The Aerotech linear stage is capable of 0.3 μm bi-directional accuracy at a velocity of 300 mm/s while exerting a peak force of 31.5 N. The linear stage uses a Renishaw RGH24B15F00A Non-contact Quadrature Linear Encoder with 20 nm position resolution. Position feedback for hardware control is accomplished with an Aerotech NLDrive10-40-A-IOPSO-MXH drive and amplifier (http://www.aerotech.com/products/amps/nd.html) (See Appendix A for detailed drawings). The NLDrive10-40-A-IOPSO-MXH can maintain a commanded machine resolution of 0.1 μm. Communication between the drive and the computer is accomplished with IEEE-1394 FireWire™ at a communication rate of 8 kHz with the Real-Rime VenturCom RTX environment.

Force measurements in the ECDMA are measured in line with the major axis of the polymer using a 50 N capacity Futek L2357 S-beam load cell. The 4-wire bridge Futek load cell is connected to a Vishay 2311 Signal Conditioning Amplifier (http://www.vishay.com/brands/measurements_group) with 10 VDC excitation and an output gain of 1,000. The Vishay amplifier and 50 N capacity load cell produce a 1.863 mN resolvable force measurement for isotonic control and polymer characterization (See Appendix A for calibration).

Electrochemical actuation within the ECDMA is controlled by an AMEL 2053 Research Potentiostat/ Galvanostat (http://www.amelchem.com/product/electrochem/line2000/ 2053/2053.html). Current ranges for the AMEL 2053 output can be adjusted from 1 μA to 1 A over seven decades. Selectable current ranges allow for a wide range of electrochemical characterization windows of the polymer's oxidation state and provide a variety of current input ranges for system identification of the polymer. The AMEL 2053's output can be modulated to 1 mV of the commanded analog voltage, allowing for high resolution electrochemistry.

Data acquisition is performed with a National Instruments PCI-6052E PCI card and BNC-2110 terminal block (http://www.ni.com/dataacquisition). The 6052E is capable of a ± 10 V range with 16 bit input/ output resolution at a sample rate of 333 kHz. Aside from monitoring position, all input and output voltages were accomplished with the 6052E.

The Aerotech NLDrive10-40-A-IOPSO-MXH includes two 16 bit analog inputs and two 18 bit analog outputs, which could be used for electrochemical actuation and data acquisition. However this solution was not implemented in the final embodiment of the ECDMA in Figure 4-5 because hardware communication between the computer and NLDrive10 provide a lower feedback control bandwidth than the National Instruments PCI-6052E data acquisition unit.

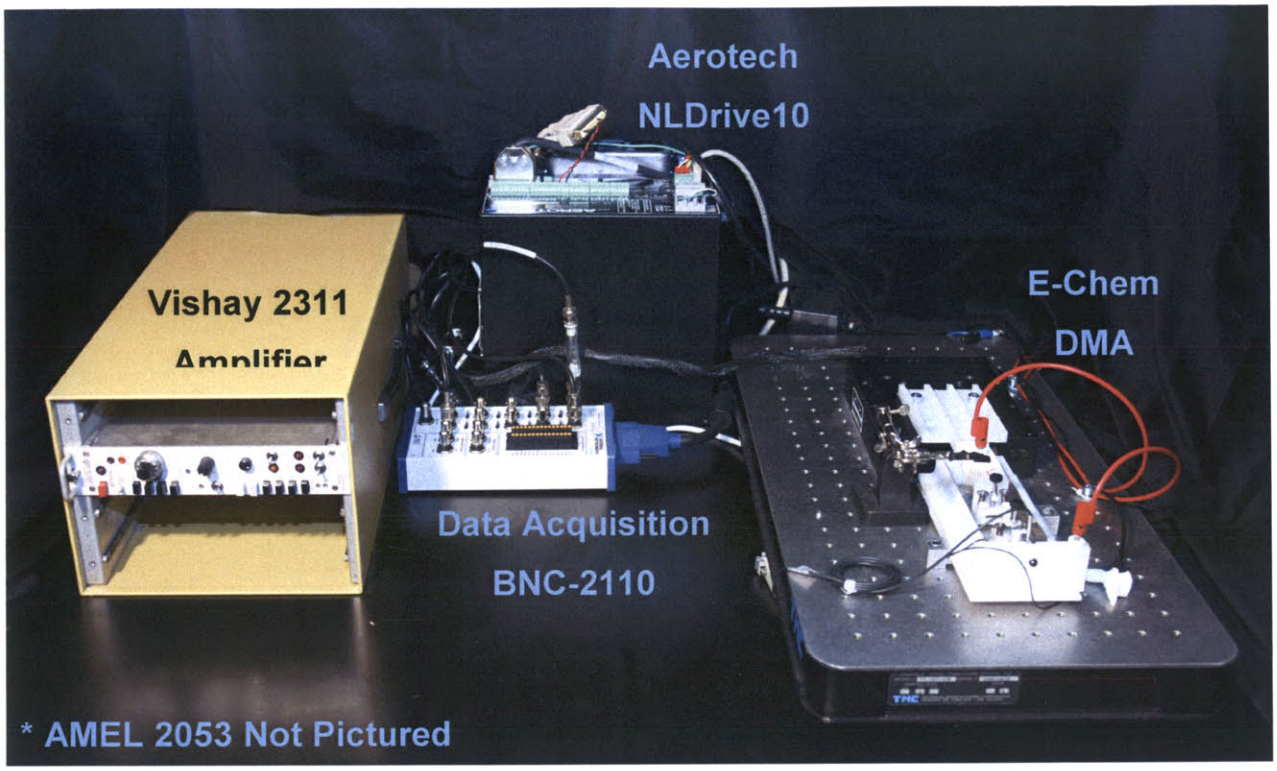

Figure 4-5: Hardware Components for ECDMA.

The schematic in Figure 4-6 depicts the hardware configuration for the ECDMA.

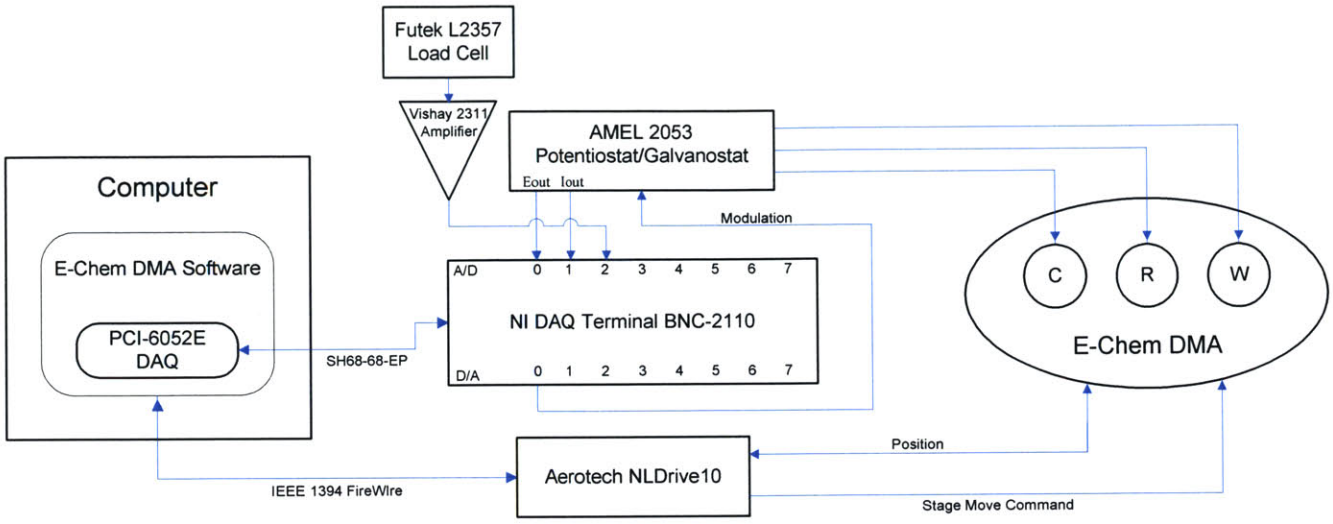

Figure 4-6: ECDMA Instrument Schematic. Note that C, R, and W refer to the counter, reference and working electrodes.

4.2.2 Software Development

All programming for the graphical user interface and operation of the electrochemical DMA was written using the Visual Basic language in Microsoft Visual Studio .NET 2003 (See Appendix A).

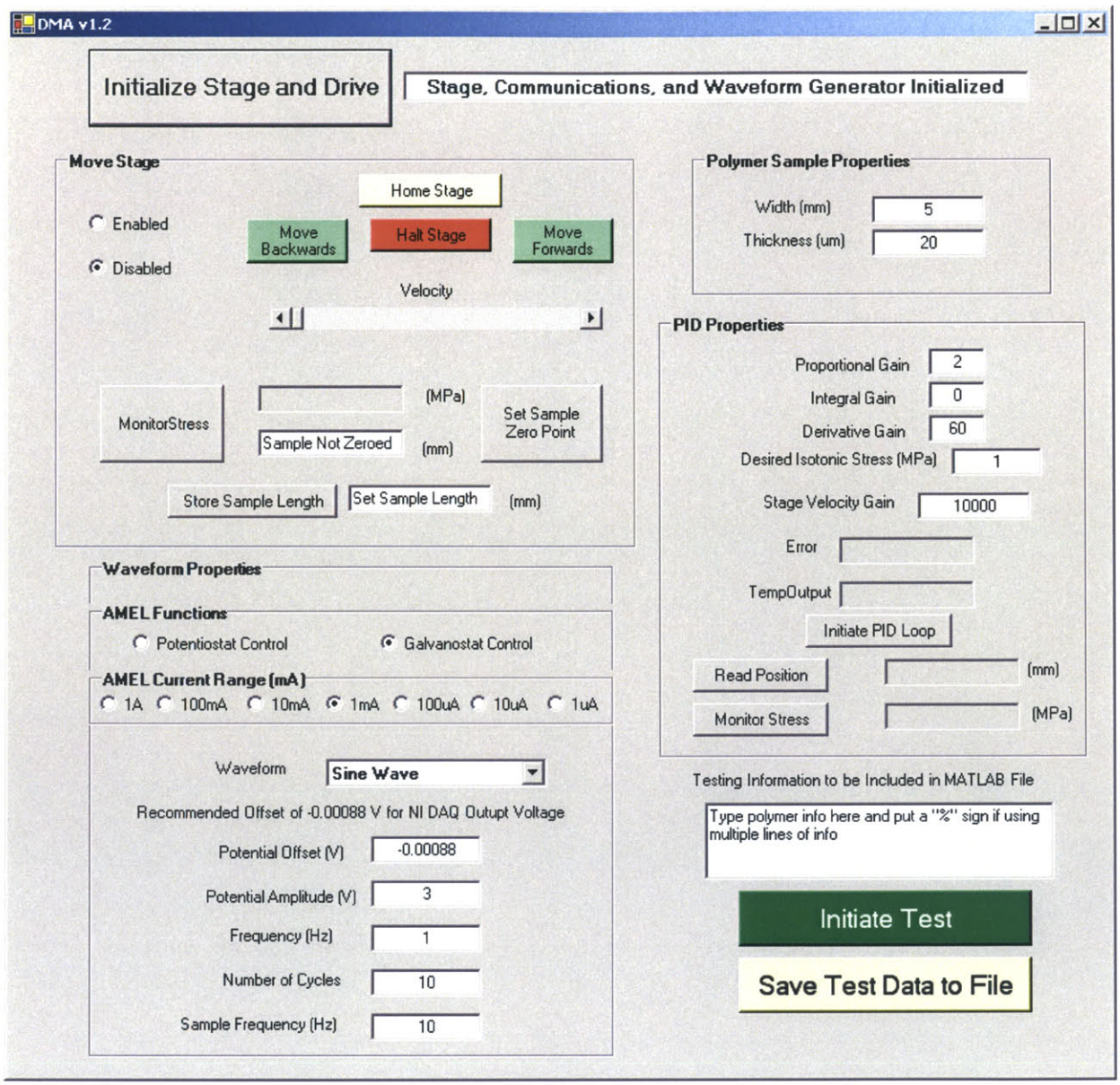

Figure 4-7: ECDMA graphical user interface for polymer characterization.

The ECDMA program communicates with the Aerotech and National Instruments hardware via the AerotechDLL.dll and Interop.nidaq32.dll. All communications with the Aerotech NLDrive10 are line executed library commands to either read the linear position encoder or command a stage movement. Input readings with the 6052E data acquisition hardware are collected with line executed library commands in the software.

A commanded analog output voltage voltage is executed at 1 MHz from locally stored binary waveforms on the PCI-6052E.

The E-Chem. graphical user interface (GUI) provides a flexible environment for electrochemical characterization of conducting polymers. Electrochemical voltammetry can be performed with the following waveforms from the drop down menu in the GUI:

- Sine Wave
- Triangle Wave
- Square Wave
- Delayed Impulse Wave
- Impulse System ID Wave
- Stepped Ramp Wave

The offset, amplitude, frequency, and number of cycles for each wave can be input through the GUI. Once the waveform is selected, each electrochemical stimulus can be executed in either isotonic or isometric conditions also specified through the GUI. If desired, a custom isotonic or isometric profile can also be loaded as a binary waveform into the program.

The E-Chem. GUI also provides a convenient method for defining the material properties of the conducting polymer sample. All material properties, experiment notes, electrochemical data, and active mechanical data are written to a MATLAB file for analysis after each experiment is executed with the ECDMA program.

4.3 Electrochemical Dynamic Mechanical Analyzer Specifications

The electrochemical dynamic mechanical analyzer encompasses a high resolution instrument capable of both normal (1 mm to 10 mm) and macro-length conducting polymer characterization. In addition to classical conducting polymer characterization

such as static isotonic and isometric tests, the ECDMA's platform provides the capability for new characterization techniques. Custom defined isotonic and isometric profiles loaded into the software allow the user to perform system identification on the polymer actuator for specific design applications. Other uses for the ECDMA include stretch alignment of polymer films and pseudo-random binary sequence (PSRB) system identification of polymers, which have also been proven possible with this instrument.

The specifications in Table 4.1 provide an overview of the instrument's capabilities.

Table 4.1: Electrochemical DMA Specifications*

Aerotech ALS130-050	Specification
Total Displacement	50 mm
Maximum Velocity	300 mm/sec
Maximum Acceleration	10 m/s^2
Maximum Tangential Load	100 N
Continuous Tangential Force	31.5 N
Commanded Position Resolution	0.1 μm
Linear Position Encoder Resolution	20 nm
***Futek L2357 Load Cell**	
[1] Maximum Capacity	50 N
[1] Minimum Resolution	1.863 mN (amplifier gain of 1,000)
[2] Maximum Capacity	1 N
[2] Minimum Resolution	69.25 μN (amplifier gain of 1,000)
Control and Data Acquisition	
Isotonic PID Control Loop Bandwidth (Software)	4 kHz
Isotonic PID Control Loop Bandwidth (Hardware)	~ 1 kHz
Maximum Data Acquisition Sample Rate	1 kHz
Analog Input and Output Resolution	16 bit (1 mV effective)
Maximum Potential	± 50 V
Maximum Current	± 1.2 A
Modulated Electrochemical Resolution	1 mV
Galvanostat Ranges	7 decades: 1 μA to 1 A
Modulated Potential (Current) Response Time	0.7 μsec (10 μsec)
Electrochemical Waveform Types	6 Preset or Custom Binary Waveform
Testing Conditions	Voltammetry, Isotonic, Isometric

*** Two different capacity L2357 load cells 1 and 2 can be interchanged in the ECDMA to account for the anticipated load.**

4.4 *Macro-Length Conducting Polymer Characterization*

The completed ECDMA performs well for various sample lengths and testing conditions. Figure 4-8 below depicts the electrochemical input and mechanical response of a polymer film to a 22 mA impulse waveform under isotonic conditions.

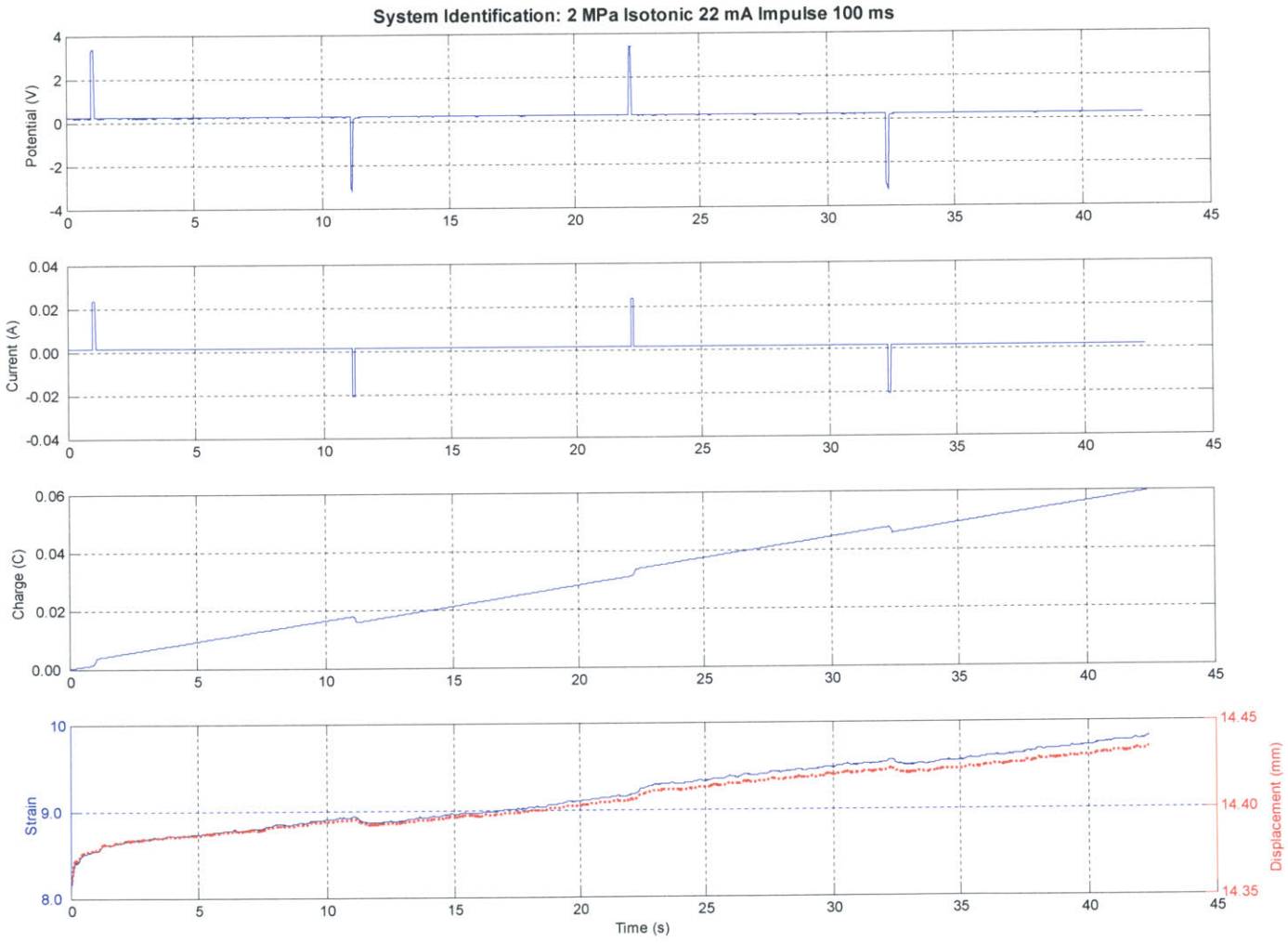

Figure 4-8: Polymer response to 100 ms impulse of 22 mA in 2 MPa isotonic conditions.

An impulse input into the polymer provides an insight into the polymer's electrochemical response. By further investigating the response in the window of 10 to 25 seconds, a

clear step in the polymer's mechanical strain is observed in relation to the charge in Figure 4-9.

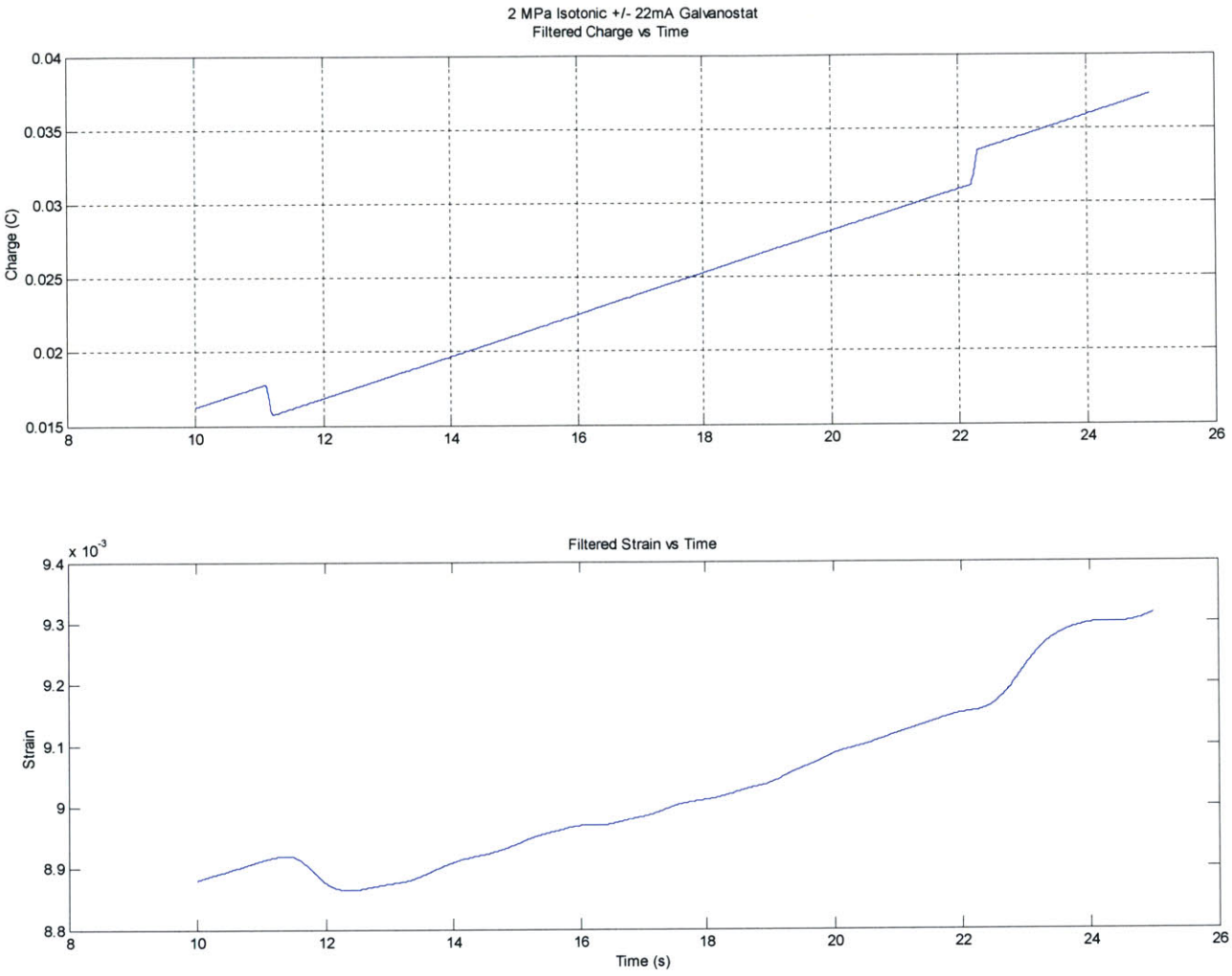

Figure 4-9: Polymer strain response to an impulse of charge.

The results are further analyzed with respect to the slope of the plotted data to determine a system response as plotted in Figure 4-10. Inspection of the rise time of the strain yields a 6.3×10^{-5} change in strain within the 75% to 25% range of the rise time, which compromised 570 ms. Further testing revealed that 20 to 25 mA impulse for 0.1 s was the peak current that the polymer could withstand before electrochemical degradation.

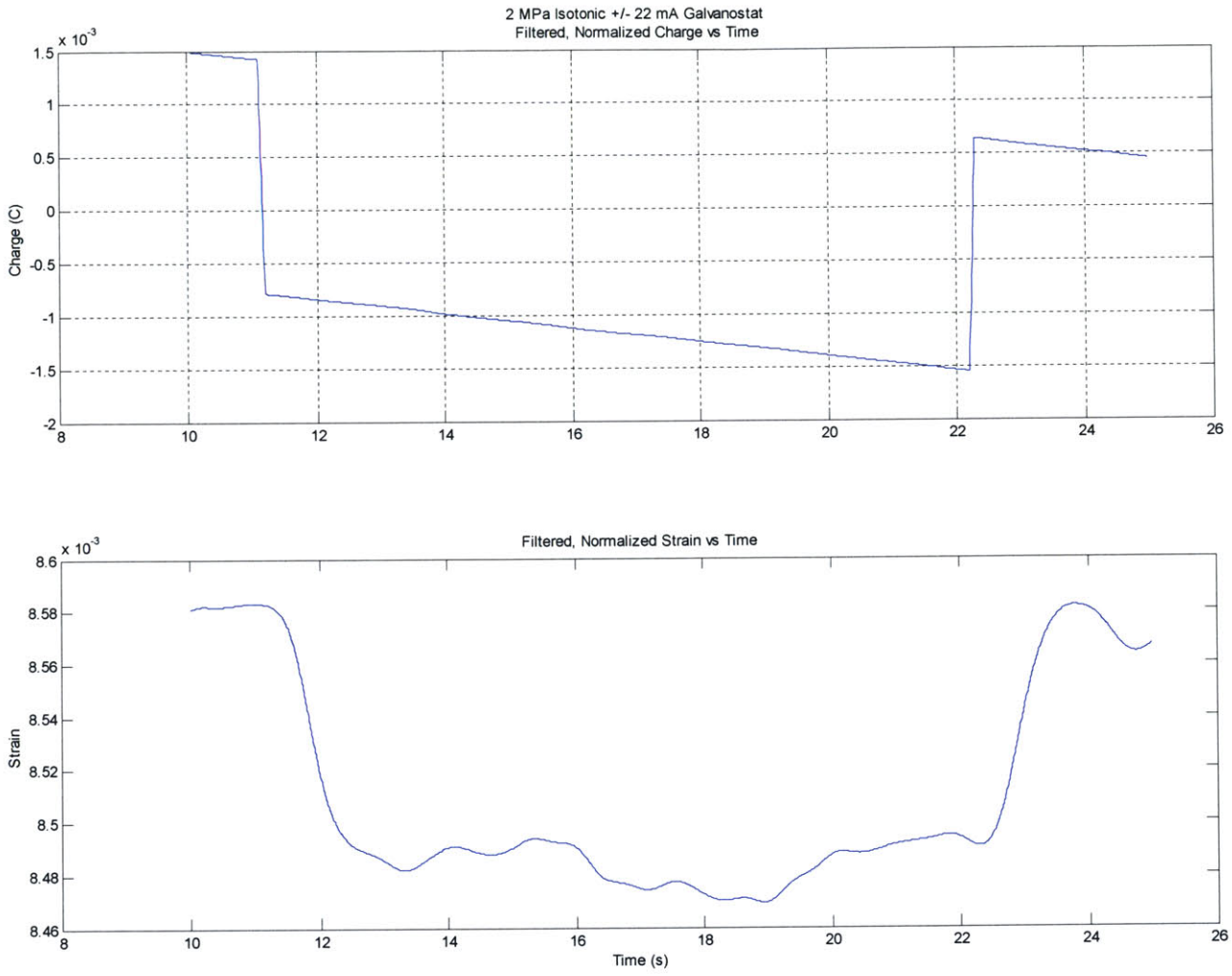

Figure 4-10: Normalized strain and charge with respect to slope.

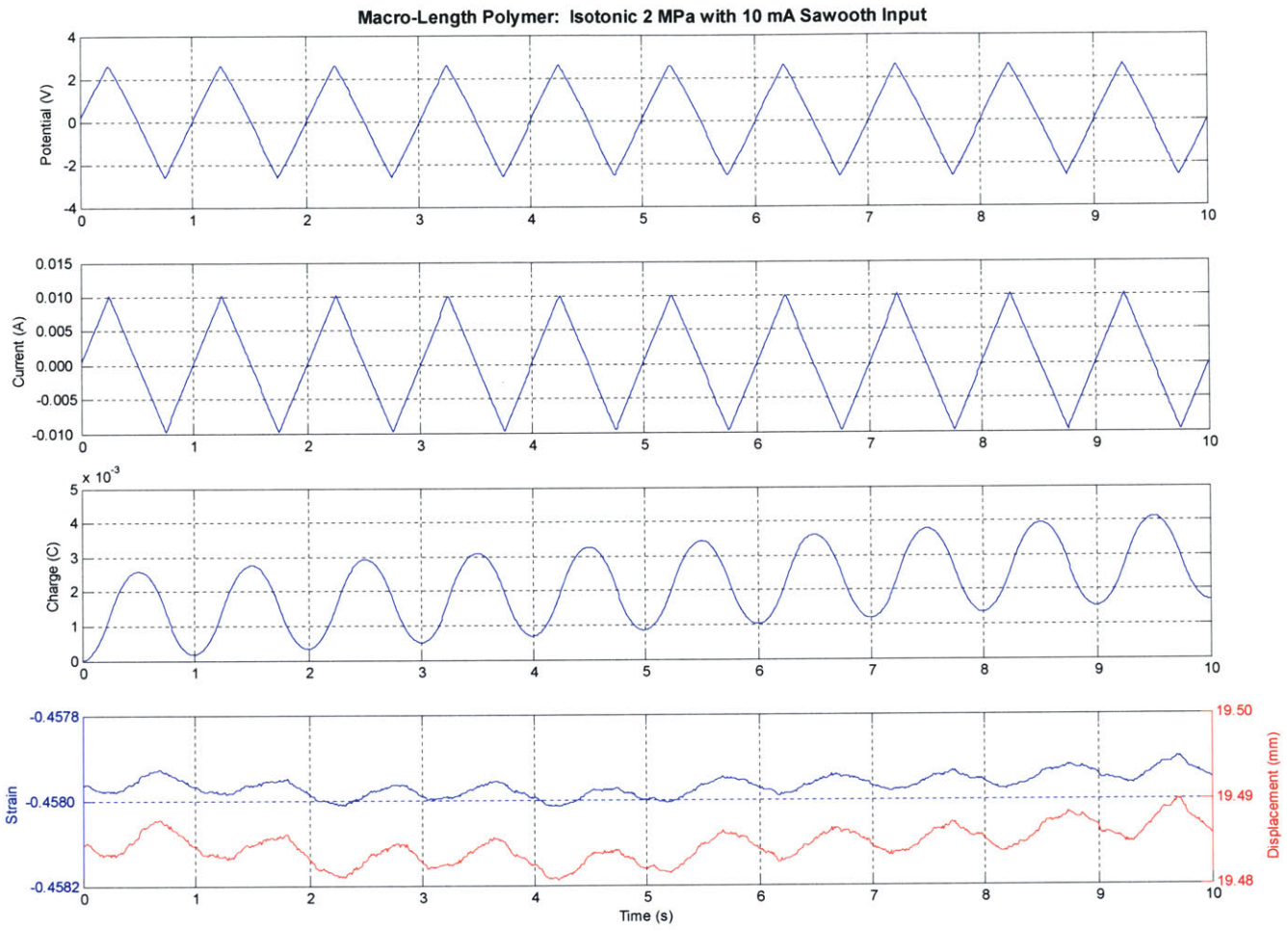

Figure 4-11: ECDMA chharacterization of a 81.5 mm long polymer film

The ECDMA's capability to test macro-length polymers is demonstrated in Figure 4-11, where an 81.5 mm film was characterized with a 10 mA sawtooth input held under under 2 MPa isotonic conditions.

4.5 Conclusion and Future Work

For the first time an electrochemical dynamic mechanical analyzer instrument has been developed that is capable of characterizing varying polymer sample sizes from 1 to 1250

mm under custom electrical and mechanical stimuli. The instrument was successfully able to characterize the response of macro-length polymers and identify a current range for system identification of fast response polymer actuators.

The potential for system identification and advancements in the engineering of polymer actuators is significantly increased with this instrument. In the future it is hoped that pseudo random binary and stochastic inputs used with the ECDMA will enhance the understanding of the polymer actuator's system response to electrochemical and mechanical loads.

4.6 Chapter References

[1] Madden, J.D., *Conducting Polymer Actuators*, Ph.D. Thesis, Massachusetts Institute of Technology,Cambridge, MA, **2000**.

[2] Spinks, G., Wallace, G., Lu Liu, L., Zhou, D. "Conducting Polymers Electromechanical Actuators and Strain Sensors" *Macromol. Symp.* **V. 192**, (2003): 161 – 169.

[3] Rinderknecht, D., "Design of a Dynamic Mechanical Analyzer for the Active Characterization of Conducting Polymer Actuators," S.B. Thesis, Massachusetts Institute of Technology, Cambridge, MA, **2002**.

Chapter 5

Rotary Motor Development

5.1 Introduction

Conducting polymer actuators have been traditionally studied with regard to linear actuation. The application of rotary motion to conducting polymers aims to achieve an actuating device capable of meeting the needs of applications requiring displacements beyond the traditional 2 to 4 % achieved by EAPs, specifically PPy. This Chapter focuses on the use of a finite actuator technologies applied for finite and infinite rotary displacement. The novel concept of generating rotary motion from traditionally linear conducting polymer systems can be achieved with and without mechanical components as later described in this Chapter (Sections 5.3 and 5.4).

5.2 Background and Prior Art

The conventional DC electric motor, invented over 100 years ago, is still the most popular motor in many applications despite its inadequacies. Although electric motors provide a cheap and common solution, they are unable to deliver high torque at low revolutions, they emit electromagnetic fields interfering with some applications, and they are unable to be easily scaled below 1.0×10^{-6} m^3 without sacrificing efficiency and performance [1]. Without the discovery of new raw materials, it is unlikely that electric motors will overcome their shortcomings. As consumer technologies move towards smaller micro-sized products, the need for miniature motors with high torque is being addressed in research and industry initiatives.

In particular, current motion solutions such as a piezoelectric ultrasonic motors and the development of a rotary motor design powered by electrostrictive polymers will be discussed in this Section.

Ultrasonic piezoelectric motors were first proposed in 1945 by Williams and Brown, but it was not until 1973 that Barth of IBM invented the first practical ultrasonic motor [2]. Piezoelectric motors have positive characteristics such as low speed and high torque, compact size, and quiet operation, but they are hindered by the need for a high frequency power supply and drooping-torque speed characteristics. Since Barth's novel motor design, two variations of the ultrasonic motor have evolved: the standing-wave and the propagating-wave types. The standing-wave can be described in the classical wave formula

$$u_s(x,t) = A \cdot \cos kx \cdot \cos \omega t. \tag{5.1}$$

The propagating-wave is expressed as

$$u_p(x,t) = A \cdot \cos(kx - \omega t), \tag{5.2}$$

which can be expanded with the trigonometric relation

$$u_p(x,t) = A \cdot \cos kx \cdot \omega t + A \cdot \cos(kx - \frac{\pi}{2}) \cdot \cos(\omega t - \frac{\pi}{2}). \tag{5.3}$$

Equation 5.3 exposes a key design principle for the propagating wave developed from the superposition of two standing waves differing by 90° in phase. The phase difference in time and space allows for controllable movements in both directions with a sacrifice in efficiency needed from two vibration sources.

Few standing-wave ultrasonic motors have found commercial applications due to difficulties in mechanical coupling from the "pecking" vibratory coupler and stator and the ability to only actuate in one direction. Although preloading appears to be a simple solution between the piezo vibrator and the stator, preloading can only be applied to the extent that the vibratory ellipse locus is deformed in half[1]. Preload does improve the maximum thrust, however the vibratory electromechanical coupling efficiency is reduced and an intermittent rotational torque still exists.

A multi-mode-single-vibrator standing wave motor developed by Koc in the following picture (Figure 5-1) is one of the few standing wave motors to find an appropriate balance between preload and vibratory excitement [3].

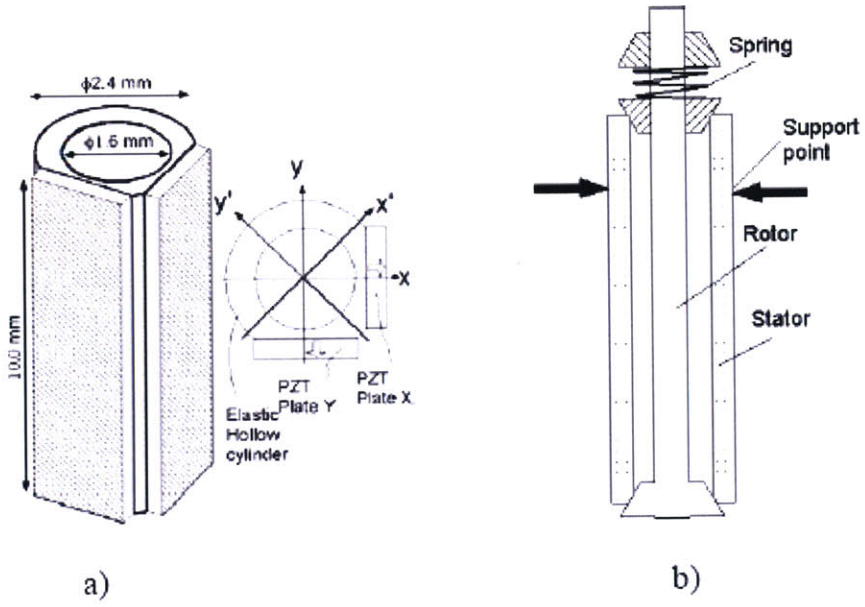

Figure 5-1: Multi-mode-single-vibrator standing wave motor. The a) structure of the stator and the b) assembly of the motor generate bending in modes x' and y' directions when only one plate is driven with an AC signal. The 2.4 mm in diameter and 10 mm long motor outputs 1.8 mNm torque with a peak speed of 60 rad/s, 60×10^{-3} W power and a 25% efficiency. (Copied from [3])

One of the most successful commercial ultrasonic motors is the propagating wave rotary motor developed by Sashida [4]. Variations of Sashida's basic design create a traveling elastic wave arising from the rotor's contact with a rippled surface driven by alternating sine and cosine voltage inputs as pictured in Figure 5-2. Sashida's design has found commercial use in the Canon EOS line of lenses because of the motor's small size, silent drive, and low power consumption compared to DC electric motors.

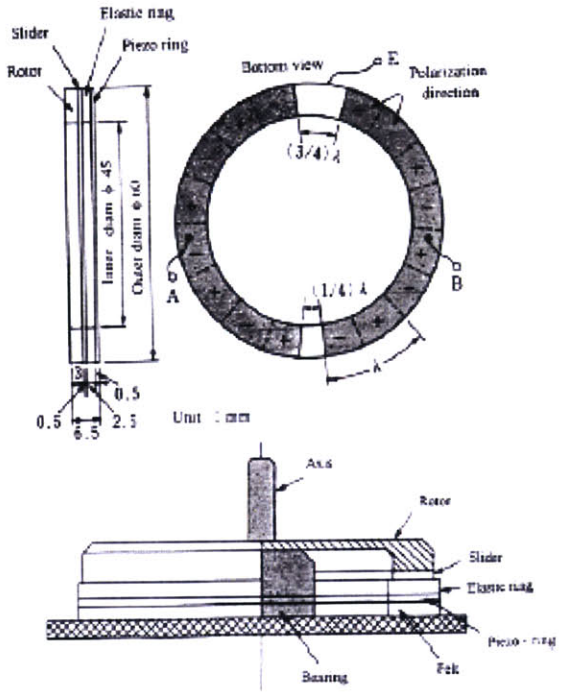

Figure 5-2: The Sashida stator structure and alternating sine and cosine voltage input layout. (Copied from [4])

A torque verses speed plot Figure 5-3 performed by Sashida demonstrates the high torque at low velocity needed in applications for his first motor dimensioned to 60 mm in diameter and 2.5 mm in height. A key design improvement into Sashida's motor is the toothed elastic ring. The teeth improve the mechanical coupling between the piezo vibration and the output shaft displacement for higher speeds, improved torque, and a reduction in intermittent coupling.

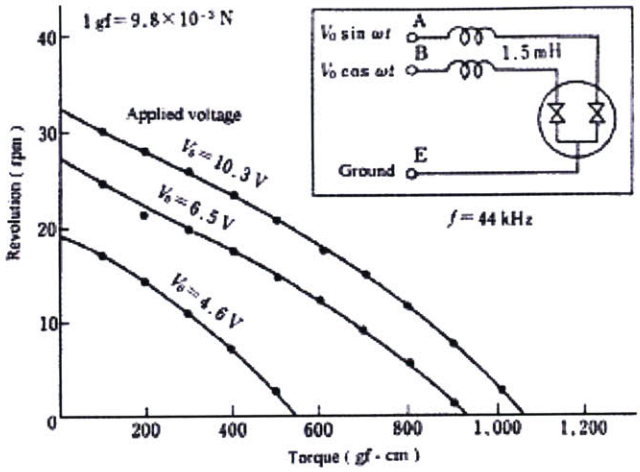

Figure 5-3: Motor performance of Sashida's original surfing rotary motor. (Copied from [4])

Ultrasonic piezoelectric motors have promise as a small niche technology for precise movement over a short time period not requiring constant forces. Despite the technological promise, ultrasonic motors have tremendous hurdles to be crossed because of a poor coupling efficiency, adverse thermal affects, and questionable robustness. Other technologies of finite displacement applied to create infinite output displacement still need even more research such as shape memory alloy and electroactivate polymer motors.

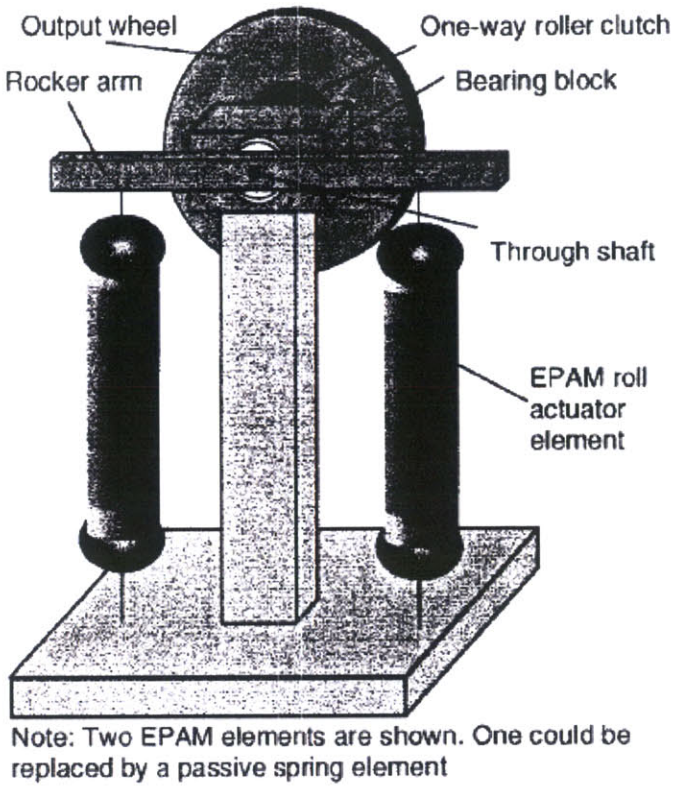

Figure 5-4: Simple Rotary Motor Based on EPAM Actuator Elements. (Copied from [5])

The concept of an EAP rotary engine was first envisioned by Kornbluh et al. [5]in 1998. Further prior art regarding the concept of electoractive polymer rotary motors are evidenced by US Patent # 6,084,321 Hunter et al. which has since been further refined by US Patents 6,249076 and 6,806,621. Kornbluh's successfully manufactured electroactive polymer based rotary motor prototype employed electrostrictive polymer actuating materials (EPAMs) as the preferred EAP actuator. The EPAM actuator actively displaced the motor's rocker arm and one way clutch as pictured in Figure 5-4. The EPAM rotary motor was able to achieve a maximum output rotational speed of 110 rpm and a maximum torque of 1.5 mN·m. Operating the EPAM element at its resonant frequency resulted in a maximum shaft output power density of about 100 W/kg. Kornbluh states that optimizing the EPAM actuator with the full 34 J/kg specific energy could theoretically produce a rotary motor power density of 300 W/kg, which would be on par with Sashida's motor and other piezoelectric actuators.

Although no literature can be found on Kornbluh's motor developing beyond its initial embodiment in 1998, his concept model proves the capability of conducting polymers actuators generating infinite rotary motion.

5.3 Helical Twisted Film Rotary Motor

5.3.1 Concept

A classical micrometer design requires the strain hardened induced plastic deformation of a single twisted metal film with two Sections that have opposing clockwise and counter-clockwise orientations. A dial indicator then placed at the meeting point of the opposing twisted orientations would subtend an angular tip displacement as the strain hardened micrometer was either compressed or expanded. This embodiment of a classical micrometer was able to produce angular displacements up to 40,000 times greater than the linear compression/ expansion of the device [Jones, F., *Ingenious Mechanisms for Designers and Inventors, Vol. III,* Industrial Press. 1997].

The classical micrometer provides a design benchmark for a helical twisted conducting polymer film rotary motor. Due to difficulties inducing plastic deformations in conducting polymers, a novel isometric approach was developed. A conducting polymer's active electrochemical properties can circumvent the polymer's inability to be plastically deformed to a desired geometry by inducing active tension within the twisted film. The electrochemical reduction across the polymer film would in effect mimic the tensile deformation of the classical micrometer as it is stretched. The following Sections will discuss finite element and analytical models describing the helical film motor followed by manufacturing techniques and experimental results.

5.3.2 Analytical Rotary Motion Model

The ANSYS finite element model in Section 5.3.3.2 serves as a useful visual tool for observing the difference in angular displacement between various geometric models, but fails to accurately predict the angular displacement value. Due to its limitations, an analytical model developed in this Section describes the expected experimental rotation from the helical twisted film motor.

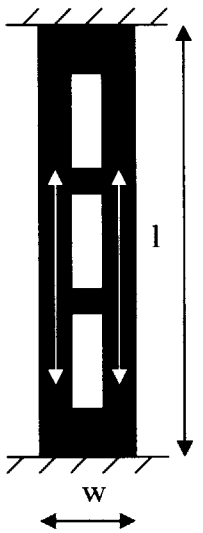

Figure 5-5: Geometry of helical film prior to twisting.

Rotary motion within a twisted conducting polymer film is generated due to the unique geometry of the polymer film. Rectangular cutouts in the film allow for a twisted film with a geometry analogous to the double helix shape of DNA. The two sub-planar films created lie along sides A and B pictured in Figure 5-5. The cross-Sectional geometry of the sub-planar films A and B then undergo a change in curvature from the induced electrochemical strain upon oxidation and reduction of the conducting polymer film. The change in curvature is monitored by the angular displacement of gauges which lie tangent to the sub-planar film's cross-Sectional curvature. The following analytical Equations predict the rotary motion created from the curvature change in the sub-planar films A and B.

We begin with the initial geometry of the polymer film rotary motor prior to twisting, which yields the length l and width w of the motor in Figure 5-5. Figure 5-6 depicts the height, h, and diameter of the twisted helix, $d(\varepsilon)$, as a function of the electrochemical strain ε. For purposes of this derivation, the analytical model presented assumes that the electrochemical strain undergone in the polymer is uniform in all directions such that sub-planer film A and B undergo identical deformations. Therefore, only sub-planar Section A will be modeled under the assumption that the Equations of motion for sub-planar film B are identical.

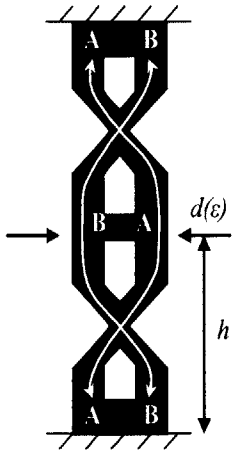

Figure 5-6: Geometry of film post helical twist.

When the planar film in Figure 5-5 is twisted and clamped as shown in Figure 5-6, the sub-planar film A forms one half of the double helical form. For the purposes of analytical modeling, sub-planar film A will be modeled as a screw which is radially unwrapped into an inclined plane as shown in Figure 5-7 where h is the polymer length undergoing one full twist, $d(\varepsilon)$, represents the width of the twisted polymer as a function of the active strain, and φ is the incline angle.

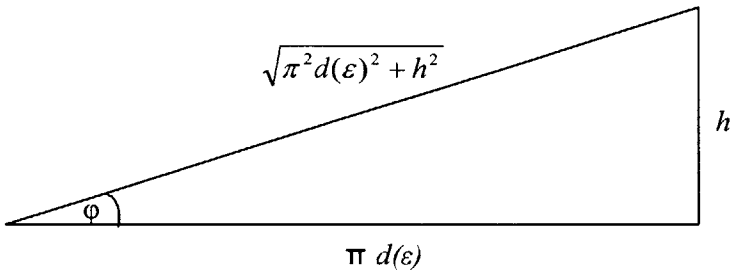

Figure 5-7: The helical screw in Figure 13 formed by the sub-planar film is expressed as an incline plane.

Geometrically, the sub-planar film A can also be represented as a circle pictured in Figure 5-8 where C is the circumference, r is the radius, s(Q) is the induced displacement as a function of charge Q, and θ is the angle that point X subtends as s changes.

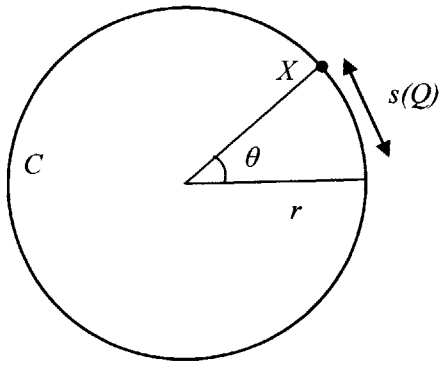

Figure 5-8: The circular representation of Figure 5-7 expresses the hypotenuse length of the incline plane equal to C with a subtended angle θ from a horizontal reference.

The following Equations relate Figure 5-7 and Figure 5-8 to establish geometric constitutive Equations.

$$s(Q) = r\,\theta\,, \tag{5.4}$$

$$C = 2\pi \cdot r \quad , \tag{5.5}$$

$$s = \frac{C}{2\pi} \cdot \theta \ . \tag{5.6}$$

Recognizing that the circumference C is equal to the hypotenuse length in Figure 5-7, we set

$$C = \sqrt{\pi^2 d(\varepsilon)^2 + h^2} \ . \tag{5.7}$$

Solving for the angle θ that point X subtends as $s(Q)$ electrochemically strains gives,

$$\theta = \frac{2\pi \cdot s(Q)}{\sqrt{[\pi \cdot d(\varepsilon)]^2 + h^2}} \ . \tag{5.8}$$

The conceptual visualization of the twisted conducting polymer film motor as a circle ideally depicts the mechanical deformations causing the rotary motion of the gauge. An axial view along the helically twisted sub-planar polymer relates the circular shape drawn in Figure 5-8 and Figure 5-9 below. The initial state of the polymer in its neutral dopant

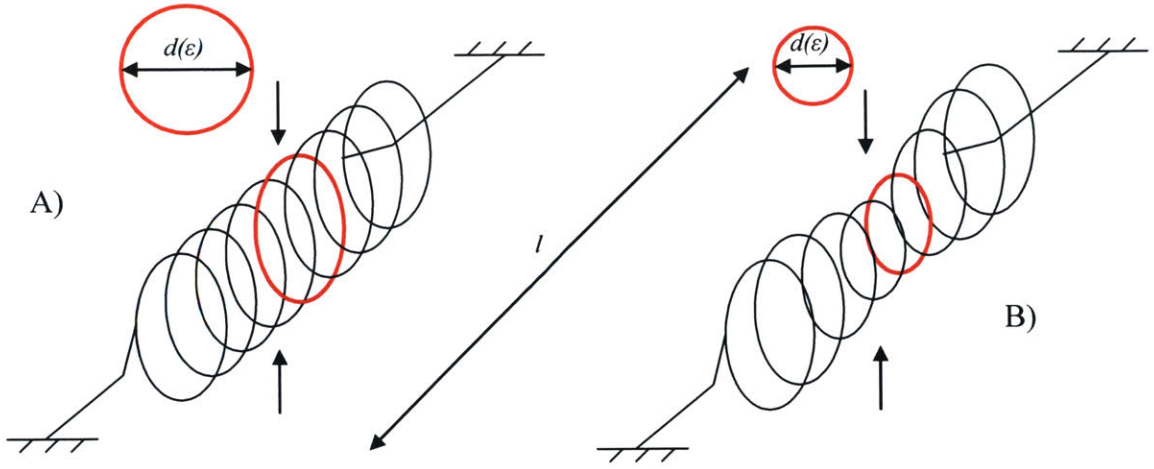

Figure 5-9: A trace of the helical sub-planar film. A) The helical film is in an initial stress state prior to reduction induced tension. B) The helical film has been reduced and the resulting contraction created a tension which reduced the inner diameter of the helical film.

state is depicted by the helical shape of the sub-planar polymer film in Figure 5-9.A. The reduced polymer state in Figure 5-9.B depicts the shape deformation undergone during electrochemically induced strain. The reduction in the sub-planar film's diameter is due to the clamped ends of the twisted radial motor. The following constitutive Equation must be satisfied where,

$$l_i = l_f \Rightarrow \therefore \Delta l = 0 . \tag{5.9}$$

Equation 5.9 states that the initial length, l_i, is equal to the final length, l_f, such that the overall change in length polymer film during electrochemical oxidation and reduction is zero. The isometric conditions in the twisted motor imply that during electrochemical actuation, the induced strain will cause 1) the cross-Sectional stress to increase and 2) the helical diameter $d(\varepsilon)$ in Figures 5-6 through 5-8 to decrease.

The motion pictured in Figure 5-9 produces a rotary motion monitored via a rotary gauge as pictured in Figure 5-10 below. The rotary gauge tracks the tangential rotary motion of

the cross-Sectional rotation of sub-planar film A during oxidation of the conducting polymer film.

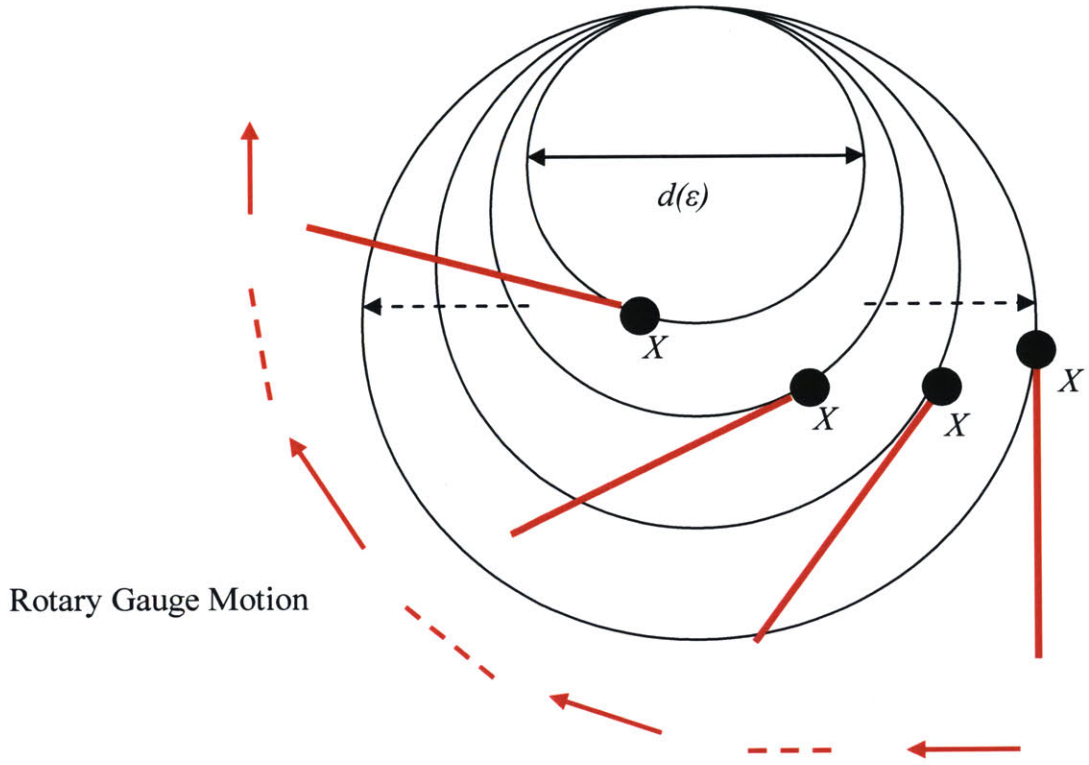

Figure 5-10: The red rotary gauge extends along the tangent of the sub-planar film at point X as an indicator of rotary motion.

The geometrical concepts of Figures 5-9 and 5-10 combine to form Figure 5-11 which depicts the geometric relationship between the induced strain within the polymer and the associated rotary deflection. From trigonometric relationships, the angle subtended by the rotary gauge as the effective diameter decreases from $d(\varepsilon)_1$ to $d(\varepsilon)_2$ during an electrochemical strain, is equivalent to $\Delta\theta$ as pictured.

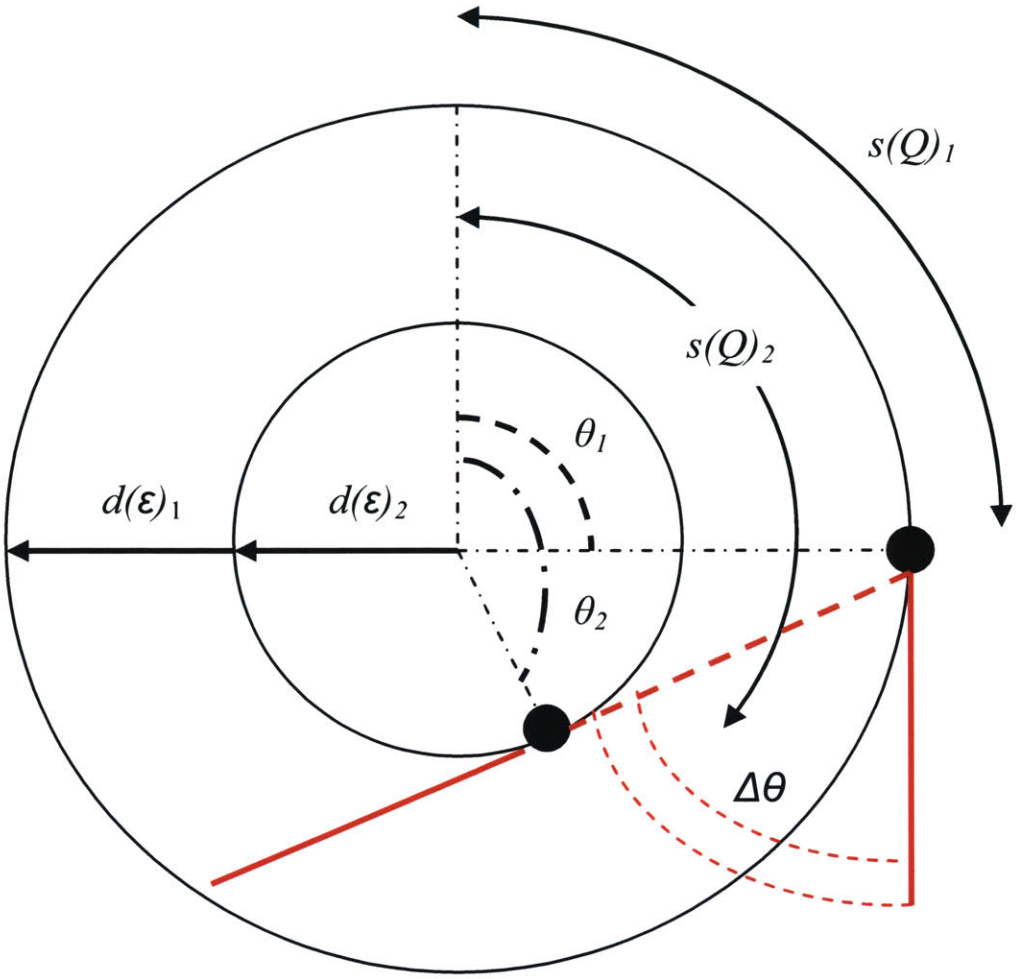

Figure 5-11: View of the major axis along the helical twisted film depicting the neutral dopant state by subscript 1 and the reduced dopant state by subscript 2.

It should also be noted that the forthcoming Equations assume that

$$\Delta s(Q) << \Delta d(\varepsilon), \tag{5.10}$$

based upon the major affects of the strain acting axially to reduce the effective diameter of the helix such that

$$s(Q)_1 = s(Q)_2. \tag{5.11}$$

Equations 5.12-5.14 below describe the geometric and constitutive relationships depicted in Figure 5-11. The constitutive equation describing the relationship between the diameter $d(\varepsilon)_i$ and angle subtended θ_i is

$$d(\varepsilon)_1\theta_1 = d(\varepsilon)_2\theta_2. \tag{5.12}$$

Solving Equation 5.12 for $\Delta\theta$ we find

$$\Delta\theta = \theta_2 - \theta_1 = \frac{d(\varepsilon)_1\theta_1}{d(\varepsilon)_2} - \frac{d(\varepsilon)_2\theta_2}{d(\varepsilon)_1}. \tag{5.13}$$

We can next solve Equation 5.12 for θ_1 and substitute that relationship into Equation 5.21 to give

$$\Delta\theta = \frac{d(\varepsilon)_1\theta_1}{d(\varepsilon)_2} - \frac{d(\varepsilon)_2}{d(\varepsilon)_1}\left(\frac{d(\varepsilon)_1\theta_1}{d(\varepsilon)_2}\right) = \left\{\frac{d(\varepsilon)_1 - d(\varepsilon)_2}{d(\varepsilon)_2}\right\}\theta_2. \tag{5.14}$$

As pictured in Figure 5-8, the angle subtended by θ_1 has a value based on a chosen reference (in this case from vertical). Substituting a similar reference for θ_1 as depicted in Figure 5-8, we will choose the following such that

$$\theta_1 = \frac{\pi}{2}. \tag{5.15}$$

Substituting Equation 5.15 into Equation 5.14, we now find that the angle subtended can be described as

$$\Delta\theta = \left\{\frac{d(\varepsilon)_1 - d(\varepsilon)_2}{2 \cdot d(\varepsilon)_2}\right\}\pi, \tag{5.16}$$

where $d(\varepsilon)_i$ is a function of the electrochemical strain. The exact value for $d(\varepsilon)_i$ can be found both through visual measurement during experimentation or from a yet to be determined correlation between the diameter of the helix and the electrochemical strain.

Coincidently, Equation 5.8 and Equation 5.16 yield comparable results if *s(Q)* is estimated to undergo a strain of 2 % such that

$$\Delta\theta = \frac{2\pi \cdot s(Q)}{\sqrt{[\pi \cdot d(\varepsilon)]^2 + h^2}} \cong \left\{\frac{d(\varepsilon)_1 - d(\varepsilon)_2}{2 \cdot d(\varepsilon)_2}\right\}\pi. \tag{5.17}$$

The analytical model in this Section accurately describes the rotary motion of the helical motor. To better visualize the motion of the motor, the following Section uses finite element analysis to determine where maximum rotary motion occurs within the helical motor's geometry.

5.3.3 Finite Element Linear and Rotary Models

This Section describes the utilization of finite element analyses for a conducting polymer actuator, specifically polypyrrole. Two analyses are presented in this Section. The first analysis provides a thorough investigation into the capability of FEA to describe the electrochemical actuation of PPy. The second analysis demonstrates the fundamental rotary motion achieved by the helical twisted film motor under isotonic conditions. For

both cases the established design parameters are based on analytical, computational, and experimental modeling of the mechanical properties of polypyrrole.

5.3.3.1 Finite Element Modeling of Electrochemical Actuation in Polypyrrole

Analytical models [6,7] describing actuation of polypyrrole are based on electromechanical and chemical coupling of the polymer and ions in the electrolyte sink. In order to represent the model within FEA, the analytical model needs to be further investigated to establish a model that is acceptable in the ADINA finite element software package. Much focus is placed on the proper dimensional analysis needed to adapt the published analytical models to the ADINA software (http://www.adina.com). Once the model has been adequately adapted to a coupled thermo-mechanical system, the ADINA results can be compared to initial analytical Equations and experimental results for polypyrrole testing.

The analytical model of polypyrrole is derived from the diffusive-elastic 'metal' model, which describes the polymer as an electrolytic capacitor with charging throughout its volume. The charging in the polymer produces a coupled electromechanical and chemical reaction as described by the strain equation

$$\varepsilon_{xx} = \frac{(1-2\nu)q_V^2}{2EC_V V^2} + \frac{\sigma_x}{E}, \tag{5.18}$$

where ε_{xx} is the strain along the major axis, ν is Poisson's ratio, q_v is the charge stored in the polymer, E is Young's Modulus, C_v is the volumetric capacitance, V is the polymer volume, and σ_x is the applied stress. Equation 5.18 can be rewritten as

$$\varepsilon_{xx} = \frac{\alpha q_v}{V} + \frac{\sigma_x}{E}, \tag{5.19}$$

where α is defined [6] as $\alpha = \frac{(1-2\nu)q_V}{2EC_V V} = \frac{(1-2\nu)e_V}{2E}$, (5.20)

and e_v is the applied potential. The strain to charge ratio, α, in Equations 5.19 and 5.20 are analogous to a thermal expansion coefficient, but for charge rather than temperature. Using dimensional analysis and the Buckingham Pi Theorem [http://scienceworld.wolfram.com/physics/BuckinghamsPiTheorem.html], the strain to charge ratio as defined in the electromehanical and chemically coupled Equations can be found for the desired thermo-mechanically coupled Equations needed for ADINA as described below:

$$\alpha = \frac{(1-2\nu)C_v e_v}{E}, \tag{5.21}$$

where C_v is the specific heat and e_v is the average applied temperature; thus creating the two dimensionally equivalent formulas for α. The thermo-mechanical α has the dimension θ^{-1}, which matches the intuitional units of $\left[\frac{1}{Potential}\right]$. The next parameter needed for a thermo-mechanical ADINA analysis is the thermal conductivity, *k*.

The solution to Fick's Law [http://en.wikipedia.org/wiki/Fick's_law_of_diffusion] for the diffusion process of ions in the polymer is analogous to the solution of current through a transmission line, which Madden [7] noted can be modeled using a reticulated network of linear circuit elements. The reticulated network allows for a linear representation of the conducting polymer network to ease the study and match well with the computational analysis using the ADINA software package. The diffusion transmission line below uses

an electrical circuit configuration with voltage equivalent to the polymer's ion concentration and the current equivalent to the ion flow into the polypyrrole.

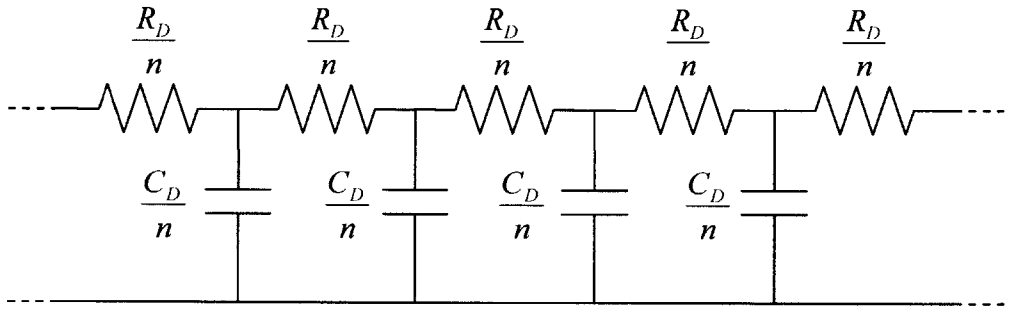

Figure 5-12: Diffusion Transmission Line modeled as an Electrical Circuit

The elements, n, in the transmission line represent each monomer in the polymer chain as the ions flow through the network and encounter the diffusive resistance, R_D, and the diffusive capacitance, C_D. The electrical circuit above can be represented as a matrix in the Laplace domain (Laplace variable s) as described by Bowers [8] where the polymer's double-layer ion concentration is V_p and i_D is the ion flow in the polymer. The diffusive resistance pictured in the transmission line is described by the equation for

$$R_D = \frac{2a\delta}{DC_p}, \tag{5.22}$$

where a is the thickness, δ is the double layer ion thickness, D is the diffusivity, and C_p is the polymer's double layer capacitance. To convert from the diffusive resistance to the thermal conductivity, the following relationship must be implied

$$k = \frac{1}{R_D} = \left(\frac{DC_p}{2a\delta}\right), \tag{5.23}$$

where k is the thermal conductivity. To complete the thermo-mechanical model, the specific heat $C_{v\text{-}thermal}$ must be found from the electrical capacitance $C_{v\text{-}electrical}$ as described by

$$C_{v-thermal} = \frac{C_{v-electrical}}{\rho}, \text{ where } \rho \text{ is the polymer's density.} \tag{5.24}$$

The formulas for α, k, and $C_{v\text{-}thermal}$ complete the necessary conversions from the electromechanical and chemically coupled analytical model of the conducting polymer (polypyrrole) to an acceptable thermo-mechanical system for use with the ADINA software. The necessary constants for the finite element analysis are listed below in Table 5.1 along with their equivalent dimension. The actual values used for the ADINA analysis are found using the MATLAB script attached in the Appendix B.

Table 5.1: Dimensional Analysis Results for Finite Element Analysis

Electrochemical and mechanical		**Thermo-mechanical**		**Dimension**
$\alpha = \frac{(1-2\nu)q_V}{2EC_V V} = \frac{(1-2\nu)e_V}{2E}$	→	$\alpha = \frac{(1-2\nu)C_v e_v}{E}$	→	$\Delta\Theta^{-1}$
$R_D = \frac{2a\delta}{DC_p}$	→	$k = \frac{1}{R_D} = \left(\frac{DC_p}{2a\delta}\right)$	→	$MLT^{-3}\Theta^{-1}$
$C_{v-electrical}$	→	$C_{v-thermal} = \frac{C_{v-electrical}}{\rho}$	→	$L^2T^{-2}\Theta^{-1}$
Δ *Voltage (Potential)*	→	Δ Temperature	→	$\Delta\ \Theta$

The thermo-mechanically coupled constants above allow for an experimental result to be comparatively modeled. A polypyrrole sample was electrochemically deposited to obtain a thickness of 20 μm as described by Schmid. The sample was then removed and characterized in a dynamic mechanical analyzer under isotonic loading at 2 MPa. The voltage was then increased from 0.0 V to 1.0 V from the open circuit potential for active testing. The data from the experiments was plotted to observe the steady state displacement for a correlating voltage input with MATLAB (See Appendix B). The displacements in the Figure 5-13 depict the steady state polymer response to a stepped potential input.

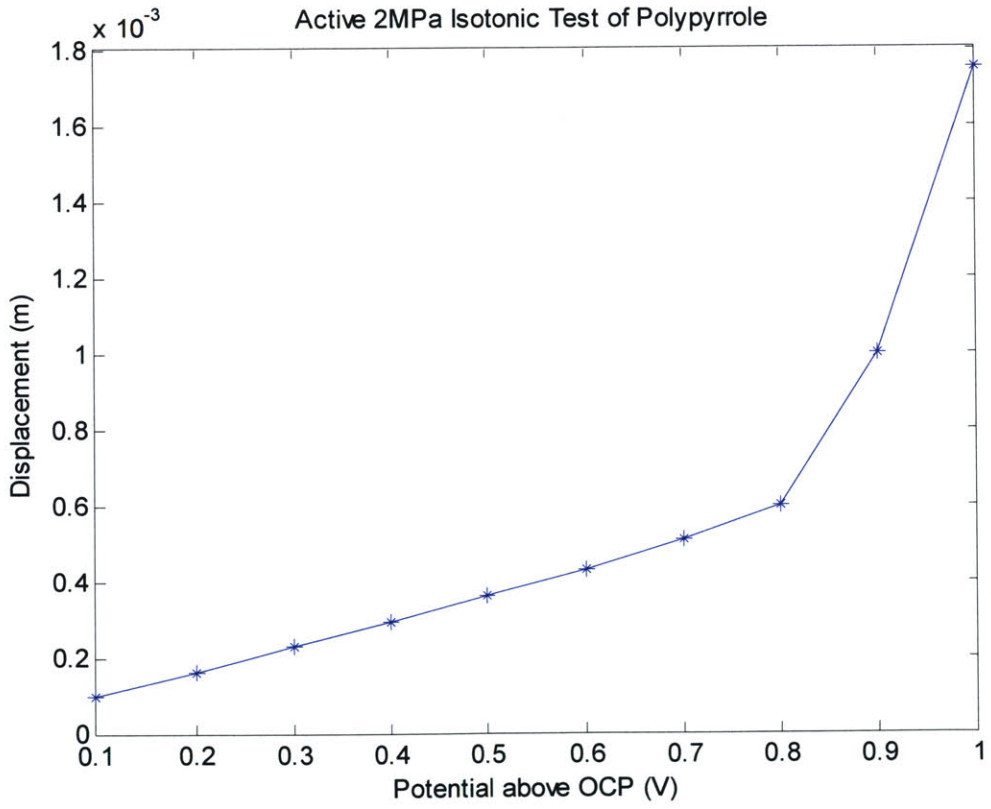

Figure 5-13: The experimental displacement obtained from active testing of polypyrrole under a 2 MPa load.

As expected the conducting polymer's response is linear prior to its degradation point (~1.0 V), which approaches a non-linear solution.

The experiment was replicated using ADINA and the thermal analysis environment ADINA-T with the previously determined variables in Table 5.1 and the dimensions described in the Appendix B. A potential (temperature) was applied along the length of the 2D model to create a potential in the ADINA-T GUI within the linear response domain of the polypyrrole. An identical mesh as used in ADINA-T was then created in the ADINA GUI with an applied load of 2 MPa to the length of the polymer as pictured in Figure 5-14 below.

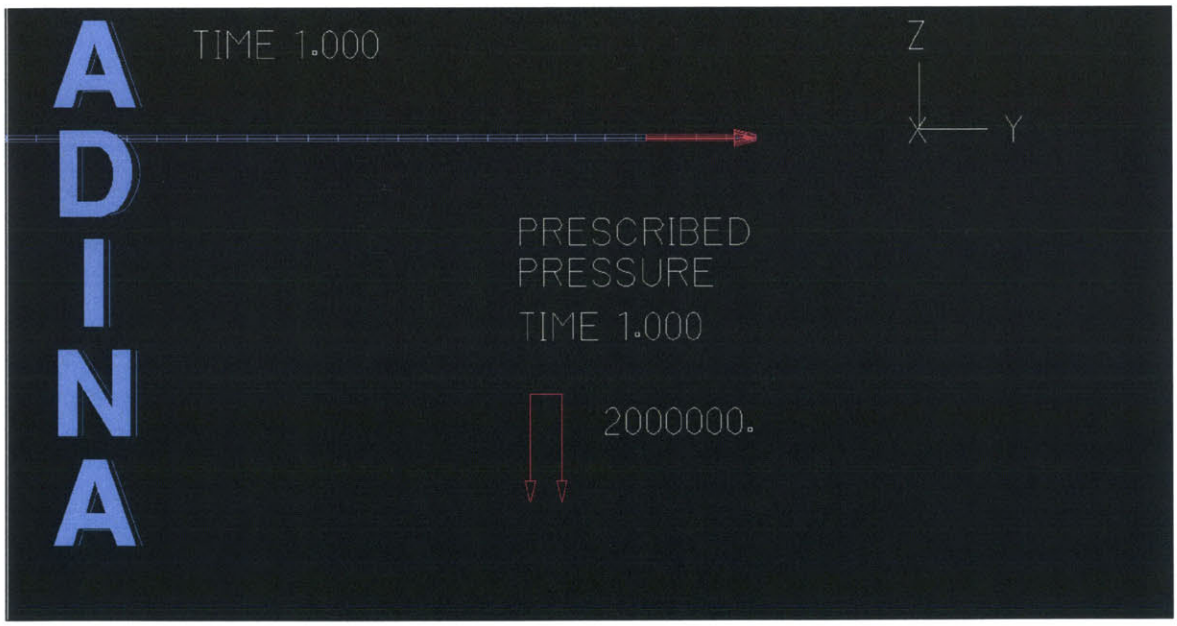

Figure 5-14: An isotonic 2 MPa load is applied to one end of the polymer.

The opposing end of the polymer (not pictured in Figure 5-14) was subjected to a boundary condition that constrained all degrees of freedom. The material properties were then defined as seen in Table 5.2 below.

Table 5.2: The material properties of the polymer for a mechanical analysis.

Temperature	Young's Modulus	Poisson's Ratio	Mean Coefficient of Thermal Expansion
0.0	10^{-8}	0.4	0.065
20.0	10^{-8}	0.4	0.065

Multiple meshes of different densities were used until a satisfactory result was obtained with an error on the same scale as the accepted analytical model while still maintaining a low cost analysis.

The final 100 × 2 mesh produced the following displacements as plotted against the experimental and analytical results also in Figure 5-15.

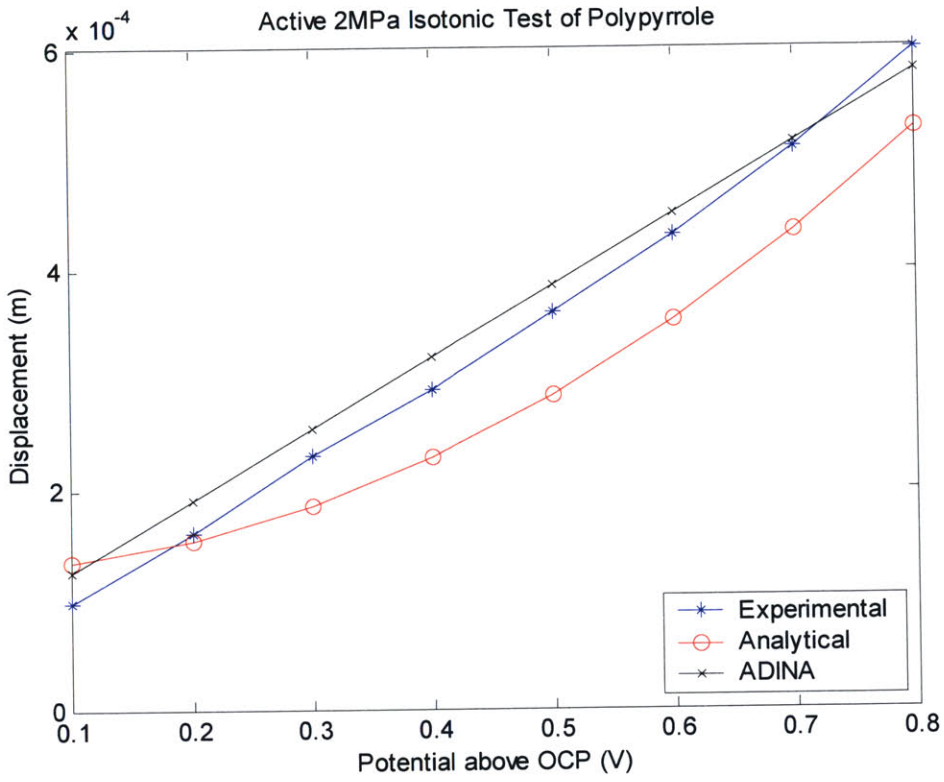

Figure 5-15: Analytical, experimental, and ADINA predictions of polymer displacement.

The analytical and computational models offer adequate representations of the experimental results obtained from the isotonic testing. The linear assumptions built into the ADINA model accurately match the experimental results within the linear domain, but quickly break down as the potential extends beyond 0.8 V. The percent error from the experimental error is less for the ADINA model than the analytical model as pictured in Figure 5-16 below.

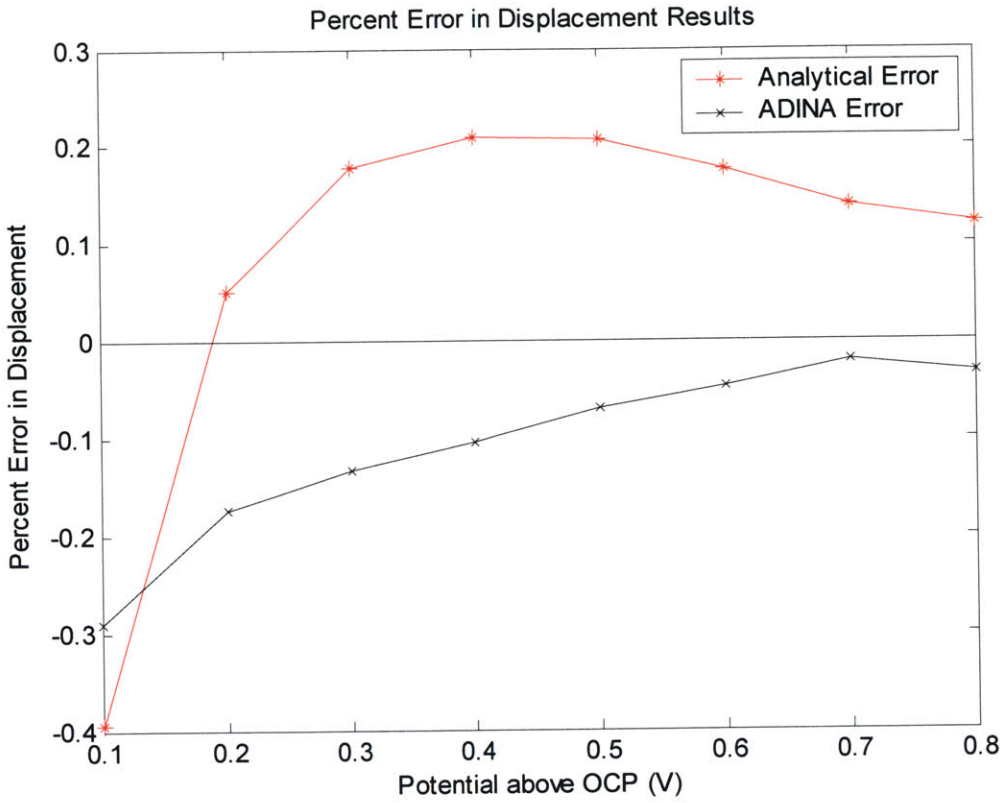

Figure 5-16: Percent error of the ADINA and analytical models.

Although up to a 29 % error exists in the ADINA model, which is above typically acceptable error values, the ADINA model more accurately represents the experimental results than the scientifically accepted analytical model. The predicted errors from the finite element ADINA model and the analytical model provided by Bowers can be attributed to the assumption that the polypyrrole film is a perfectly linear isotropic film without abnormalities. For the purposes of predicting actuation to allow engineering design of the geometry, both models are considered acceptable within the linear regime.

5.3.3.2 Finite Element Modeling of Rotary Motion in Helical Twisted Conducting Polymer Film

Having established an acceptable finite element model describing the actuation of polypyrrole through dimensional analysis, this Section will further employ finite element techniques to visualize the rotary motion obtained from linear isometric actuation of the helical twisted polypyrrole motor. ANSYS Workbench 9.0 and the variables described in Section 5.3.3.1 were used for the dynamic analysis of rotary motion in this Section.

Computer aided drawings (CAD) of the helical twisted polymer motor were created in the Solid Edge v16 software package [http://www.solidedge.com/] as an assembly of helically twisted Sections with a rotary gauge tangentially attached to each segment of the film. The assembly was then imported into the ANSYS Workbench 9.0 environment as a linear isotropic model. The opposing ends of the helical motor lying in the z-plane were then constrained in all degrees of freedom to represent the experimental isometric conditions for the helical rotary motor device. A given thermal load of 20 °C was then applied to the entire geometry along with the same material properties as described in Table 5.2 of Section 5.3.3.1 as pictured in Figure 5-17 below.

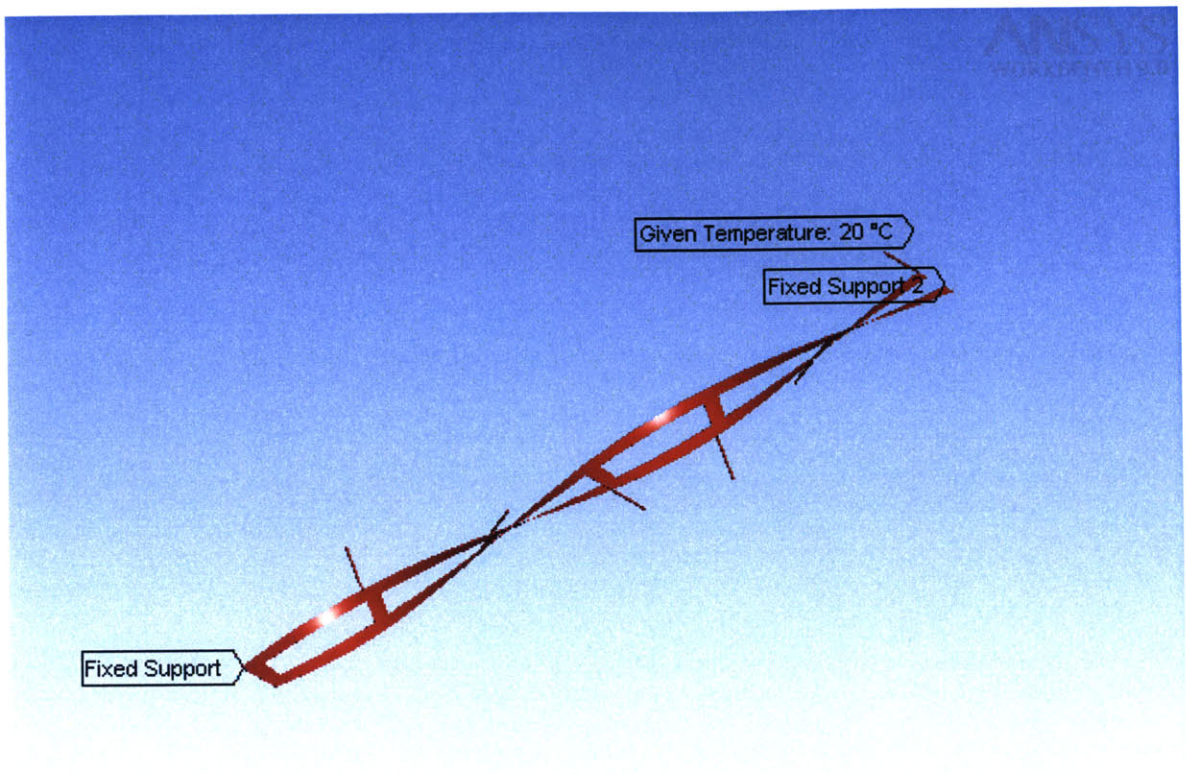

Figure 5-17: The fixed constraints and uniform potential load on the helical motor.

The ANSYS Workbench then solved for the total deformation undergone by the helical motor as pictured in Figure 5-18 below.

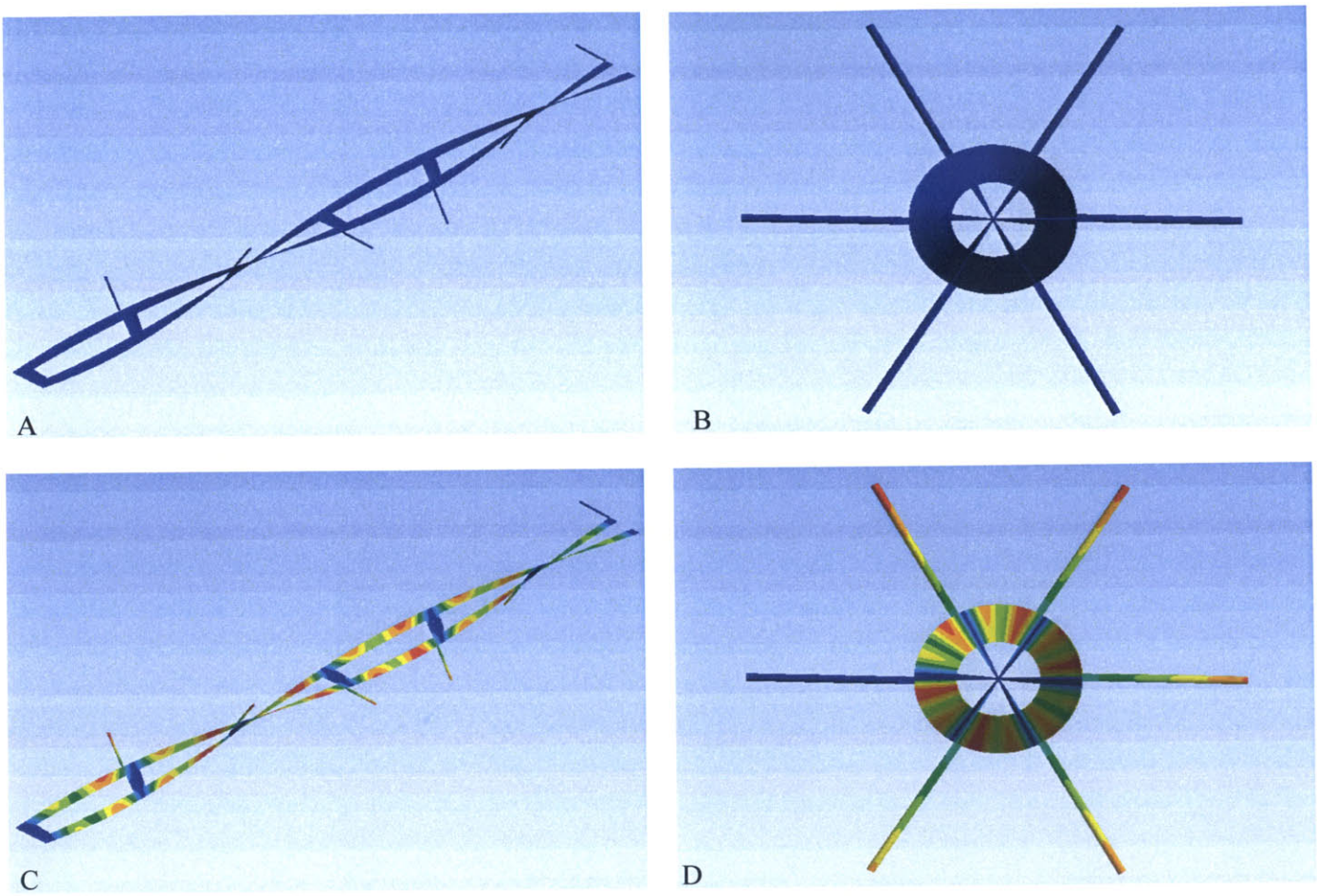

Figure 5-18: Pictures of the helical twist polymer motor in ANSYS Workbench A) Undeformed isometric view B) Undeformed axial view C) Deformed isometric view D) Deformed axial view.

The rotational deformation undergone by Figure 5-18.D can be best visualized with deformation vectors as shown in Figure 5-19. The maximum angular displacement

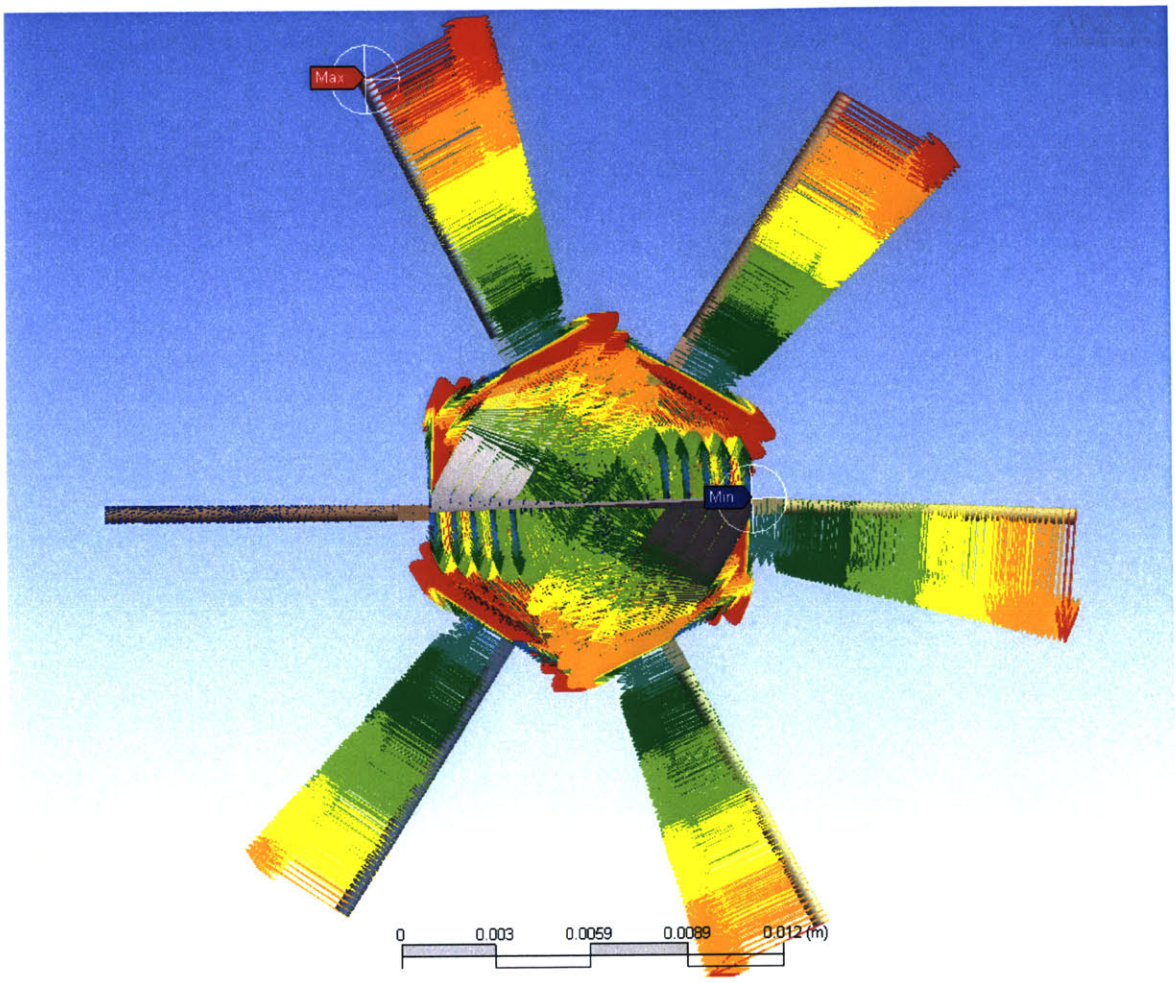

Figure 5-19: Rotational deformation expressed with vectors.

occurs at the outer tip of the angular gauge. When compared to experimental results, the ANSYS finite element model grossly underestimates the angular displacement subtended by the rotary gauge. The underestimate of the angular displacement can be attributed to the model's assumption that the polypyrrole material properties describe a linear isotropic material. This assumption does not allow for curvature of the tensioned film about the axis that the helical film is wrapped. As pictured in Figure 5-20 below, the deformations of the film only occur normal to the original geometry and do not exhibit curvature.

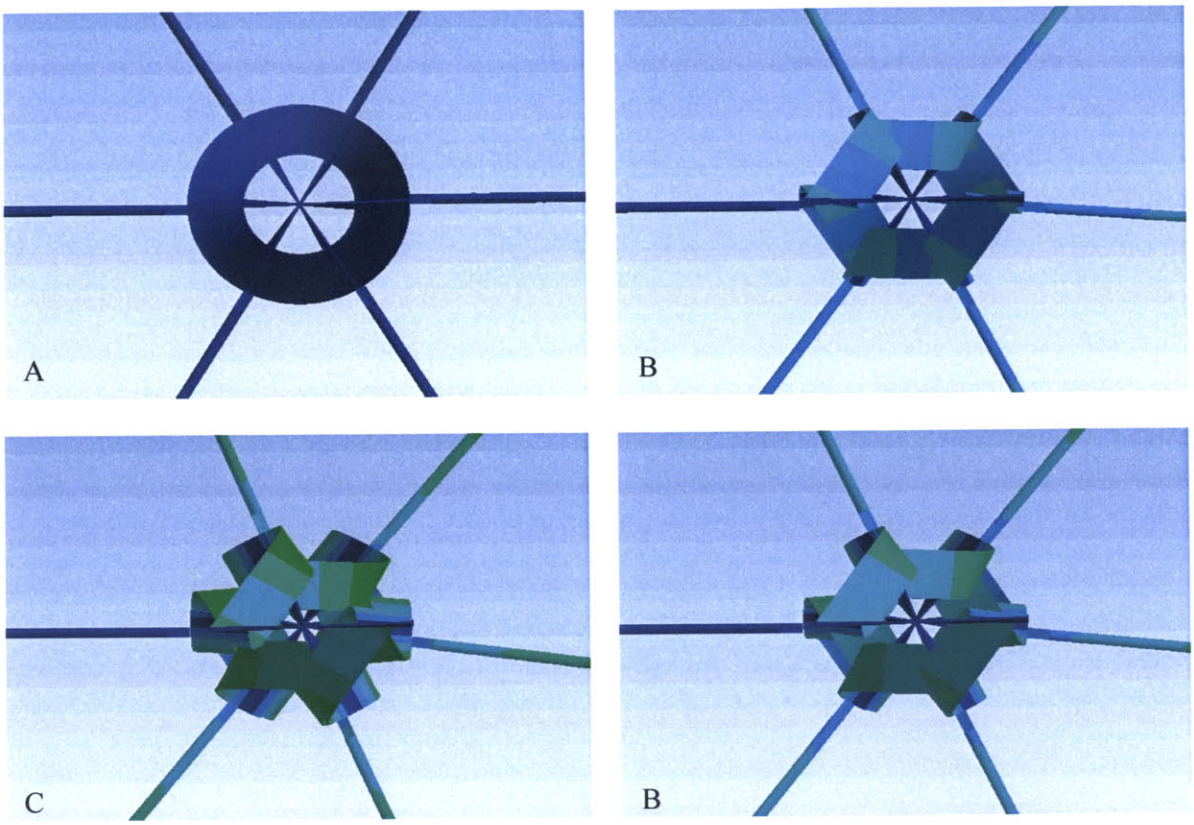

Figure 5-20: FEM sub-planar film displacements do not display curvature.

Since the model's boundary conditions do not account for buckling conditions in the sub-planar film due to anisotropic properties, curvature of the film about the central axis does not exist. Were the model to exhibit curvature about the central axis, the rotary gauge would subtend an increased angular tip displacement tangent to the curvature.

The ANSYS Workbench 9.0 finite element model lacks as an accurate description of the magnitude of the helical twisted film motor's angular displacement. However, the model serves as a powerful tool to prove that rotary motion can be obtained from a linear isometric reduction of the polymer without additional mechanical components. Moreover, the ANSYS model allows the engineer to manipulate geometric constraints of

the helical motor with a reliable representation of the difference in rotary motion between different geometries.

5.3.4 Design and Manufacturing

Construction of the helical twisted film rotary motor begins with the electrochemical deposition of the conducting polymer film. For the experiments carried out in this Section, the conducting polymer polypyrrole served as the conducting polymer of choice. Polypyrrole was synthesized in 0.05 M tetraethylammonium hexaflourophosphate, 0.05 M distilled pyrrolye, and 1 % by volume distilled H_2O in propylene carbonate solution. The solution was then placed in a – 40 °C heat transfer bath during deposition. The galvanostatic deposition employed a copper counter electrode and carbon working electrode to pass a 0.8 A/m^2 current density to electrochemically deposit the film for 12 to 15 hours. The deposition process produced films of 20 to 35 μm in thickness for construction of the helical rotary motor.

Polypyrrole films were then placed on a sacrificial acrylic sheet to be laser cut to the desired geometry as pictured below in Figure 5-21. Using a Trotec Speedy II (http://www.trotec.net) with the grey 50 mm lens at power 70, speed 20, and frequency 3000 Hz, the polymer was cut accurately with no noticeable adverse affects.

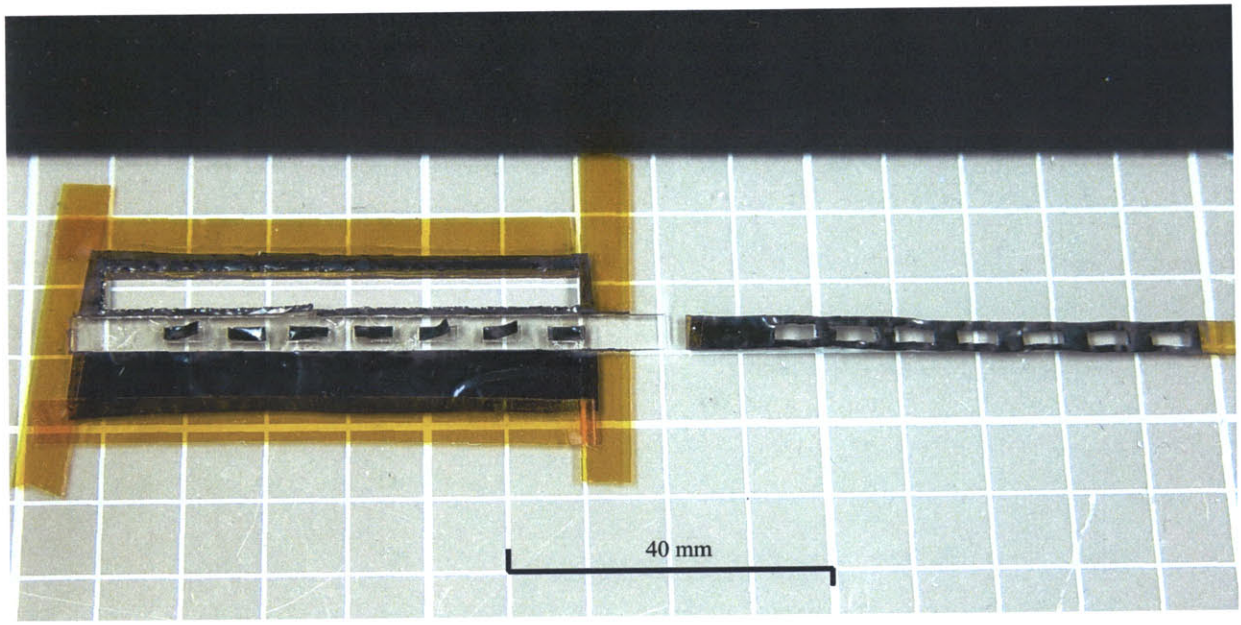

Figure 5-21: Polypyrrole film on a sacrificial acrylic substrate and the resulting laser cut geometry.

To assist in visualizing the rotary motion undergone by the helical motor during reduction, 300 μm glass capillaries were adhered using carbon epoxy as pictured in Figure 5-22.

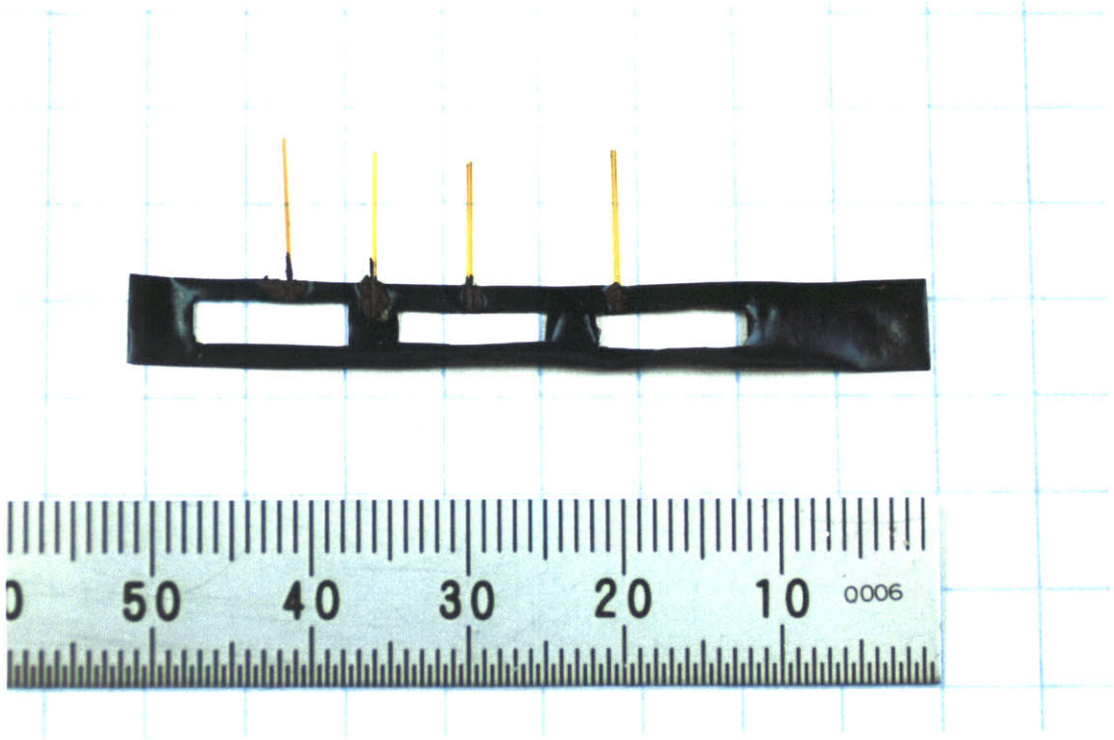

Figure 5-22: Glass capillaries adhered to PPy using conductive carbon epoxy along the tangent of the film.

The polymer film is then twisted into a helical shape as pictured in Figure 5-23.A and Figure 5-23.B.

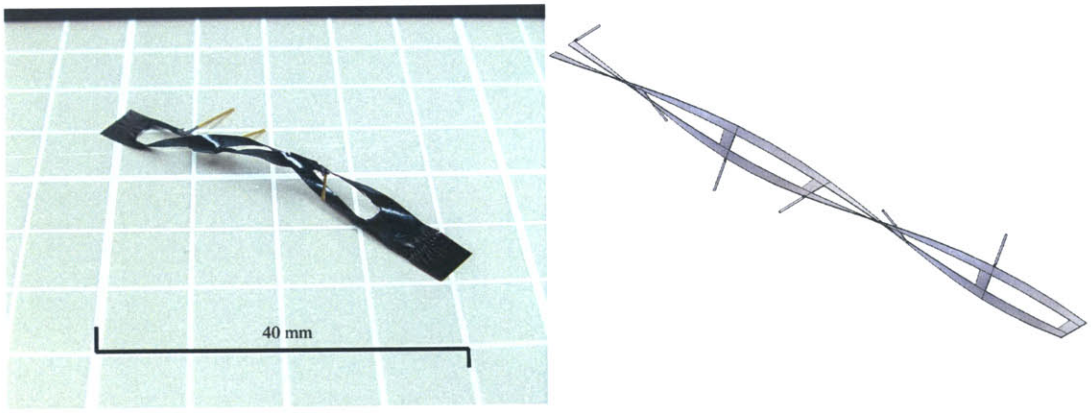

Figure 5-23: The manufactured helical twisted polymer film in Figure 5-23.A and computer aided drawing in Figure 5-23.B.

5.3.5 Experimental Procedures and Results

Characterization and actuation of the helical twisted film motor is conducted within the ECDMA. The particular 85 mm by 5 mm helical motor characterized in this Section has seven 5 mm by 2 mm cutouts evenly spaced between the clamped ends. The helical film motor is clamped and tensioned to 0.2 MPa to optimize motion of the rotary gauges. The stage is then locked in place for testing. The final mounting configuration of the motor is depicted in Figure 5-24.

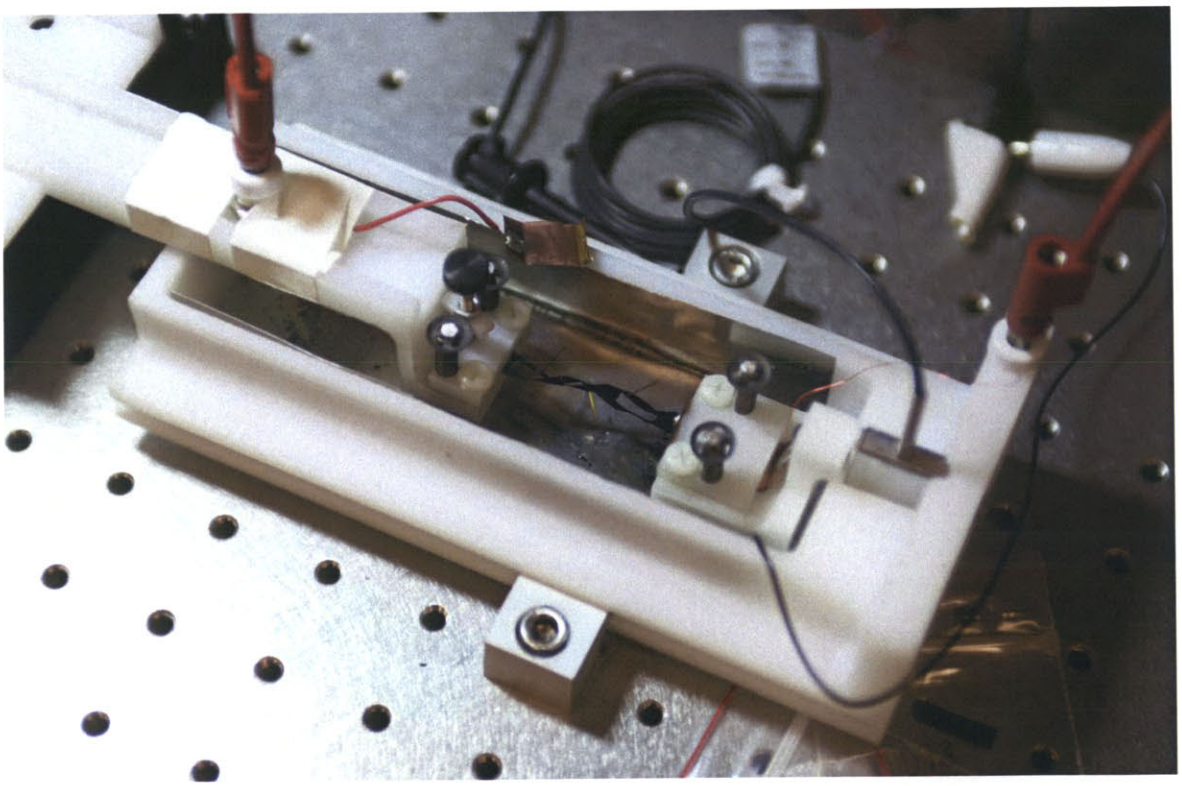

Figure 5-24: Helical twisted film motor mounted in ECDMA.

The helical motor was actuated under galvanostat control with square waves of differing amplitudes as pictured in Figure 5-25.

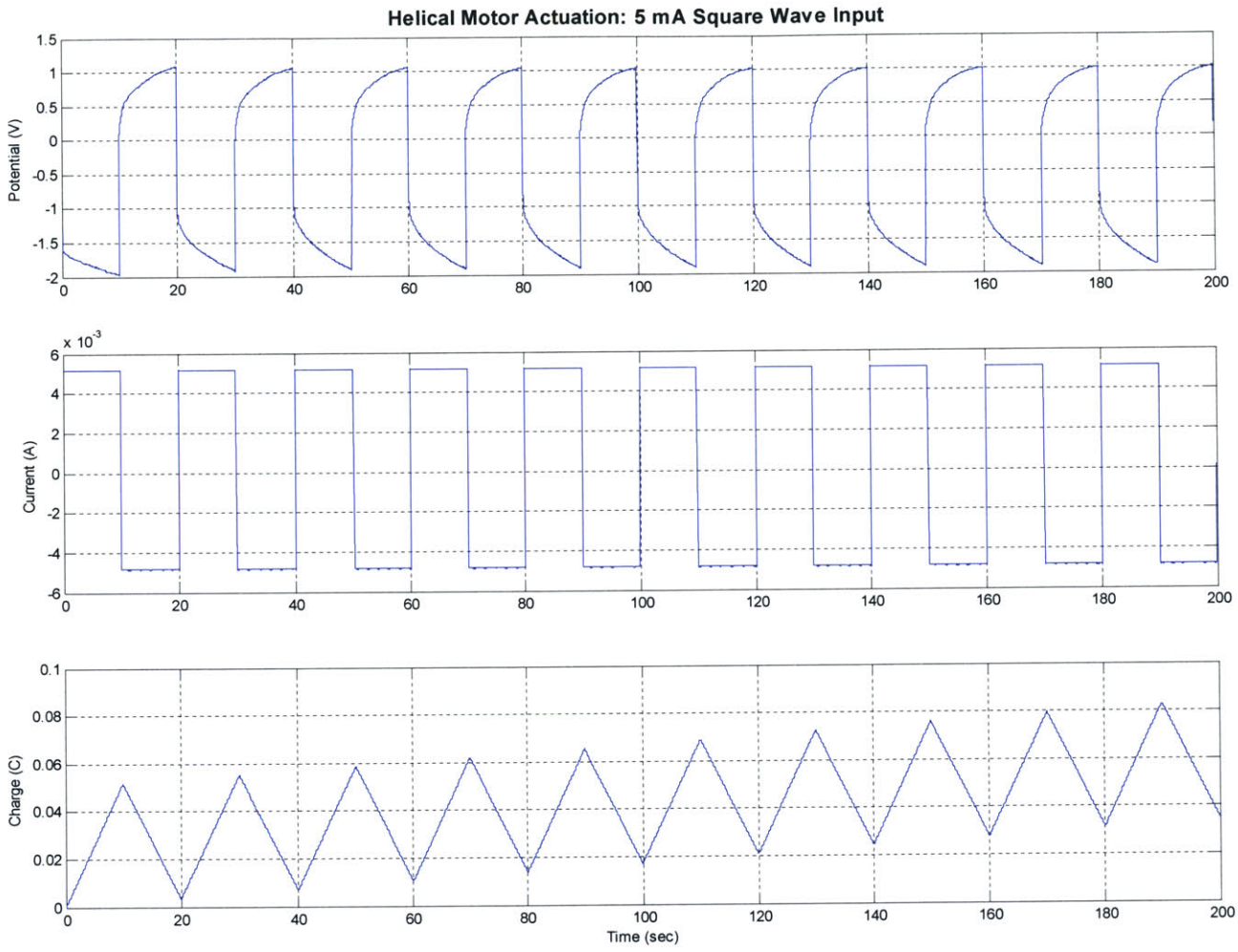

Figure 5-25: Electrochemical response for the helical motor with a 5 mA square wave input.

The electrochemical input produces an active strain within the motor that induces rotary motion. Rotary gauges placed in the center of each cutout capture the maximum rotary displacement as shown by finite element analysis in Section 5.3.3.2. The resulting motion was monitored and recorded using a Canon XLS1S Digital Video Recorder. The video camera was operated to capture full field (non-interlaced) imaging at 30 frames per

second at a resolution of 720 by 480 pixels. All videos were then transferred to a computer as an uncompressed AVI file for analysis.

Still images of the helical motor were then captured from the video for image processing with Adobe Premiere Pro 1.5 and Adobe Photoshop 7.0. [http://www.adobe.com] Images of the rotary gauge at either extreme of its motion were overlaid in Photoshop to determine the angle subtended by the gauge

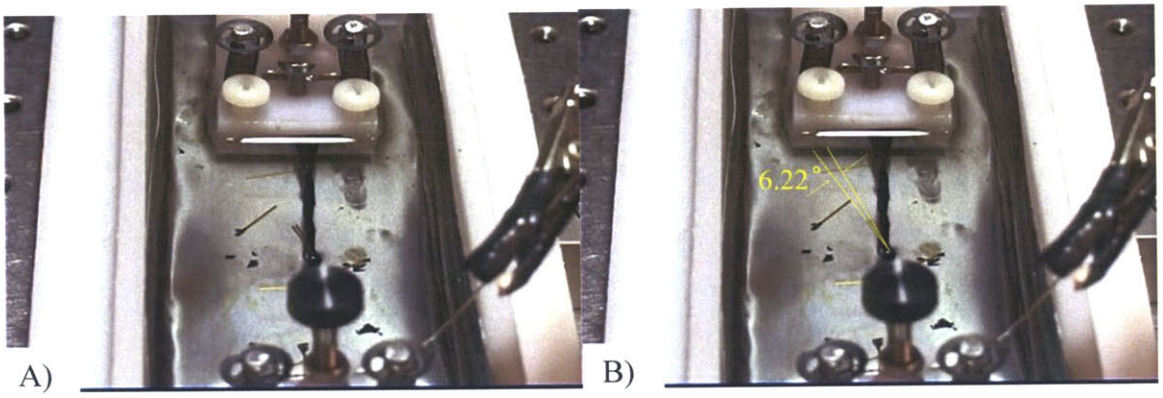

Figure 5-26: Overlaying images depicting rotary Motion from 5 mA input.

as pictured in Figure 5-26. The angle subtended was determined by placing vectors over the rotary gauges in Photoshop as pictured in Figure 5-26 B. The bounding rectangle for each vector yielded the dimensions of 258 × 193 pixels and 264 × 156 pixels. Using trigonometry from the dimensions of the bounding rectangles, the angular displacement of the rotary gauge was 6.22° from the camera's viewing angle above the experiment. The exact viewing angle and distance of the camera from there experiment were not recorded to determine the exact angular rotation of the rotary gauge.

5.4 Conducting Polymer Actuated Rotary Eccentric Motor

5.4.1 Concept

A conducting polymer actuated rotary eccentric motor generates infinite rotary displacements of an eccentric about its axis from finite linear displacements. Compared

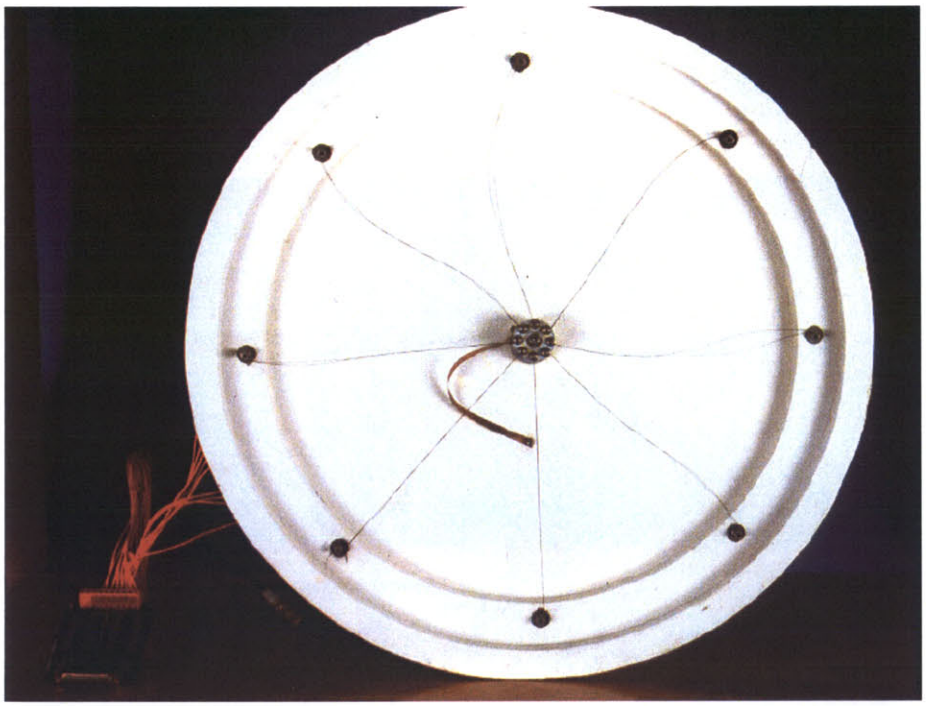

A)

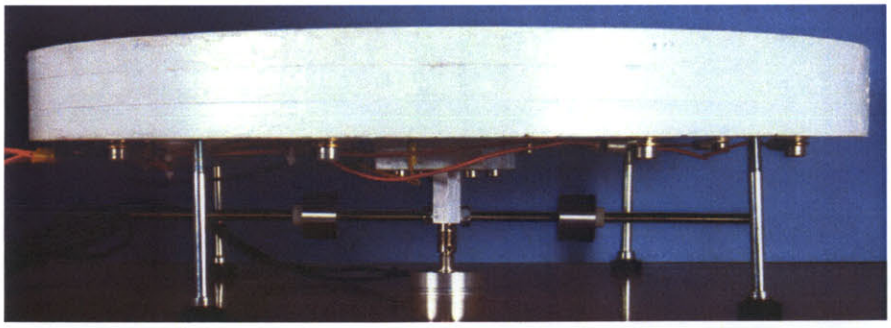

B)

Figure 5-27: The NiTi Rotary motor by Lafontaine [9] produced a peak shaft speed of 6.7 rotations per second and a peak torque of 0.1 Nm. A) Top View. B) Side View

to the helical twist EAP film motor, this motor allows for the output shaft to be readily

connected to a device and is also not limited to only 360° of rotation. The design and inspiration for this motor begat from a nickel titanium shape memory powered rotary motor [9] pictured in Figure 5-27 and from US Patents # 6,249,076 and # 6,806,621.

Although the embodiments of conducting polymer rotary eccentric motors have been published, no motors constructed to date have demonstrated working functionality. Figure 5-28 represents a rotary eccentric motor patented by Kornbluh that uses electroactive polymers to create the motion.

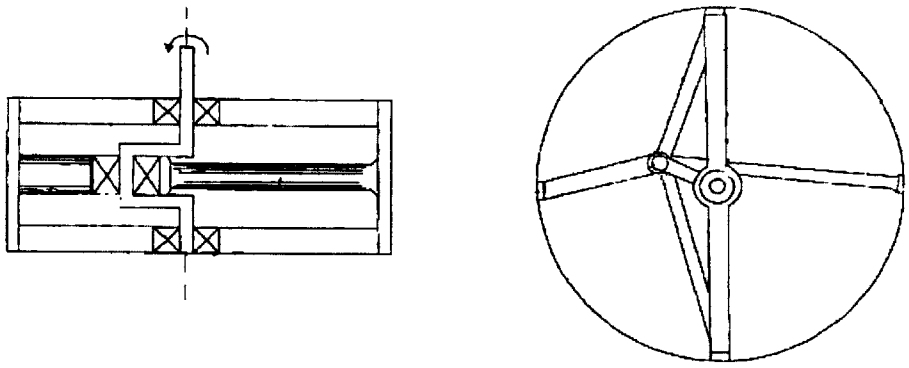

Figure 5-28: Eectroactive polymer rotary motor diagram. (Copied from Heim et al. US Patent # 6,806,621)

Both Lafontaine and Kornbluh's motor designs impacted the design presented in the following Section for a conducting polymer based rotary eccentric motor.

5.4.2 Proposed Design

To address the possibility of an electroactive polymer motor, this paper will switch its focus to the design and theoretical performance of such a motor. The design assumes a

low speed, proof of concept model focusing on the design parameters for the motor's rotary eccentric and polymer film geometry. Particular conceptual advantages of the conducting polymer driven engine include a constant torque output no matter the engine's RPM, the ability to recover energy into the system from the conducting polymer's actuation, a higher power to mass ratio than today's electric DC motors, and the ability to eliminate the need for bulky gear assemblies.

The rotary eccentric design is based on the assumption that the conducting polymer will be radially attached at multiple points as depicted in Figure 5-29. Each piece of PPy will contract once during a revolution such that the major lobe of the eccentric will point in the same direction of the EAP undergoing the largest strain. Major parameters relevant to design include: 1) the achievable active strain for the PPy under a given load, 2) the strain rate of the PPy, 3) the moment created by the eccentric's off axis mounting, and 4) momentum's ability to maintain constant output shaft velocity.

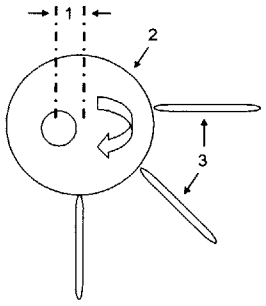

Figure 5-29: Rotary eccentric schematic. The rotary eccentric is off axis by distance (1). The eccentric (2) has numerous pieces of PPy (3) attached for rotation in the direction of the arrow as the PPy contracts in sequence. The major lobe of the eccentric will always be facing the active Section of PPy.

The principal model for the active strain achieved in polypyrrole reveals a linear electro-mechanically coupled system as described by the diffusive elastic model in Equation 1.1 of Chapter 1. In order to achieve the maximum possible strain, Equation 1.1 must be iteratively solved using the following time constants [4,10]

$$\tau_D = \frac{b^2}{4 \cdot D}, \tag{5.25}$$

$$\tau_{RCV} = R \cdot C_v \cdot Vol = \frac{g \cdot b}{2 \cdot \sigma_e} \cdot C_v, \tag{5.26}$$

$$\tau_{RCVP} = R_p \cdot C_v = \frac{l^2}{4 \cdot \sigma_p} \cdot C_v, \tag{5.27}$$

where b is the PPy thickness, g is the maximum allowable distance between electrodes, l is the length of the PPy film, D is the effective film diffusion coefficient, R is the system resistance from the electrolyte and film, C_v is the volumetric capacitance, σ_e is the electrolyte conductivity, and σ_p is the polymer conductivity. The time constants in Equations 5.25 – 5.27 can be optimized by increasing the polypyrrole surface area to volume ratio. However, a high surface area to volume geometry sacrifices the polymer's active peak force and passive strength. In conjunction with the polymer models, basic mechanics must be considered for the system.

The fundamental Equation governing the success of the conducting polymer actuated engine is the force required to move the eccentric. The torque needed to turn the eccentric is a function of the off axis lobe angle θ as described by

$$\tau(\theta) = -m \cdot g(l \cdot \sin\theta) = I \cdot \alpha, \tag{5.28}$$

where τ is the torque needed to rotate the eccentric, m is the mass of the eccentric, g is gravity, l is the distance from the center of mass to the point of rotation, θ is the angle of the major lobe from gravity's neutral axis, I is the moment of inertia for the eccentric, and α is the angular acceleration. Equation 5.28 assumes no friction about the point of

rotation and implies the peak force will occur when the major lobe angle is 90°. Reducing the peak force required to accelerate the eccentric can be accomplished by incorporating a flywheel into the motor design that can also maintain constant shaft velocity at steady-state. The angular momentum created by the flywheel can be modeled by

$$L = m \cdot r^2 \cdot \omega = I \cdot \omega, \tag{5.29}$$

where L is the angular momentum, r is the distance from the point or rotation, and ω is the angular velocity.

Equations 5.25 and 5.27 provide the key elements in evaluating the possibility and design specifications for a polypyrrole based device. Solving for the maximum allowable thickness and length as a function of time, allow for a better understanding of the geometric constraints placed on the polypyrrole.

The graph in Figure 5-30 below uses Equation 5.27 to determine the maximum allowable length and also infer the maximum attainable strain for a given time constant.

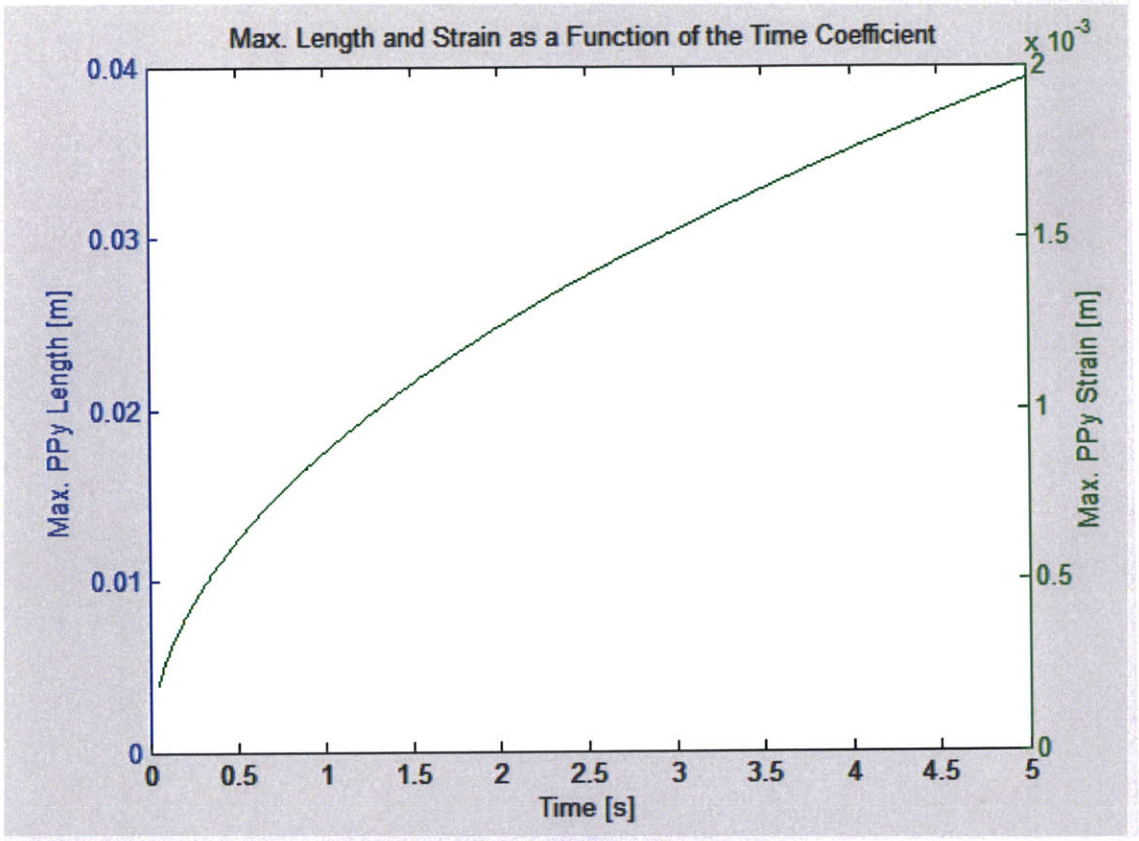

Figure 5-30: The maximum PPy length possible while still being able to perform a complete contraction is determined from the time constant for diffusion. Assuming a 5% contraction from doping, the maximum PPy strain is also plotted above.

In order to have a better feel for the peak force that can be produced by the polypyrrole, Equation 5.25 is solved for the maximum allowable thickness as plotted below in Figure 5-31. In order to attain the peak force produced by the polypyrrole, a width of 10 mm was assumed to determine the cross Sectional area which was then multiplied a peak stress of 30 MPa for a given time constant.

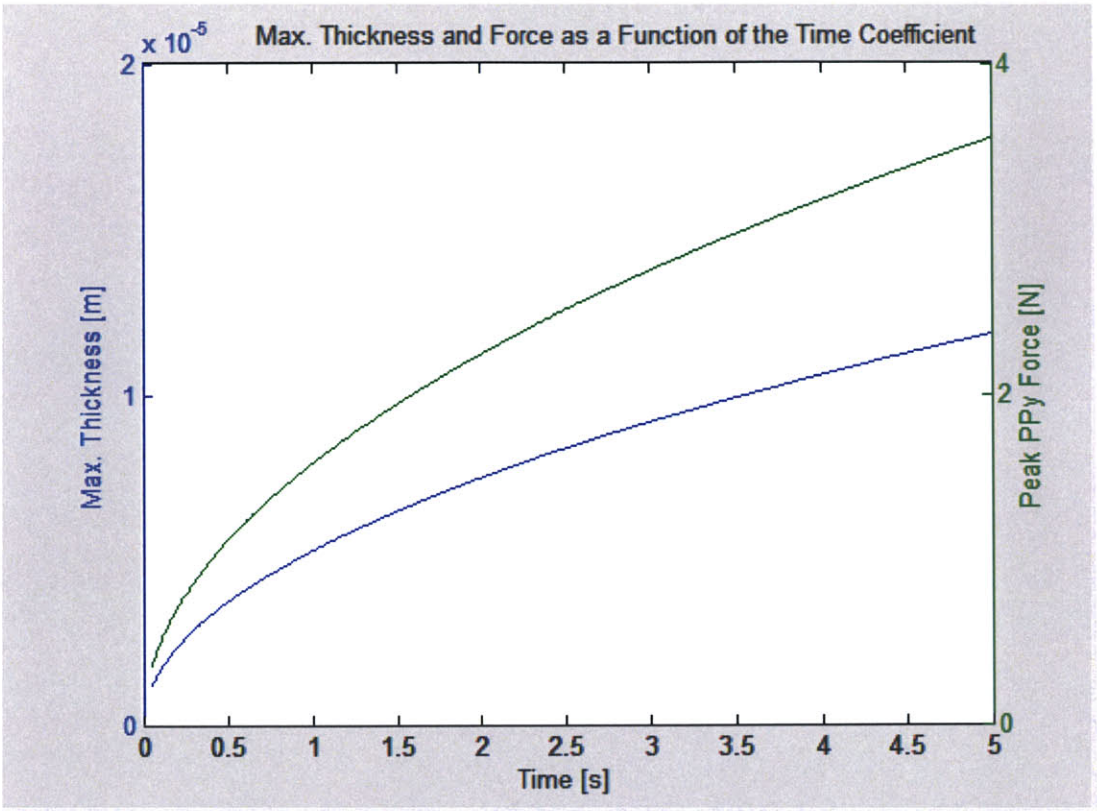

Figure 5-31: The maximum allowable thickness that will achieve a contraction within the polymer's volumetric RC charging time constant is determined in conjunction with the peak PPy force as a function of time.

For the rotary eccentric, the three dependant variables that must be chosen to determine the geometry of the conducting polymer are: 1) the desired speed of operation, 2) the force required to turn the eccentric, and 3) the distance of eccentricity of the crankshaft. Further investigation into Figures 5-30 and 5-31 reveals that choosing the force or distance of the eccentric as the dominant functional variable can lead to headaches in film geometry. For instance, if large forces are sought as the dominant variable, films can quickly approach millimeter thicknesses which are difficult to electrochemically deposit and take minutes or hours for full oxidation. On the other hand, choosing time as your dominant function variable, allows you to quickly determine if the suggested theoretical polypyrrole geometry is feasible and if the associated strains and forces will meet the

design's demands. In accordance with the justification above, the motor's RPMs are chosen as the dominant design parameter for this paper.

To achieve an operation frequency of 60 RPMs or 1 Hz, the polypyrrole will have to contract within a 0.5 s and then expand in an additional 0.5 s. Although this is desired, Figure 5-30 shows that the maximum allowable length of the PPy is approximately 120 mm with an associated strain of 60 μm which is too small for a practical eccentric on the macroscale. Therefore a time constant of 3 seconds was chosen since strains will be produced on the millimeter scale corresponding to a speed of 10 RPM. Now that an appropriate speed has been chosen, the polymer geometry and design can move forward (See Appendix B for further analysis).

The first step used to design the motor is to calculate the work undergone by the polypyrrole to move the eccentric one rotation. Assuming that the motor is manufactured from a nonconductive material such as delrin, the eccentric volume and mass are estimated to be approximately 5.0×10^{-6} m^3 and 0.01 kg. The work can then be calculated from the force necessary to lift the eccentric a distance of 1.5 mm as

$$Wecc = Mecc \cdot g \cdot Ff, \tag{5.30}$$

where *Wecc* [J] is the work, *Mecc* [kg] is the mass of the eccentric, g [$m \cdot s^{-2}$] is the acceleration of gravity, and *Ff* is a frictional factor. The work required to move the eccentric is estimated to be 1.1×10^{-4} J. The volume of polypyrrole necessary to achieve *Wecc* and *Wppy* [$J \cdot m^{-3}$] is the work per unit volume associated with polypyrrole

$$PPyVol_{\min} \geq \frac{Wecc}{Wppy}, \tag{5.31}$$

where $PPyVol_{min}$ [m^3] is the minimum volume of polypyrrole necessary can be estimated as 1.1×10^{-9} m^3. The peak charge needed to fully oxidize the polymer can be found form

$$I_{peak} = \frac{C_v \cdot V \cdot Vppy}{\tau_D} = \frac{Charge}{\tau_D}, \tag{5.32}$$

where I_{peak} [A] is the peak current and V [V] is the applied voltage. Using a volumetric film capacitance of 1.3×10^8 $F \cdot m^3$ and applied voltage of ± 2.5 V with diffusion time constant of 3 s, the peak current required for doping is approximately 0.12 A. The above derivations and results allow for the polypyrrole geometry and electrode distance to now be calculated from the modification of Equations 5.25 through 5.27.

The maximum allowable thickness of the polypyrrole film to achieve a contraction within 3 seconds, can be found by modifying Equation 5.25 as

$$b \leq \sqrt{4 \cdot \tau_D \cdot D}, \tag{5.33}$$

with a 7×10^{-12} $m^2 \cdot s^{-1}$ diffusion coefficient for polypyrrole. A thickness of approximately 9 μm was calculated. This is an easily achievable thickness from common electrochemical deposition techniques. The maximum allowable length can next be determined from Equation 5.25 by solving for l as shown below,

$$l = \sqrt{\frac{2 \cdot \tau_{RCVP} \cdot \sigma_p}{C_v}}, \tag{5.34}$$

with a polymer conductivity of 1 x 10^4 $S \cdot m^{-1}$. Solving for l when τ_{RCVP} is 3 seconds, the maximum allowable length is approximately 30 mm which will undergo a strain of 5% and contract 1.5 mm. Therefore the rotary eccentric can have a 1.5 mm off axis eccentric crank distance. Finally the maximum allowable gap distance between the working and

counter electrode can be determined from Equation 5.26. Although the gap distance is one of the least critical dimensions for the motor, the gap distance still provides a parameter than can affect the feasibility of design. Solving for g in Equation 5.26 yields

$$g = \frac{2 \cdot \tau_{RCV} \cdot \sigma_e}{b \cdot C_v}. \tag{5.35}$$

Substituting in an electrical conductivity of 3 $S \cdot m^{-1}$ and a τ_{RCV} of 3 s, the desired gap distance should not exceed 15 mm. The $PPyVol_{min}$ can be determined from the geometry results in Equations 5.33 and 5.34 to solve for the number of polymer films, n, required to obtain the desired force without sacrificing the desired actuation speed

$$n = \frac{PPyVol_{\min}}{l \cdot b \cdot w}, \tag{5.36}$$

The design parameters and returned values yield $n \approx 0.4$ indicating that the specified width of 10 mm can be reduced in half to conserve space and potentially improve actuation speeds without sacrificing the desired force.

Finally, the average current required for activation can be determined from

$$I_{avg} = \frac{\varepsilon \cdot Vol}{\alpha \cdot \tau}, \tag{5.37}$$

where the assumed polypyrrole strain is 5% and the strain to charge ratio is set at 10×10^{-10} $m^3 \cdot C^{-1}$. The average current required for oxidation of the motor design above is approximately 20 mA under the assumption that the polymer and electrolyte are the sole sources of electrical resistance in the system.

In summary, a film of polypyrrole which is 9 μm thick and 30 mm long will produce stains large enough to rotate an eccentric crank mounted 0.75 mm off axis and attain a speed of 10 RPM. The motor can be driven from two alkaline AA batteries at ± 2.5 V with a peak current of 120 mA. Each polymer film will be able to deliver 2.8 N of force to the motor's eccentric. The addition of a flywheel to the motor will also improve the motor's speed. The momentum maintained by the flywheel will add an associated passive force to assist in PPy film expansion and reduce the passive eccentric force during film contraction.

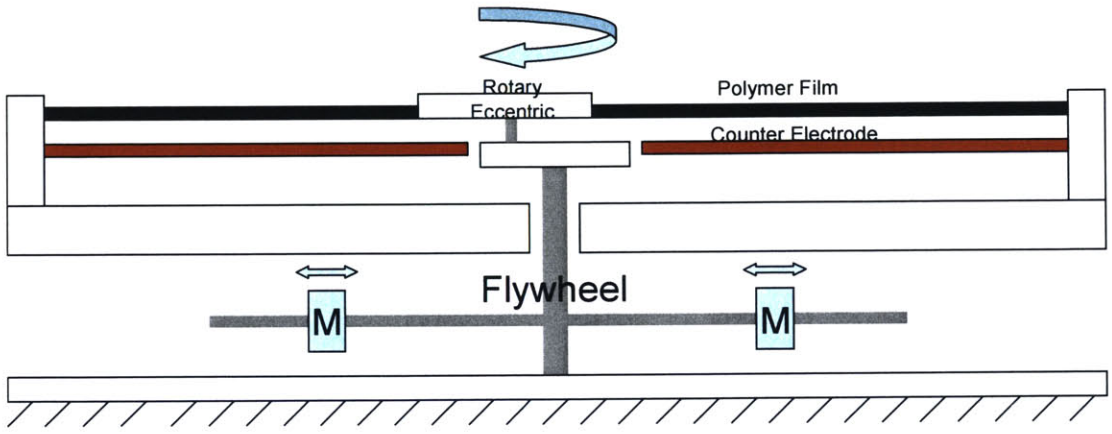

Figure 5-32: Side view of the conducting polymer motor. The polymer film to the left of the eccentric is fully oxidized and therefore contracted whereas the film on the right is fully unoxidized and expanded.

The design of the conducting polymer rotary motor reveals inherent flaws in the polymer, particularly the slow actuation speed of the film from poor electro-mechanical coupling and small attainable strains of 2 to 8 %. Although current advancements have been made to achieve strains of 12 % [7,11], much research still needs to be done for developing films with higher strains and conductivities. If a film is optimized according to the

Equations presented in this paper, it is possible to construct a 10 nm film which is several millimeters long with a diffusion time coefficient of 3 μs, capable of strain rates of 3000 $\%\cdot s^{-1}$, and have a power to mass ratio of 30 $kW\cdot kg^{-1}$, 30 times greater than an internal combustion engine [7]. Is this feasible? Although the conjecture is years away from reality, current research suggests that it is possible to achieve the power and rate described. Such enticing actuation possibilities provide the conclusion that conducting polymers provide one of the most attractive solutions to micro and nano actuation in the foreseeable future. Progressing past the current hurdles of manufacturing and assembly at such small levels will advance conducting polymers as a feasible and desired actuation solution.

5.5 *Conclusion and Future Work*

The helical twisted polymer film rotary motor's simple design offers many unique benefits. The helical rotary motor can produce a large gain factor from its translation of linear motion into rotary motion of a subtended angular displacement. Moreover, the helical rotary motor can be manufactured from a single film without additional mechanical components that inefficiently convert linear to rotary motion.

The results obtained from the ADINA model has not been published before and offers significant advances for design and materials research with conducting polymers. A computational model of the polymer can potentially reduce the time needed for scientists to overcome one of the greatest hurdles facing conducting polymers: high strain rates. The proven ability to obtain an accurate model for conducting polymers within finite element analysis software allows for researchers to implement creative geometries and other advancements that would decrease the diffusive resistance, R_D. A reduction in the diffusive resistance will increase the actuation speed of the polymer and its potential as a viable actuator device. Future modeling of conducting polymers should focus on a more accurate analytical model and transient 3D finite element analysis to accelerate the development of conducting polymer control in devices.

The conducting polymer based rotary eccentric motor developed in this Section provides a theoretical design for the polymer actuators and motor housing. Future work to construct the rotary eccentric motor should focus on system identification of the polymer for a feed forward potential input to drive the motor to its peak performance capabilities.

5.6 *Chapter References*

[1] Uchino, K. "Piezoelectric Ultrasonic Motors: Overview" *Smart Mater. Struct.* **V. 7**, (1998): 273-285.

[2] Barth, H.V. *IBM Technical Disclosure Bulletin.* **V. 16**: 2263.

[3] Koç, B., Başaran, D., Akın, T., Erden, A., "Design of a Piezoelectric Ultrasonic Motor for Micro-Robotic Application," *The 6th International Conference on Mechatronic Design and Modeling (MDM), Capadocia, TURKEY,* **(2002)**.

[4] Sashida, T. *Mech. Automation Japan.* **V. 15,** (1983):31.

[5] Kornbluh, R., Perline, R., Eckerle, J., Joseph, J. "Electrostrictive Polymer Artificial Muscle Actuators." *Proceedings of the 1998 IEEE International Conference on Robotics & Automation, Leuven, Belgium,* (May 1998): 2147-2154.

[6] Bowers, T., "Modeling, Simulation, and Control of a Polypyrrole-Based Conducting Polymer Actuator", S.M. Thesis, Massachusetts Institute of Technology, Cambridge, MA, **(2004)**.

[7] Madden, J.D., "Conducting Polymer Actuators," Ph.D. Thesis, Massachusetts Institute of Technology, Cambridge, MA, (2000): 156-192.

[8] Schmid, B., "Device Design and Mechanical Modeling of Conducting Polymer Actuators," S.B. Thesis, Massachusetts Institute of Technology, Cambridge, MA, **(2003)**.

[9] Lafontaine, S. *Fast Shape Memory Alloy Actuators*, PhD Thesis, McGill University, Montreal, Canada. (Jul. **1997**).

[10] Madden, J.D., Madden, P.G., Hunter, I.W. "Conducting Polymer Actuators as Engineering Materials." *Proceedings of SPIE 9th Annual Symposium on Smart Structures and Materials: Electroactive Polymer Actuators and Devices*, Yoseph Bar-Cohen, Ed., SPIE, San Jose CA, **V. 4695,** (2002): 176-190.

[11] Bay, L., West, K., Sommer-Larsen, P., Skaarup, S., Benslimane, M. "A Conducting Polymer Artificial Muscle with 12 % Linear Strain." *Advanced Materials*. **V. 15, No. 3,** Feb. 5, (2003): 310 - 313.

Appendix A: ECDMA

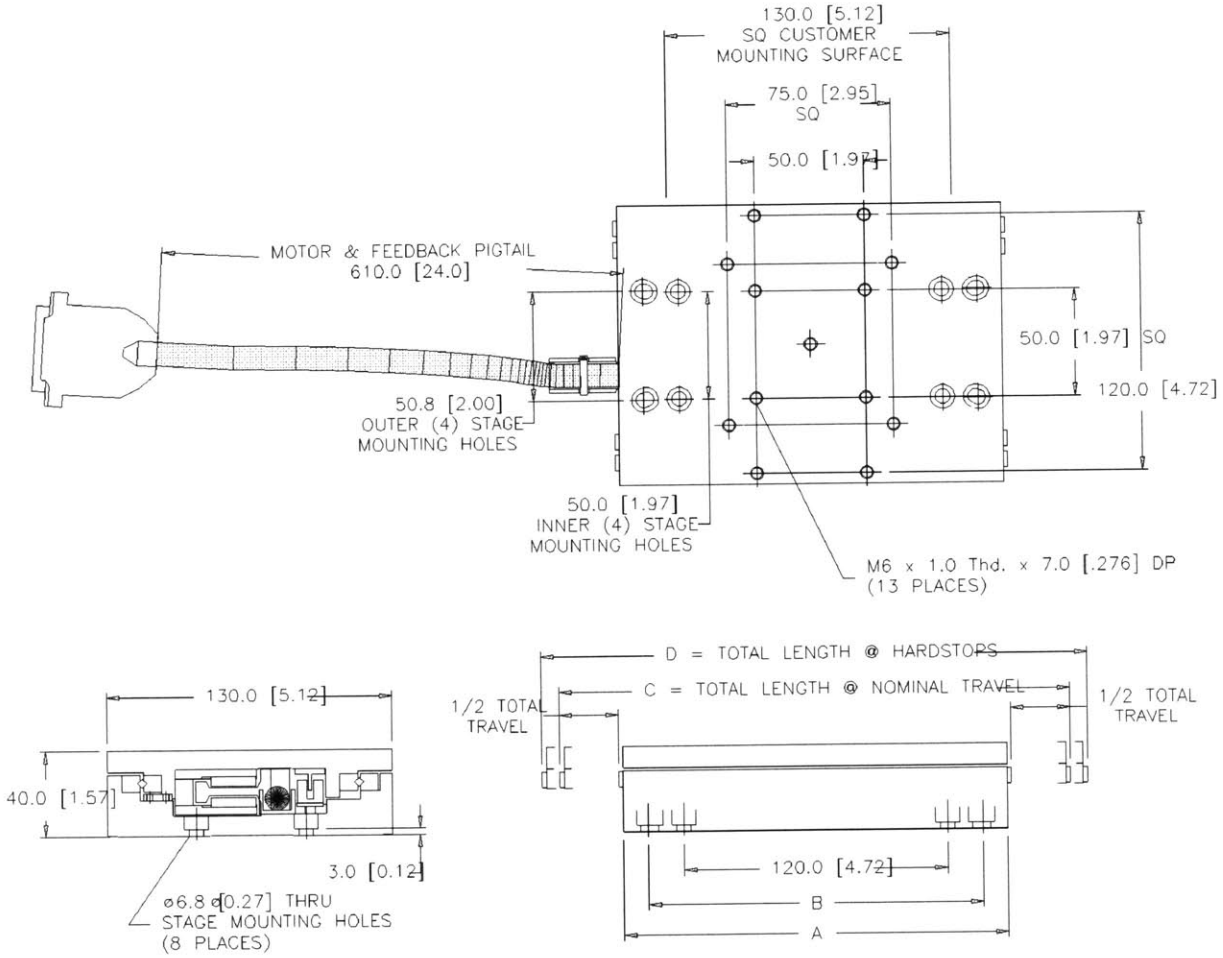

Basic Model	Total Travel	Dimensions – Millimeters [Inches]			
		A	B	C	D
ALS130-025	25.0 [1.00]	125.0 [4.92]	--------	179.0 [7.05]	195.0 [7.68]
ALS130-050	50.0 [2.00]	175.0 [6.89]	150.0 [5.91]	229.0 [9.02]	245.0 [9.65]
ALS130-100	100.0 [4.00]	225.0 [8.86]	150.0 [5.91]	329.0 [12.95]	345.0 [13.58]
ALS130-150	150.0 [6.00]	275.0 [10.83]	200.0 [7.87]	429.0 [16.89]	445.0 [17.52]

A.1 Aerotech ALS130-050 Technical Drawing

[Copied from http://www.Aerotech.com]

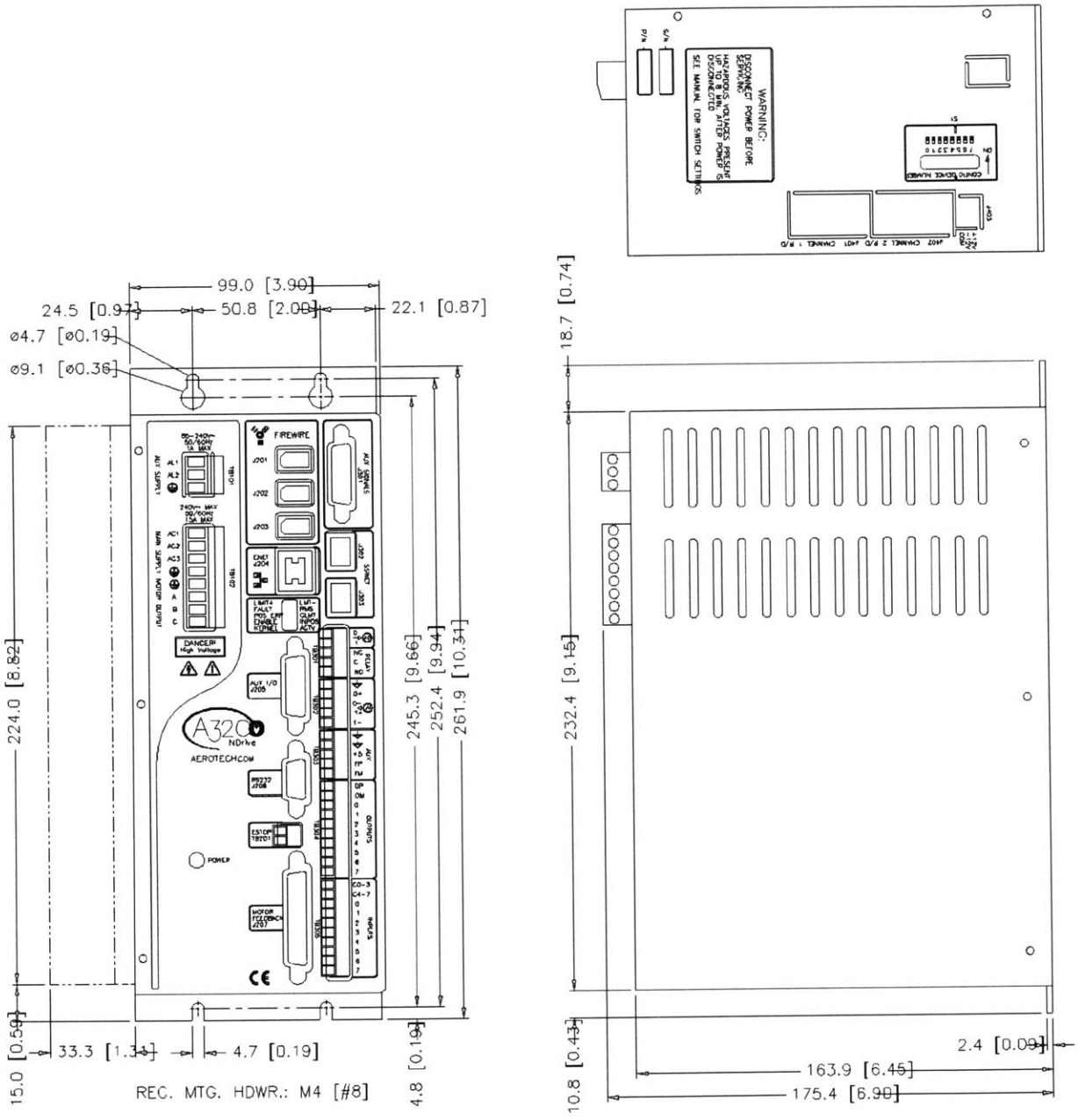

A.2 Aerotech NLDrive10 Technical Drawing

[Copied from http://www.Aerotech.com]

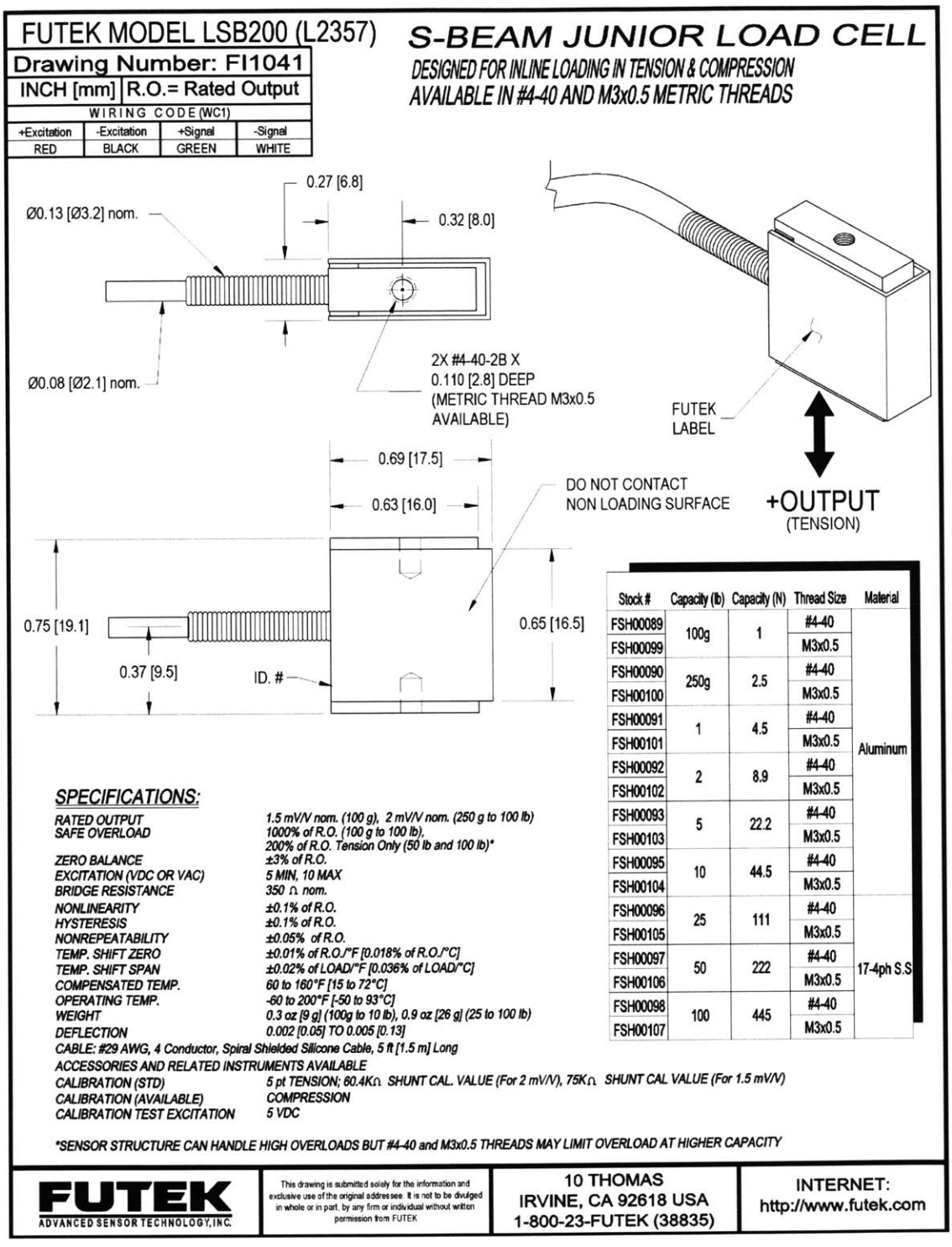

A.3 Futek L2357 Load Cell Specifications

[Copied from http://www.futek.com]

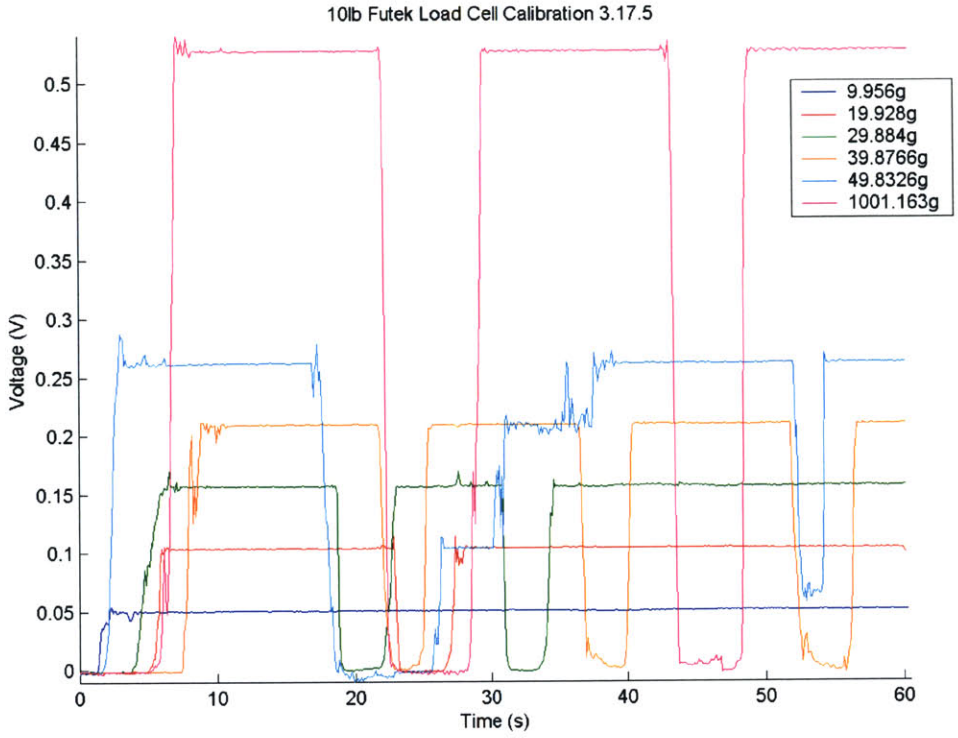

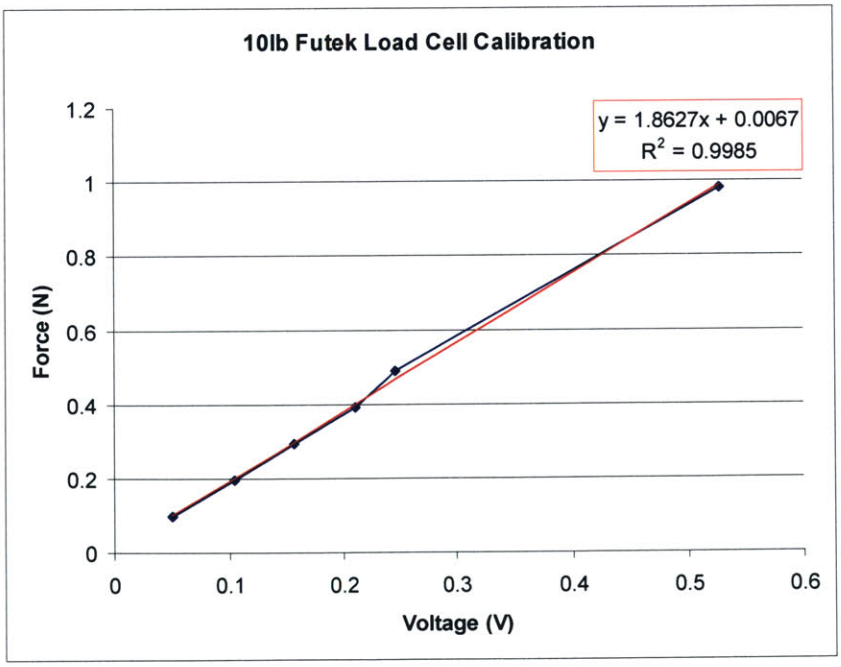

A.4 Futek Load Cell Calibration

A.5 ECDMA Visual Basic .NET 2003 Code


```
Imports System.Threading

Public Class Form1
  Inherits System.Windows.Forms.Form

#End Region
  'Single Point Input and Output Functions
  Declare Function AI_VRead Lib "nidaq32.dll" (ByVal deviceNumber As Int16, ByVal chan As Int16,
ByVal gain As Int16, ByRef voltage As Double) As Int16
  Declare Function AO_Update Lib "nidaq32.dll" (ByVal deviceNumber As Int16) As Int16
  Declare Function AO_VWrite Lib "nidaq32.dll" (ByVal deviceNUmber As Int16, ByVal chan As Int16,
ByVal voltage As Double) As Int16

  'NIDAQ Configuration and Device Info
  Declare Function AO_Configure Lib "nidaq32.dll" (ByVal deciceNumber As Int16, ByVal chan As
Int16, ByVal outputPolarity As Int16, ByVal intOrExtRef As Int16, ByVal refVoltage As Double, ByVal
updateMode As Int16) As Int16

  'Funtions for buffering an output
  Declare Function WFM_ClockRate Lib "nidaq32.dll" (ByVal deviceNumber As Int16, ByVal group As
Int16, ByVal whichClock As Int16, ByVal timebase As Int16, ByVal interval As Int32, ByVal mode As
Int16) As Int16
  Declare Function WFM_Group_Control Lib "nidaq32.dll" (ByVal deviceNumber As Int16, ByVal group
As Int16, ByVal operation As Int16) As Int16
  Declare Function WFM_Group_Setup Lib "nidaq32.dll" (ByVal deviceNumber As Int16, ByVal
numChans As Int16, ByVal chanVect() As Int16, ByVal group As Int16) As Int16
  Declare Function WFM_Load Lib "nidaq32.dll" (ByVal deviceNumber As Int16, ByVal numChans As
Int16, ByVal chanVect() As Int16, ByVal buffer() As Int16, ByVal count As Int32, ByVal iterations As
Int32, ByVal mode As Int16) As Int16
  Declare Function WFM_Rate Lib "nidaq32.dll" (ByVal rate As Double, ByVal units As Int16, ByVal
timebase As Int16, ByVal updateInterval As Int32) As Int16
  Declare Function WFM_Scale Lib "nidaq32.dll" (ByVal deviceNumber As Int16, ByVal chan As Int16,
ByVal count As Int32, ByVal gain As Double, ByVal voltArray As Double(), ByVal binArray() As Int16)
As Int16

  'Aerotech Initialze Drive Functions
  Declare Function AerSysOpen Lib "A32SYS.DLL" (ByVal dwDeviceID As Long, ByVal dwCard As
Long, ByRef phAerCtrl As Long) As Long
  Declare Function AerSysInitSystem Lib "A32Sys.Dll" (ByVal hAerCtrl As Long, ByVal bReset As
Long, ByVal mAxis As Long, ByVal mTask As Long, ByVal pszFile As String, ByRef pdwParmType As
Long, ByRef pdwParmNum As Long, ByRef pdwIndex As Long) As Long
  Declare Function AerSysStart Lib "A32SYS.DLL" (ByVal dwReset As Long, ByRef phAerCtrl As
Long) As Long

  'Aerotech Function to retreive the position
```

```
  Declare Function AerParmGetValue Lib "A32SYS.DLL" (ByVal hAerCtrl As Integer, ByVal
dwParmType As Integer, ByVal dwIndex As Integer, ByVal dwParm As Integer, ByVal
dwConvertToUserUnits As Integer, ByRef pdwValue As Double) As Integer

  'Aerotech Move related functions
  Declare Function AerMoveEnable Lib "A32SYS.DLL" (ByVal hAerCtrl As Integer, ByVal iAxis As
Integer) As Integer
  Declare Function AerMoveDisable Lib "A32SYS.DLL" (ByVal hAerCtrl As Integer, ByVal iAxis As
Integer) As Integer
  Declare Function AerMoveHome Lib "A32SYS.DLL" (ByVal hAerCtrl As Integer, ByVal iAxis As
Integer) As Integer
  Declare Function AerMoveFreerun Lib "A32SYS.DLL" (ByVal hAerCtrl As Integer, ByVal iAxis As
Integer, ByVal lDir As Integer, ByVal dwSpeed As Integer) As Integer
  Declare Function AerMoveHalt Lib "A32SYS.DLL" (ByVal hAerCtrl As Integer, ByVal iAxis As
Integer) As Integer



  'Global Variables
  Dim hAerCtl As Long = 0
  Dim phAerCtrl As Integer
  Dim ErrorCode As UInt32
  Dim IRc As Integer
  Dim PosDisp_Thread As Boolean = False
  Dim AI_Thread As Boolean = False
  Dim PIDLoop_Thread As Boolean = False
  Dim DataCollection_Thread As Boolean = False
  Dim WvFormOutput_Thread As Boolean = False
  Dim AnalogInThread As New Thread(AddressOf AnalogInMonitor)
  Dim PositionDisplayThread As New Thread(AddressOf PositionDisplayMonitor)
  Dim PIDLoopThread As New Thread(AddressOf PIDLoop)

  Dim Data(,) As Double
  Dim NInput As Long
  Dim WvfrmData() As Double
  Dim NewtonsPerVolt As Double = 1.8627 'N/V calibration factor with 10x gain
  Dim SampleArea As Double
  Dim Amplitude As Double
  Dim pos As Double
  Dim SampleZero As Double
  Dim SampLength As Double
  Dim Offset As Double
  Dim WaveformFrequency As Double
  Dim doutValue As Double
  Dim NumSamplesPerCycle As Integer
  Dim LastData As Integer
  Dim CurrentRange As Double
  Dim Potentiostat As Boolean = True
  Dim RampSystemID As Boolean = False
  Dim TestType As Integer ' 0 = Isotonic, 1 = Isometric
  Dim Pgain As Double
  Dim Igain As Double
  Dim Dgain As Double
```

```
  Private Sub InitiateTest_Click(ByVal sender As System.Object, ByVal e As System.EventArgs) Handles
InitiateTest.Click

    'General Variables to set array sizes and loop lengths
    Dim j As Integer = 0
    LastData = Convert.ToInt32(SampFreq.Text * NumberCycles.Text / WaveformFreq.Text)
    ReDim Data(LastData * 2, 4)
    Dim status As Int16
    SampleZero = Convert.ToDouble(ZeroSample.Text)
    SampLength = Convert.ToDouble(SampleLength.Text)

    'Varuables for Analog Input Voltages
    Dim ForceVoltage As Double
    Dim EOutVOltage As Double
    Dim IOutVoltage As Double

    'Variables related to the timing of the task
    Dim dTSample As Long = 10000000 / Convert.ToDouble(SampFreq.Text)
    Dim Tnot As DateTime
    Dim TSample As Long
    Dim TotalTime As Long = 10000000 * Convert.ToDouble(NumberCycles.Text) /
Convert.ToDouble(WaveformFreq.Text)
    Dim CurrentTime As DateTime

    'Variables for the PID (Isotonic) Loop
    Dim PIDTime As Double = 100 ' PID Loop Frequency (Sampling Time Increment)
    Dim PID_RunState As Integer = 0 ' 0 if no points stored, 1 if 1 point stored, 2 if 2 points stored
    Dim Err As Double
    Dim ErrLast As Double
    Dim IntLast As Double 'Integral Term
    Dim ErrLastLast As Double
    Dim TemporaryOutput As Double
    Dim PIDControl As Integer
    Dim PIDVelocity As Integer
    Dim SetPoint As Double = Convert.ToDouble(Stress_SetPoint.Text)  ' Stress (MPa) Setpoint
    Dim VelFactor As Double = Convert.ToDouble(StageVelFactor.Text)
    Dim Pgain As Double = Convert.ToDouble(GainP.Text) ' Proportional Gain
    Dim Igain As Double = Convert.ToDouble(GainI.Text) ' Integral Gain
    Dim Dgain As Double = Convert.ToDouble(GainD.Text) 'Derivative Gain
    Dim Aero As New AerotechDLL.AerIO
    Dim hAerCtrl As UInt32
    hAerCtrl = Convert.ToUInt32(phAerCtrl)
    Dim PIDCount As Long = 1
    Dim PIDDir As Integer
    Dim pos As Double
    Dim LdCellStress As Double
    SampleArea = Convert.ToDouble(SampleWidth.Text * SampleThickness.Text * 0.001) 'mm^2

    'Variables and values for Output Waveform to drive AMEL
    NumSamplesPerCycle = 500000
```

```
Amplitude = Convert.ToDouble(WaveformAmp.Text)
Offset = Convert.ToDouble(PotentialOffset.Text)
WaveformFrequency = Convert.ToDouble(WaveformFreq.Text)

   Dim Wvfrmdata() As Double = FunctionGenerator(signalTypeComboBox.SelectedIndex)
   Dim count As Int32
   count = Wvfrmdata.Length()
   Dim binaryWvfrm As Int16() = New Int16(Wvfrmdata.GetUpperBound(0)) {}
   Dim chanVect As Int16() = New Int16(0) {}
   Dim OutputFreq As Double = Convert.ToDouble(WaveformFreq.Text)
   Dim iterations As Int16 = Convert.ToInt16(NumberCycles.Text)

   status = WFM_Group_Control(1, 1, 0)
   status = WFM_Scale(1, 0, count + 1, 1, WvfrmData, binaryWvfrm)
   status = WFM_Load(1, 1, chanVect, binaryWvfrm, count, iterations, 0)
   status = WFM_ClockRate(1, 1, 0, 1, 2, 0)
   Tnot = Now
   TSample = Tnot.Ticks
   CurrentTime = Tnot

   'Output the analog waveform on the NIDAQ BNC-2110
status = WFM_Group_Control(1, 1, 1)

   Do Until CurrentTime.Ticks >= Tnot.Ticks + TotalTime

   status = AI_VRead(1, 2, 1, ForceVoltage)
   LdCellStress = ForceVoltage * NewtonsPerVolt / SampleArea
   Err = SetPoint - LdCellStress
   ' Positive Err indicates state stress too low
   ' Negative Err indicates stress state is too high

   If PID_RunState = 0 Then
      TemporaryOutput = Pgain * Err + Igain * Err
      ErrLast = Err
      IntLast = Igain * Err
      PID_RunState = 1
   End If

   If PID_RunState = 1 Then
      Err = SetPoint - LdCellStress
      TemporaryOutput = Pgain * Err + IntLast + Igain * Err + Dgain * (Err - ErrLast)
      ErrLast = Err
      IntLast = IntLast + Igain * Err
   End If

   If TemporaryOutput >= 0 Then
      PIDDir = 1
   ElseIf TemporaryOutput <= 0 Then
      PIDDir = -1
   End If

   IRc = AerMoveFreerun(phAerCtrl, 0, PIDDir, Math.Abs(TemporaryOutput * VelFactor))
```

```
        CurrentTime = Now

        If CurrentTime.Ticks >= TSample + dTSample Then
          'Get Analog Input Voltage From Potentiostat (E Out)
          status = AI_VRead(1, 0, 1, EOutVOltage)

          'Get Analog Input Voltage From Potentiostat (I Out)
          status = AI_VRead(1, 1, 1, IOutVoltage)

          'Get Analog Input Voltage (Stress)
          status = AI_VRead(1, 2, 1, ForceVoltage)

          'Get Position (mm)

          IRc = AerParmGetValue(phAerCtrl, 0, 0, 41, 1, pos)

          'Record Data to temporary memory
          'Col 1 = Time, Col 2 = Load Cell Voltage , Col 3 = Position, Col 4 = AMEL E Out, Col 5 =
AMEL I Out
          Data(j, 0) = CurrentTime.Ticks
          Data(j, 1) = ForceVoltage
          Data(j, 2) = pos * 0.000025
          Data(j, 3) = EOutVOltage
          Data(j, 4) = IOutVoltage

          j = j + 1
          TSample = dTSample + TSample
        End If
      Loop
        IRc = AerMoveHalt(phAerCtrl, 0)
        TxtInitStatus.Text = "The test is complete."

    End Sub
    Private Function FunctionGenerator(ByVal selectedIndex As Integer) As Double()
      Dim Wvfrmdata() As Double = {}
      Select Case selectedIndex
        Case 0
          Wvfrmdata = GenerateSineWave()
        Case 1
          Wvfrmdata = GenerateTriangleWave()
        Case 2
          Wvfrmdata = GenerateSquareWave()
        Case 3
          Wvfrmdata = GenerateStepIDWave()
        Case 4
          Wvfrmdata = GenerateImpulseIDWave()
        Case 5
          Wvfrmdata = GenerateRampedStepWave()
        Case Else
          Wvfrmdata = GenerateSineWave()
      End Select
      Return Wvfrmdata
    End Function
```

```
    Private Function GenerateSineWave() As Double()
        Dim Wvfrmdata(NumSamplesPerCycle / WaveformFrequency) As Double

        Dim j As Integer
        For j = 0 To (NumSamplesPerCycle / WaveformFrequency) - 1
            Wvfrmdata(j) = ((Math.Sin(Math.PI * 2 * j * WaveformFrequency / NumSamplesPerCycle) *
Amplitude) + Offset)
        Next
        Return Wvfrmdata
    End Function

    Private Function GenerateTriangleWave() As Double()
        Dim Wvfrmdata(NumSamplesPerCycle / WaveformFrequency) As Double
        Dim j, k As Integer
        Dim Increment As Double = 4 * Amplitude / (Wvfrmdata.Length)

        Wvfrmdata(0) = Offset

        For j = 1 To Convert.ToInt32(Wvfrmdata.Length / 4) - 1
            Wvfrmdata(j) = Wvfrmdata(j - 1) + Increment
        Next
        For k = j To Convert.ToInt32(Wvfrmdata.Length / 2) + j
            Wvfrmdata(k) = Wvfrmdata(k - 1) - Increment
        Next
        For j = k To Wvfrmdata.Length - 2
            Wvfrmdata(j) = Wvfrmdata(j - 1) + Increment
        Next

        Wvfrmdata(j) = Offset

        Return Wvfrmdata
    End Function

    Private Function GenerateSquareWave() As Double()
        Dim Wvfrmdata(NumSamplesPerCycle / WaveformFrequency) As Double
        Dim j, k As Integer

        Wvfrmdata(0) = Offset
        For j = 1 To Convert.ToInt32(Wvfrmdata.Length / 2)
            Wvfrmdata(j) = Offset + Amplitude
        Next
        For k = j To Wvfrmdata.Length - 2
            Wvfrmdata(k) = Offset - Amplitude
        Next
        Wvfrmdata(k) = Offset
        Return Wvfrmdata
    End Function

    Private Function GenerateStepIDWave() As Double()
        Dim Wvfrmdata(NumSamplesPerCycle / WaveformFrequency) As Double
        Dim i, j, k, m, n As Integer

        Wvfrmdata(0) = Offset
```

```
    For i = 1 To Convert.ToInt32(Wvfrmdata.Length / 21.2)
      Wvfrmdata(i) = Offset
    Next
    For j = i To Convert.ToInt32(1.1 * Wvfrmdata.Length / 21.2)
      Wvfrmdata(j) = Offset + Amplitude
    Next
    For k = j To Convert.ToInt32(11.1 * Wvfrmdata.Length / 21.2)
      Wvfrmdata(k) = Offset
    Next
    For m = k To Convert.ToInt32(11.2 * Wvfrmdata.Length / 21.2)
      Wvfrmdata(m) = Offset - Amplitude
    Next
    For n = m To Convert.ToInt32(Wvfrmdata.Length - 2)
      Wvfrmdata(n) = Offset
    Next

    Return Wvfrmdata
End Function

Private Function GenerateImpulseIDWave() As Double()
    Dim Wvfrmdata(NumSamplesPerCycle / WaveformFrequency) As Double
    Dim i, j, k, m, n As Integer

    Wvfrmdata(0) = Offset
    For i = 1 To Convert.ToInt32(5 * Wvfrmdata.Length / 20.2)
      Wvfrmdata(i) = Offset
    Next
    For j = i To Convert.ToInt32(5.1 * Wvfrmdata.Length / 20.2)
      Wvfrmdata(j) = Offset + Amplitude
    Next
    For k = j To Convert.ToInt32(15.1 * Wvfrmdata.Length / 20.2)
      Wvfrmdata(k) = Offset
    Next
    For m = k To Convert.ToInt32(15.2 * Wvfrmdata.Length / 20.2)
      Wvfrmdata(m) = Offset - Amplitude
    Next
    For n = m To Convert.ToInt32(Wvfrmdata.Length - 2)
      Wvfrmdata(n) = Offset
    Next

    Return Wvfrmdata
End Function


Private Function GenerateRampedStepWave() As Double()


    Dim Wvfrmdata(NumSamplesPerCycle / WaveformFrequency) As Double
    Dim a, b, c, d, e, f, g, h, i, j, k, l, m, n, o, p, q, r, s, t As Integer
    Wvfrmdata(0) = Offset
    For a = 1 To Convert.ToInt32(100 * Wvfrmdata.Length / 1000)
      Wvfrmdata(a) = Offset + 0 * Amplitude
    Next
```

```
For b = a + 1 To Convert.ToInt32(200 * Wvfrmdata.Length / 1000)
   Wvfrmdata(b) = Offset + 1 * Amplitude
Next
For c = b + 1 To Convert.ToInt32(300 * Wvfrmdata.Length / 1000)
   Wvfrmdata(c) = Offset + 2 * Amplitude
Next
For d = c + 1 To Convert.ToInt32(400 * Wvfrmdata.Length / 1000)
   Wvfrmdata(d) = Offset + 3 * Amplitude
Next
For e = d + 1 To Convert.ToInt32(500 * Wvfrmdata.Length / 1000)
   Wvfrmdata(e) = Offset + 4 * Amplitude
Next
For f = e To Convert.ToInt32(600 * Wvfrmdata.Length / 1000)
   Wvfrmdata(f) = Offset + 5 * Amplitude
Next
For g = f To Convert.ToInt32(700 * Wvfrmdata.Length / 1000)
   Wvfrmdata(g) = Offset + 6 * Amplitude
Next
For h = g To Convert.ToInt32(800 * Wvfrmdata.Length / 1000)
   Wvfrmdata(f) = Offset + 7 * Amplitude
Next
For i = h To Convert.ToInt32(900 * Wvfrmdata.Length / 1000)
   Wvfrmdata(i) = Offset + 8 * Amplitude
Next
For j = i + 1 To Convert.ToInt32(1000 * Wvfrmdata.Length / 1000 - 200)
   Wvfrmdata(j) = Offset + 9 * Amplitude
Next

'Switch to reverse charge through the ramp waveform

'For k = j + 1 To Convert.ToInt32(11 * Wvfrmdata.Length / 20)
'   Wvfrmdata(k) = Offset - 10 * Amplitude
'Next
'For l = k + 1 To Convert.ToInt32(12 * Wvfrmdata.Length / 20)
'   Wvfrmdata(l) = Offset - 9 * Amplitude
'Next
'For m = l + 1 To Convert.ToInt32(13 * Wvfrmdata.Length / 20)
'   Wvfrmdata(m) = Offset - 8 * Amplitude
'Next
'For n = m + 1 To Convert.ToInt32(14 * Wvfrmdata.Length / 20)
'   Wvfrmdata(n) = Offset - 7 * Amplitude
'Next
'For o = n + 1 To Convert.ToInt32(15 * Wvfrmdata.Length / 20)
'   Wvfrmdata(o) = Offset - 6 * Amplitude
'Next
'For p = o + 1 To Convert.ToInt32(16 * Wvfrmdata.Length / 20)
'   Wvfrmdata(p) = Offset - 5 * Amplitude
'Next
'For q = p + 1 To Convert.ToInt32(17 * Wvfrmdata.Length / 20)
'   Wvfrmdata(q) = Offset - 4 * Amplitude
'Next
'For r = q + 1 To Convert.ToInt32(18 * Wvfrmdata.Length / 20)
'   Wvfrmdata(r) = Offset - 3 * Amplitude
```

```
        'Next
        'For s = r + 1 To Convert.ToInt32(19 * Wvfrmdata.Length / 20)
        '   Wvfrmdata(e) = Offset - 2 * Amplitude
        'Next
        'For t = s + 1 To Wvfrmdata.Length - 2
        '   Wvfrmdata(t) = Offset - Amplitude
        'Next
        Wvfrmdata(t) = Offset
        Return Wvfrmdata
    End Function

    Private Sub InitializaStageAndDrive_Click(ByVal sender As System.Object, ByVal e As
System.EventArgs) Handles InitializaStageAndDrive.Click
        'Initialize stage and open communications with drive to perform experiment

        Dim eRc As String

        Dim sfilepath As String
        Dim lparmtype As UInt32
        Dim lparmnum As UInt32
        Dim lparmindex As UInt32

        sfilepath = ""
        eRc = "Stage, Communications, and Waveform Generator Initialized"

        Dim Aero As New AerotechDLL.AerSys
        Dim ErrorCode As UInt32
        Dim DeviceID As UInt32
        Dim CardId As UInt32

        DeviceID = Convert.ToUInt32(0)
        CardId = Convert.ToUInt32(0)
        ErrorCode = Aero.A32SysOpen(DeviceID, CardId, phAerCtrl)
        ErrorCode = Aero.A32SysStart(Convert.ToUInt32(1), phAerCtrl)
        ErrorCode = Aero.A32SysInitSystem(phAerCtrl, Convert.ToUInt32(0),
Convert.ToUInt32(&HFFFFFF), Convert.ToUInt32(&HFF), "", lparmtype, lparmnum, lparmindex)

        TxtInitStatus.Text = eRc 'Initialization Status

    End Sub

    Private Sub RadioButton1_CheckedChanged(ByVal sender As System.Object, ByVal e As
System.EventArgs) Handles Enable_X_Button.CheckedChanged
        'Enable X-axis for testing - initiated by user
        IRc = AerMoveEnable(phAerCtrl, 0)
    End Sub

    Private Sub Disable_X_Button_CheckedChanged(ByVal sender As System.Object, ByVal e As
System.EventArgs) Handles Disable_X_Button.CheckedChanged
        'Disable the X-axis on the stage - default mode
        IRc = AerMoveDisable(phAerCtrl, 0)
    End Sub
```

```
  Private Sub Home_Stage_Click(ByVal sender As System.Object, ByVal e As System.EventArgs)
Handles Home_Stage.Click
    'Home the stage
    IRc = AerMoveHome(phAerCtrl, 0)
  End Sub
  Private Sub StageVelocity_Scroll(ByVal sender As System.Object, ByVal e As
System.Windows.Forms.ScrollEventArgs) Handles StageVelocity.Scroll
    'Set stage velocity from scrollbar
    Dim StageVelocity_scroll As Long
    StageVelocity_scroll = StageVelocity.Value
  End Sub
  Private Sub Move_Forwards_Click(ByVal sender As System.Object, ByVal e As System.EventArgs)
Handles Move_Forwards.Click
    'Move stage forwards
    IRc = AerMoveFreerun(phAerCtrl, 0, -1, StageVelocity.Value)
  End Sub
  Private Sub Move_Backwards_Click(ByVal sender As System.Object, ByVal e As System.EventArgs)
Handles Move_Backwards.Click
    'Move stage backwards
    IRc = AerMoveFreerun(phAerCtrl, 0, 1, StageVelocity.Value)
  End Sub
  Private Sub Button1_Click(ByVal sender As System.Object, ByVal e As System.EventArgs) Handles
Button1.Click
    'Halt stage movement
    IRc = AerMoveHalt(phAerCtrl, 0)
  End Sub

  Private Sub StressUpdate_Click(ByVal sender As System.Object, ByVal e As System.EventArgs)
Handles StressUpdate.Click
    If AI_Thread Then
      AI_Thread = False
      AnalogInThread.Suspend()
      Exit Sub
    Else
      AI_Thread = True
      If AnalogInThread.IsAlive() Then
        AnalogInThread.Resume()
      Else
        AnalogInThread.Start()
      End If
    End If
  End Sub
  Public Sub AnalogInMonitor()

    Dim status As Int16
    Dim ForceVoltage As Double
    Dim LdCellStress As Double
    SampleArea = Convert.ToDouble(SampleWidth.Text * SampleThickness.Text * 0.001) 'mm^2

    Do Until AI_Thread = False
      status = AI_VRead(1, 2, 1, ForceVoltage)
      LdCellStress = ForceVoltage * NewtonsPerVolt / SampleArea
      AIMonitor.Text = LdCellStress
```

```
        AIMonitor2.Text = LdCellStress
        AnalogInThread.Sleep(200)
      Loop

    End Sub

    Private Sub OneAmp_CheckedChanged(ByVal sender As System.Object, ByVal e As
System.EventArgs) Handles OneAmp.CheckedChanged
      CurrentRange = 1  ' Sets Current Range to 1 Amp
    End Sub

    Private Sub HundredmAmp_CheckedChanged(ByVal sender As System.Object, ByVal e As
System.EventArgs) Handles HundredmAmp.CheckedChanged
      CurrentRange = 0.1 ' Sets Current Range to 100 mA
    End Sub

    Private Sub TenmAmp_CheckedChanged(ByVal sender As System.Object, ByVal e As
System.EventArgs) Handles TenmAmp.CheckedChanged
      CurrentRange = 0.01 'Sets Current Range to 10 mA
    End Sub

    Private Sub OnemAmp_CheckedChanged(ByVal sender As System.Object, ByVal e As
System.EventArgs) Handles OnemAmp.CheckedChanged
      CurrentRange = 0.001 ' Sets Current Range to 1 mA
    End Sub

    Private Sub HundredMicroAmp_CheckedChanged(ByVal sender As System.Object, ByVal e As
System.EventArgs) Handles HundredMicroAmp.CheckedChanged
      CurrentRange = 0.0001 ' Sets Current Range to 100uA
    End Sub

    Private Sub TenMicroAmp_CheckedChanged(ByVal sender As System.Object, ByVal e As
System.EventArgs) Handles TenMicroAmp.CheckedChanged
      CurrentRange = 0.00001 ' Sets Current Range to 10 uA
    End Sub

    Private Sub OneMicroAmp_CheckedChanged(ByVal sender As System.Object, ByVal e As
System.EventArgs) Handles OneMicroAmp.CheckedChanged
      CurrentRange = 0.000001 ' Sets Current Range to 1 uA
    End Sub

    Private Sub SaveToFile_Click(ByVal sender As System.Object, ByVal e As System.EventArgs) Handles
SaveToFile.Click
      ' Saves the Data array into a text format to be edited in MATLAB
      ' Code derived from Nate Vandesteeg who deserves some recognition

      'Be sure code is appropriately updated with RadioButtons for Current Range and also whether
      'you are driving the polymer in a Potentiostat or Galvanostat mode to account for the Slave
      'and Command voltages.  This should also be printed in the file below.

      Dim i As Long
      Dim DateTime As Date
      Dim FileName As String
```

```
    Dim State As Double
    SampleArea = Convert.ToDouble(SampleWidth.Text * SampleThickness.Text * 0.001) 'mm^2
    Dim Info As String
    Info = Convert.ToString(FileInfo.Text)

    TxtInitStatus.Text = "Data Being Written to File"

    DateTime = Now
    FileName = "test" & Convert.ToString(Format(DateTime, "MMddyyHmm")) & ".m"

    FileOpen(1, FileName, OpenMode.Output)

    PrintLine(1, "%Matlab Script file: " & FileName)
    PrintLine(1, "%" + Convert.ToString(Format(DateTime, "MMddyy-H:mm:ss")))
    PrintLine(1, " Fn = 'test" & Convert.ToString(Format(DateTime, "MMddyyHmm")) & ".m'")
    PrintLine(1, "%Aerotech DMA Program by Bryan Schmid Feb 10, 2004")
    PrintLine(1)
    PrintLine(1, "%*******NOTES")
    PrintLine(1, "%    " & Info & "% (Relevant Notes)")
    PrintLine(1)
    PrintLine(1, "%Configuration")
    PrintLine(1, "%*******AMEL Configuration")
    PrintLine(1, "%    " & Convert.ToString(CurrentRange) & " A (Current Range)")

    If Potentiostat Then
      Potentiostat = True
      PrintLine(1, "%    AMEL in Potentiostat Mode")
    Else
      PrintLine(1, "%    AMEL in Galvanostat Mode")
    End If

    PrintLine(1, "%*******Aerotech PID Loop")
    PrintLine(1, "%    " & Convert.ToString(GainP.Text) & "  Proportional Gain")
    PrintLine(1, "%    " & Convert.ToString(GainI.Text) & "  Integral Gain")
    PrintLine(1, "%    " & Convert.ToString(GainD.Text) & "  Derivative Gain")
    PrintLine(1, "%    " & Convert.ToString(StageVelFactor.Text) & "  Stage Velocity Gain")
    PrintLine(1, "%    " & Convert.ToString(Stress_SetPoint.Text) & "  Desired Stress")
    PrintLine(1, "%*******Aerotech Stage Position Units")
    PrintLine(1, "%    " & Convert.ToString(0.000025) & "  Machine Count Factor to mm")
    PrintLine(1, "%*******Futek Load Cell Parameters")
    PrintLine(1, "%    " & Convert.ToString(NewtonsPerVolt) & "   Newtons Per Volt conversion")
    PrintLine(1, "%*******Sample Properties")
    PrintLine(1, "%    " & Convert.ToString(SampleWidth.Text) & " mm (Width)")
    PrintLine(1, "%    " & Convert.ToString(SampLength) & " mm (Length)")
    PrintLine(1, "%    " & Convert.ToString(SampleThickness) & " um (Thickness)")
    PrintLine(1, "%    " & Convert.ToString(SampleArea) & " mm^2 (Area)")
    PrintLine(1, "%    " & Convert.ToString(ZeroSample.Text) & " mm (Sample Zero)")

    PrintLine(1)
    PrintLine(1, "%*******Processed Data")
    PrintLine(1, "%Matrix form: [Time (s), Load Cell Stress (MPa), Raw Position (mm), Strain, AMEL E
Out, AMEL I Out]")
    PrintLine(1)
```

```
    PrintLine(1, "Data = zeros(" & Convert.ToString(LastData + 1) & ",7);")
    PrintLine(1, "Data = [")

    For i = 0 To LastData - 1
      Print(1, (Data(i, 0) - Data(0, 0)) / 10000000.0# & " ")
      Print(1, NewtonsPerVolt * Data(i, 1) / SampleArea & " ")
      Print(1, Data(i, 2) & " ")
      Print(1, (((Math.Abs(SampleZero) + Data(i, 2)) - Convert.ToDouble(SampLength)) /
Convert.ToDouble(SampLength)) & " ")
      Print(1, -Data(i, 3) & " ")
      Print(1, -Data(i, 4) * CurrentRange & " ")
      PrintLine(1)
    Next
    PrintLine(1, "];")
    FileClose(1)
    TxtInitStatus.Text = "The Data File Has Been Saved to the bin"
  End Sub

  Public Sub PIDLoop()

    Dim PIDTime As Double = 100 ' PID Loop Frequency
    Dim PID_RunState As Integer ' 0 if no points stored, 1 if 1 point stored, 2 if 2 points stored
    Dim Err As Double
    Dim ErrLast As Double
    Dim IntLast As Double ' Integral term
    Dim ErrLastLast As Double
    Dim TemporaryOutput As Double
    Dim PIDControl As Integer
    Dim PIDVelocity As Integer
    'Dim SetPoint As Double = Convert.ToDouble(Stress_SetPoint.Text)  ' Stress (MPa) Setpoint
    'Dim VelFactor As Double = Convert.ToDouble(StageVelFactor.Text)
    'Dim Pgain As Double = Convert.ToDouble(GainP.Text) ' Proportional Gain
    'Dim Igain As Double = Convert.ToDouble(GainI.Text) ' Integral Gain
    'Dim Dgain As Double = Convert.ToDouble(GainD.Text) 'Derivative Gain
    Dim status As Int16
    Dim ForceVoltage As Double
    Dim LdCellStress As Double
    SampleArea = Convert.ToDouble(SampleWidth.Text * SampleThickness.Text * 0.001) 'mm^2

    Do Until PIDLoop_Thread = False

      Dim SetPoint As Double = Convert.ToDouble(Stress_SetPoint.Text)  ' Stress (MPa) Setpoint
      Dim VelFactor As Double = Convert.ToDouble(StageVelFactor.Text)
      Dim Pgain As Double = Convert.ToDouble(GainP.Text) ' Proportional Gain
      Dim Igain As Double = Convert.ToDouble(GainI.Text) ' Integral Gain
      Dim Dgain As Double = Convert.ToDouble(GainD.Text) 'Derivative Gain

      status = AI_VRead(1, 2, 1, ForceVoltage)
      LdCellStress = ForceVoltage * NewtonsPerVolt / SampleArea
      Err = SetPoint - LdCellStress
      ' Positive Err indicates state stress too low
      ' Negative Err indicates stress state is too high
```

```
        If PID_RunState = 0 Then
            TemporaryOutput = Pgain * Err + Igain * Err
            ErrLast = Err
            IntLast = Igain * Err
            PID_RunState = 1
        End If

        If PID_RunState = 1 Then
            Err = SetPoint - LdCellStress
            TemporaryOutput = Pgain * Err + IntLast + Igain * Err + Dgain * (Err - ErrLast)
            ErrLast = Err
            IntLast = IntLast + Igain * Err
        End If


        Dim PIDDir As Integer
        If TemporaryOutput >= 0 Then
            PIDDir = 1
        ElseIf TemporaryOutput <= 0 Then
            PIDDir = -1
        End If

        IRc = AerMoveFreerun(phAerCtrl, 0, PIDDir, Math.Abs(TemporaryOutput * VelFactor))
        PIDErr.Text = Err
        TempOutputMonitor.Text = TemporaryOutput
        'PIDLoopThread.Sleep(100)
    Loop

End Sub
Private Sub InitPIDLoop_Click(ByVal sender As System.Object, ByVal e As System.EventArgs)
Handles InitPIDLoop.Click

    If PIDLoop_Thread Then
        PIDLoop_Thread = False
        PIDLoopThread.Suspend()
        IRc = AerMoveHalt(phAerCtrl, 0)
        Exit Sub
    Else
        PIDLoop_Thread = True
        If PIDLoopThread.IsAlive() Then
            PIDLoopThread.Resume()
        Else
            PIDLoopThread.Start()
        End If
    End If

End Sub

Public Sub PositionDisplayMonitor()

    Dim pos As Double
    Do Until PosDisp_Thread = False
        IRc = AerParmGetValue(phAerCtrl, 0, 0, 41, 1, pos)
```

```
        Position_Display.Text = Convert.ToString(pos * 0.000025)
        PositionDisplayThread.Sleep(200)
      Loop

    End Sub
    Public Sub Read_Position_Click(ByVal sender As System.Object, ByVal e As System.EventArgs)
Handles Read_Position.Click

      If PosDisp_Thread Then
        PosDisp_Thread = False
        PositionDisplayThread.Suspend()
        Exit Sub
      Else
        PosDisp_Thread = True
        If PositionDisplayThread.IsAlive() Then
          PositionDisplayThread.Resume()
        Else
          PositionDisplayThread.Start()
        End If
      End If

    End Sub

    Private Sub ZeroSample_Button_Click(ByVal sender As System.Object, ByVal e As System.EventArgs)
Handles ZeroSample_Button.Click
      IRc = AerMoveHalt(phAerCtrl, 0)
      IRc = AerParmGetValue(phAerCtrl, 0, 0, 41, 1, pos)
      ZeroSample.Text = (pos * 0.000025) + 1.61 ' 1.61mm is the offset for the screw holding the electrode
      SampleZero = (pos * 0.000025) + 1.61 ' 1.61mm is the offset for the screw holding the electrode
    End Sub

    Private Sub SetLength_Click(ByVal sender As System.Object, ByVal e As System.EventArgs) Handles
SetLength.Click
      IRc = AerParmGetValue(phAerCtrl, 0, 0, 41, 1, pos)
      SampLength = Convert.ToDouble(Math.Abs(SampleZero) + pos * 0.000025)
      SampleLength.Text = SampLength
    End Sub
    Private Sub CheckBox1_CheckedChanged(ByVal sender As System.Object, ByVal e As
System.EventArgs)
      RampSystemID = True
    End Sub

    Private Sub StressUpdate2_Click(ByVal sender As System.Object, ByVal e As System.EventArgs)
Handles StressUpdate2.Click
      Call StressUpdate_Click(sender, e)
    End Sub
End Class
```

Appendix B: Polymer Rotary Motor

B.1 Experimental Data From Isotonic Testing

Experimental data using a voltage input as plotted below and the corresponding displacement for an isotonic load of 2MPa. The polymer has the following dimensions: length = 11.64mm, width = 3.5mm, and thickness = 19μm.

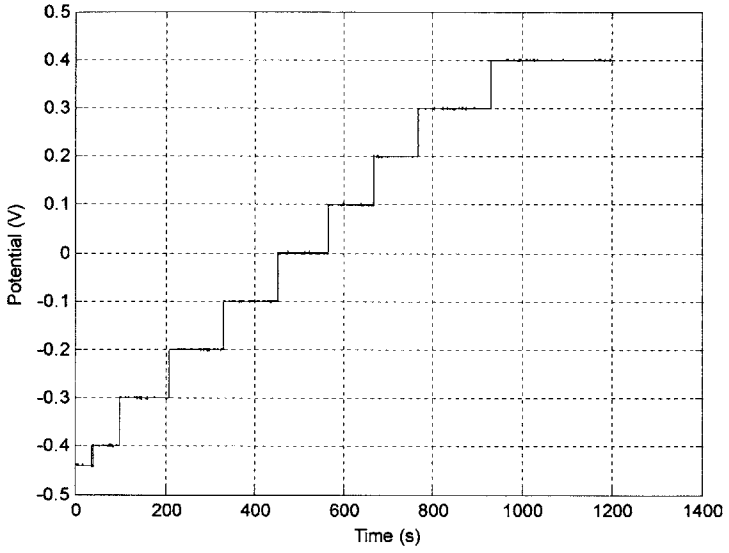

Figure B.1

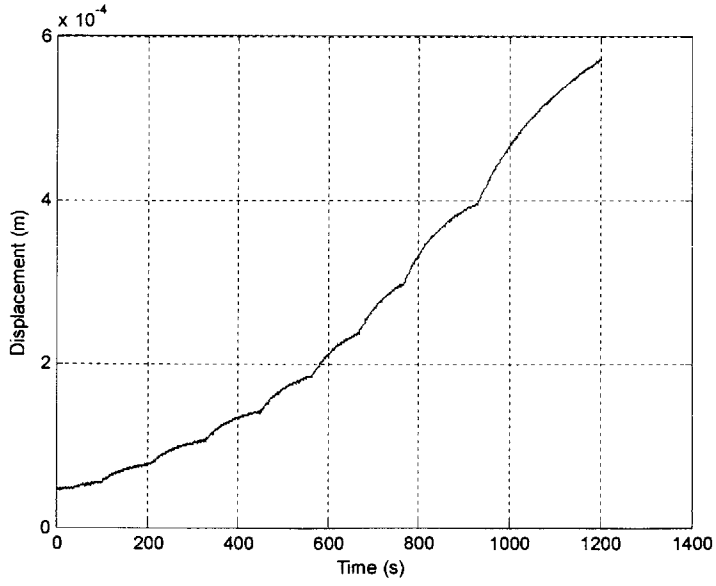

Figure B.2

B.2 MATLAB Script used for calculating non-dimensional values for finite element analysis.

```
%%%%%%%%%%%%%%%%%%%%%%%%%%%%
%%%  Bryan Schmid                    %%%
%%%  Calculations for Material Properties %%%
%%%%%%%%%%%%%%%%%%%%%%%%%%%%

ai= 19; % thickness in um of polypyrrole
a=ai*10^-6; % thickness in m of polypyrrole
delta=2.5*10^-9;  % Double layer thickness
D= 1*10^-12;  % Diffusivity Constant
Ep=120; % Constant
Epn= 8.854*10^-12; % Permitivity of Free Space
wi= 3.5 % width in mm of polypyrrole
w=wi*10^-3;  % width in m
li=11.64; % length in mm
l=li*10^-3; % length in m
nu=0.4; % Poisson's Ratio
Cv=1.3e8; % Charge Density
ev=0.5; % Potential across the polymer
E= 1e8; % Young's Modulus 0.1 GPa
rho=1.3e3; % Density of PPy

Cvt= Cv/rho; % Thermal Specific Heat (Heat Capacity) at Constant Volume

k=(D*Ep*Epn*w*l)/(a*delta^2);  % Thermal Conductivity k

alpha=((1-2*nu)*Cv*ev)/E;  % Thermal Coeff. of Expansion alpha

%%%%%%%%%%%%%%%%%%%%%%%%%%%%
%%%  Experimental Displacement Data %%%
%%%%%%%%%%%%%%%%%%%%%%%%%%%%

%%% Figure 4.0 in Project %%%

V=[.1:.1:1]; % Input potential
D=[9.7e-5  .00016  .00023  .00029  .00036  .00043  .00051  .0006  .001  .00175]; %
Displacement
plot(V,D,'-*');
xlabel('Potential above OCP (V)');
ylabel('Displacement (m)');
title('Active 2MPa Isotonic Test of Polypyrrole');
```

```
%%% Figure 5-15 %%%

figure
hold on
V=[.1:.1:.8]; % Input potential
De=[9.7e-5 .00016 .00023 .00029 .00036 .00043 .00051 .0006]; % Experimental
Displacements
Da=[.000135 .000154 .000185 .000229 .000285 .000354 .000434 .000527]; % Analytical
Displacements
Dad=[1.25e-4 1.9e-4 2.55e-4 3.2e-4 3.85e-4 4.5e-4 5.15e-4 5.8e-4]; % ADINA
Displacements
plot(V,De,'b-*');
plot(V,Da,'r-o');
plot(V,Dad,'k-x');
xlabel('Potential above OCP (V)');
ylabel('Displacement (m)');
title('Active 2MPa Isotonic Test of Polypyrrole');
legend('Experimental', 'Analytical', 'ADINA',4);

%%% Figure 5-16 %%%

figure
hold on
V=[.1:.1:.8]; % Input potential
Aa=[-.39488 .051556 .17744 .209283 .207833 .177079 .140253 .12118] % Aa is the
Analytical percent error
Aad=[-.29132 -.17284 -.13333 -.10345 -.06945 -.04651 -.0198 -.033332] % Aad is
ADINA percent error
plot(V,Aa,'r-*');
plot(V,Aad,'k-x');
xlabel('Potential above OCP (V)');
ylabel('Percent Error in Displacement');
title('Percent Error in Displacement Results')
legend('Analytical Error', 'ADINA Error');
```